

1 2 9 0



UNIVERSIDADE DE
COIMBRA

David Alexandre Mendes Carreira

**DEEP FACE RECOGNITION FOR ONLINE
STUDENT IDENTIFICATION**

Thesis submitted to the University of Coimbra in fulfillment of the requirements of the Master's Degree in Engineering Physics under the scientific supervision of Doctor David Portugal and Eng. José Faria and presented to the Physics Department of the Faculty of Sciences and Technology of the University of Coimbra.

September 2023

List of Figures

1	Architecture of a Convolutional Neural Network [49].	7
2	3x3 Kernels of the Sobel-Feldman operator used for edge detection [96].	8
3	Convolution operation using a 2×2 kernel.	8
4	Max pool, an example of a pooling operation.	9
5	Pipeline	13
6	Comparison between a) MTCNN: multi-stage, CPU real-time and multi-task learning, and b) RetinaFace: single-stage, anchor-based, CPU real-time and multi-task learning. MTCNN [133] proposes a series of bounding boxes then, through a series of refinement stages, the best solution and landmarks are found. RetinaFace [25] accomplishes, in a single-stage, face classification and bounding box regression by evaluating anchors, landmark localization and dense 3D projection for facial correspondence.	15
7	Pipeline	17
8	GoogLeNet’s inception block from the original paper [99].	22
9	ResNet’s residual block from the original paper [37].	22
10	Comparison between ResNet’s residual block (left) [17] with the inverted residual block proposed by MobileNetV2 (right) [89] and used by MobileFaceNet. Image taken from MovileNetV2’s paper [89].	24
11	VargNet’s normal block (top) and downsampling block (bottom) [134] used by VargFaceNet. Image from VargNet’s paper [134].	25

12	A normal convolution block that uses a single kernel (left) and the Mixed Depthwise Convolution proposed by MixNet [102].	26
13	Convolutional block proposed by ConvNeXt [68] (top) and the one by ConvFaceNeXt [39] (bottom). Image from the ConvFaceNeXt work [39].	27
14	Intra- and Inter-class challenge [111]. Eventhough features f_2 and f_3 belong to the same class, the euclidean distance between f_1 and f_2 is much smaller, proving the ineffectiveness of the softmax loss regarding inter-class compactness and inter-class separateness. . . .	28
15	Comparison between the classic softmax loss, modified softmax loss (NormFace) [111] and SphereFace [66].	29
16	ArcFace training process as described in the original paper [23]. . .	30
17	Demonstration of the intra-class compactness and inter-class distance of ArcFace (right) compared to Norm-Softmax (left) for 8 identities. The distance margin between classes is clear for ArcFace. Image from ArcFace’s paper [23].	31
18	Representation of training using triplet loss. Image from Facenet’s paper [92].	32
19	Results produced by the RetinaFace method over a test photo. Represented are the bounding boxes, respective confidence scores and the five facial landmarks.	37
20	Landmark based alignment. The green dot serves as an auxiliary point, resulting from the intersection of a horizontal line originating at the pivot eye and a vertical line projected from the other eye. Subsequently, the rotation angle is determined by computing the arctangent of two distances: the distance between the higher eye and the auxiliary point, and the distance from the auxiliary point to the pivot eye.	38

21	Different face capturing scenarios. The top row corresponds to 1280×720 files captured by a webcam, while the bottom row are 2309×3072 pictures from a smartphone's front facing camera.	41
22	DET (left) and ROC (right) curves. The y-axis represents the True Positive Rate (or TAR) for the ROC curves and False Negative Rate (or FRR) for the DET curves. The x-axis represents the False Positive Rate (or FAR) for both plots. Image from [88]	44
23	ROC Curves for the LFW benchmark from the Frontal group.	50
24	ROC Curves for the CALFW benchmark from the Age group.	50
25	ROC Curves for the CPLFW benchmark from the Pose group.	50
26	ROC Curves for the XQLFW benchmark from the Hard group. . . .	50
27	DET Curves for the LFW benchmark from the Frontal group.	52
28	DET Curves for the CALFW benchmark from the Age group.	52
29	DET Curves for the CPLFW benchmark from the Pose group.	53
30	DET Curves for the XQLFW benchmark from the Hard group. . . .	53
31	ROC Curves for the CFP-FF benchmark from the Frontal group. . .	99
32	ROC Curves for the AgeDB30 benchmark from the Age group. . . .	99
33	ROC Curves for the CFP-FP benchmark from the Pose group. . . .	100
34	ROC Curves for the VGGFace2 benchmark from the Hard group. .	100
35	DET Curves for the CFP-FF benchmark from the Frontal group. .	100
36	DET Curves for the AgeDB30 benchmark from the Age group. . . .	100
37	DET Curves for the CFP-FP benchmark from the Pose group. . . .	101
38	DET Curves for the VGGFace2 benchmark from the Hard group. .	101

List of Tables

1	Comparison of the training datasets. ✓- Datasets that are still available to the public. ✗- Datasets that have been removed from distribution.	19
2	Comparison of the test datasets. ✓- Datasets that are still available to the public. ✗- Datasets that have been removed from distribution.	20
3	Benchmarks' groups, their difficulty and intended evaluation purpose. * - Very easy. ***** - Very difficult.	43
4	Model's characteristics. “# Parameter” refers to the trainable parameters, “# Mult-Adds” to the number of multiplication and addition operations, “# Layers” denotes the quantity of convolutional and linear layers present in the model, “Embedding” signifies the dimensionality of the feature embedding produced by the model's output, “Inference time (s)” represents the average time taken for inference of all images from all the benchmark datasets, “Loss” is the loss function used to train the model, and “Dataset” are the training images.	48
5	Model's face verification accuracy.	49
6	TAR@FAR for all the models and benchmarks.	51
7	EER values for all the models and respective benchmarks.	53
8	MobileFaceNet accuracy scores before and after fine-tuning the whole network on QMUL-SurvFace with different ArcFace margins.	56

9	MobileFaceNet accuracy scores before and after fine-tuning the whole network on DigiFace-1M with different ArcFace margins.	57
10	TAR@FAR after fine-tuning the model with QMUL-SurvFace.	58
11	TAR@FAR after fine-tuning the model with DigiFace-1M.	58
12	MobileFaceNet accuracy scores before and after fine-tuning the network, with the first five layers frozen, on QMUL-SurvFace with different ArcFace margins.	59
13	MobileFaceNet accuracies before and after fine-tuning the network, with the first five layers frozen, on DigiFace-1M with different ArcFace margins.	60
14	TAR@FAR after fine-tuning the model, with the first five layers frozen, on QMUL-SurvFace.	60
15	TAR@FAR after fine-tuning the model, with the first five layers frozen, on DigiFace-1M.	61
16	MobileFaceNet accuracy scores before and after fine-tuning the network, with all the layers frozen aside the last two, on QMUL-SurvFace with different ArcFace margins.	61
17	MobileFaceNet accuracies before and after fine-tuning the network, with all the layers frozen aside the last two, on DigiFace-1M with different ArcFace margins.	62
18	TAR@FAR after fine-tuning the model, with all the layers frozen except the last two, on QMUL-SurvFace.	62
19	TAR@FAR after fine-tuning the model, with all the layers frozen except the last two, on DigiFace-1M.	63

Contents

Acknowledgments	i
Abstract	ii
Resumo	iii
1 Introduction	1
1.1 Context	1
1.2 Objectives	2
1.3 Dissertation structure	3
2 State of The Art	4
2.1 History of AI	4
2.2 Face Recognition - Theory Background	5
2.2.1 Convolutional Neural Networks	6
2.2.2 Training	10
2.3 A Face Recognition System	13
2.3.1 Face Detection	14
2.3.2 Face Alignment	15
2.3.3 Face Representation	16
2.4 Face Representation Pipeline	17
2.4.1 Datasets: Training and Testing Data	18
2.4.2 Feature Extractor	21
2.4.3 Loss	27

2.5	Related work	33
3	Methodology	36
3.1	Face detection	36
3.2	Face Representation	39
3.2.1	FaceNet	39
3.2.2	ResNet	40
3.2.3	MobileFaceNet	40
3.3	Finetuning data	40
3.4	Benchmarks	42
3.5	Implementation details	44
3.6	Discussion	45
4	Results	47
4.1	Models' specifications	47
4.2	Benchmarking Results	48
4.2.1	Accuracy	48
4.2.2	ROC Curves	50
4.2.3	DET Curves	52
4.2.4	Discussion	54
4.3	Training Details	54
4.4	Training Results	55
4.4.1	Discussion	63
5	Conclusion	65
5.1	Main Outcomes	65
5.2	Future work	67

Acknowledgments

Abstract

Resumo

Chapter 1

Introduction

1.1 Context

The outbreak of the COVID-19 pandemic tested the entire world on several levels and changed the concept of what is considered "normal" thereafter. The devastating health, economic and social consequences that COVID caused, spanned a need to develop novel solutions, for almost every aspect of our lives to facilitate the adaptation to the new world we are now living in.

Educational systems were no exception. In the midst of the pandemic, governments around the world forced institutions to shut down and interrupt the in-person regimen of teaching. By April 2020, most universities transitioned to an adapted remote learning paradigm [119] that lacked proper support due to the unanticipated nature of events, leading to new challenges, in particular, the legitimacy of evaluation performed remotely. To counter this problem, different approaches can be taken, namely, changing the method of evaluation, suppressing it altogether [8] or, when possible, implement continuous and automated vision-based student monitoring solutions, such as TrustID [29]. However, there are several unresolved issues that must be addressed in order to implement an end-to-end solution capable of assuring the success of such systems.

One core aspect is the face verification stage, where the visual data obtained from the monitoring system directly influences the rate of success of said stage. Another challenge is the unconstrained nature of the problem due to the purpose of the application and expected devices to be used. There is no way of controlling the conditions of capturing the visual data and consequent results, and the most likely input method will be a webcam or a smartphone's front facing camera, so a high variation in pose, resolution, illumination, etc. is foreseeable.

An additional detail that must be considered is the processing power available to execute the system¹, since solutions that benefit from higher accuracy comes at the cost of increased computational overhead, which can make real-time continuous monitoring unfeasible.

In conclusion, the method of choice must take the aforesaid into consideration and provide a trade-off between accuracy and computational cost, while also being invariant, to a certain degree, to the posed challenges of capturing the required data. Another detail to consider is the accuracy values required in this context. Because the solution is intended to perform image-based student monitoring, the accuracy values do not need to be perfect. Since the monitoring process occurs over a prolonged span of time, there are enough face verifications to supplant possible low accuracy values.

1.2 Objectives

Building upon the earlier context, the main objective of this dissertation is to evaluate Face Recognition (FR) methods on different benchmarks, compare them to the TrustID project's student monitoring solution and find a better approach. The aim is to identify the model that offers the most favorable balance of performance and computational efficiency, with the notion in mind that in this context

¹ According to the February 2023 Steam hardware survey, roughly 5% of its users do not have a dedicated GPU.

a perfect accuracy is not required. To achieve this, the following specific objectives have been established:

- Conduct a comprehensive review of state-of-the-art face recognition methods to select the prime ones.
- Implement the essential stages of a face recognition pipeline.
- Search for a better approach to TrustID's facial recognition module by evaluating the proposed methods on diverse benchmarks.
- Fine-tune using relevant datasets in an attempt to further improve the selected approach.
- Evaluate the performance of the fine-tuned method using selected benchmarks and discuss the overall best performing solution.

1.3 Dissertation structure

This dissertation is divided into several chapters. Chapter one relates to the introduction of the dissertation, it presents the context and motivation for this work, and the structure of the document. The document continues in the second chapter, it starts with an overview of the [History of Artificial Intelligence \(AI\)](#), carries out a survey about the topic's State-Of-The-Art, presented and summarized through the step-by-step analysis of the pipeline of a Face Recognition system, and ends with a comparison table of the discussed methods. In chapter three, the implemented methods and experiments are described. The forth chapter presents and discusses the results obtained. Finally, chapter five draws conclusions of the work achieved in the past several months and prospects for the future.

Chapter 2

State of The Art

This chapter gathers all the necessary background to better understand the topics and work of this dissertation. First, a brief history of Artificial Intelligence (AI) is presented. Then a review of the theoretical background behind a Face Recognition system and its components. To conclude, relevant works related to the dissertation are discussed.

2.1 History of AI

The breakthroughs of AI are predominant, and its importance in our everyday life is undeniable. The interest in the area grew immensely with all the Turing's theoretical research, the proposal of the first mathematical Artificial Neuron model in 1943 by Warren McCulloch and Walter Pitts [72] or the first successful Artificial Neural Network (ANN) by Belmont Farley and Westley Clark [30]. However, only in 1956, during the *Dartmouth Summer Research Project on Artificial Intelligence* [71], was the term "Artificial Intelligence" was firstly proposed by John McCarthy *et al.*, beginning what is now considered to be the birth of AI [130].

The succeeding two decades following the Dartmouth conference were filled with important developments. The 1959 General Problem Solver implemented by Allen Newel *et al.* [78] or Joseph Weizenbaum's ELIZA (1964), a natural language

processing tool [117]. Unfortunately, part of the interest and development around AI met an unforeseen fade after the 1969 book *The Perceptron: A Probabilistic Model for Information Storage and Organization in the Brain* [75] that reported the incapability of ANN to solve linear inseparable problems. However, the authors failed to consider other solutions already proposed that solves the linear inseparability, such as the 1965 implementation, by Ivakhnenko and Lap, of what is considered to be the first deep learning network Ia [47].

In 1979, Kunihiko Fukushima introduced the first Convolutional Neural Network (CNN), and ten years later, Yann LeCun *et al.* applied to for the first time Backpropagation [58] to a CNN, creating what is now a pillar for most of the modern competition winning networks in computer vision [91]. The study on Neural Networks continued with special attention to CNNs due to their great performance in image related tasks when compared to others networks [60]. Some relevant examples: in 2003 the MNIST record was broken by Simard *et al.* [94] and, in 2011, a GPU implementation of a CNN [21] achieved superhuman vision performance [97]. To supplement even more the importance of CNNs and GPUs, only a year later, Alex Krizhevsky *et al.* proposed a Deep CNN trained by GPUs that became the first one of this type to win the ImageNet Large Scale Visual Recognition Challenge (ILSVRC) [55]. The year of 2012 was very important for Deep Learning, CNNs and Computer Vision, beginning what's considered to be the start of the new wave, we're currently in, of interest in Artificial Intelligence.

2.2 Face Recognition - Theory Background

Face Recognition is a thoroughly debated and extensively researched task in the Computer Vision community for more than two decades [85], popularized in the early 1990s with the introduction of the Eigenfaces [106] or Fisherfaces [80] approaches. These methods project faces in a low-dimensional subspace assuming certain distributions, but lack the ability to handle uncontrolled facial changes that

breaks said assumptions. Henceforth, bringing about face recognition approaches through local-features [20, 1] that, even though, presented considerable results, were not distinctive or compact. Beginning in 2010, methods based on learnable filters have risen [127, 61], but revealed limitations when nonlinear variations are at stake.

Earlier methods for FR worked appropriately when the data was handpicked or generated on a constrained environment. However, they did not scale adequately in the real world were there are large fluctuations in, particularly, pose, age, illumination, background scenario, the presence of facial occlusion [85] and many unimaginable more [48]. These shortcomings can be dealt with by using Deep Learning, a framework of techniques that solves the nonlinear inseparable classes problem [75], more specifically a structure called Convolutional Neural Network [113].

CNNs are a type of Artificial Neural Network that exhibits an improved performance on image or video-based tasks compared to other methods [60]. They were greatly hailed in 2012, after the AlexNet [55] victory, by a great margin, in the ImageNet Large Scale Visual Recognition Challenge (ILSVRC). Just two years later, DeepFace [100] revolutionized the benchmarks scores by achieving state-of-the-art results that approached human performance, reinforcing even further the importance of Deep Learning and shifting the research path to be taken [113].

Given what has been stated so far and the proven robustness, performance, and overall results in computer vision, the methods discussed in this dissertation will therefore deal exclusively with Deep Learning approaches. For more information on other methods, please refer to [57].

2.2.1 Convolutional Neural Networks

There are several types of Neural Networks architectures, but CNNs are probably the most widely implemented model overall [124, 63]. Using CNNs for Computer Vision tasks [55, 100, 105, 132], in this specific case, Face Recognition, is not

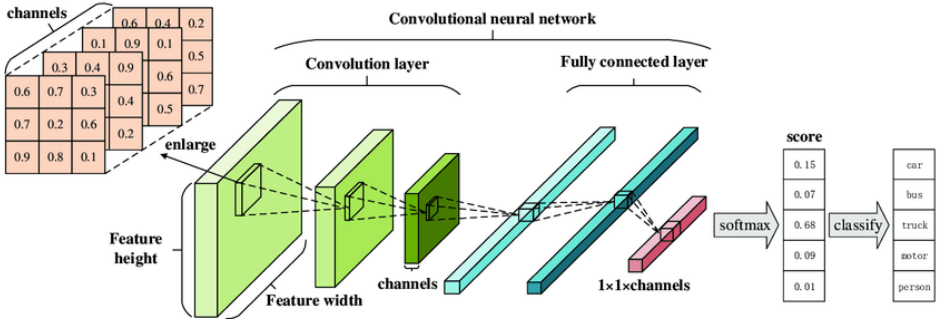


Figure 1: Architecture of a Convolutional Neural Network [49].

an arbitrary choice, but due to the fact that the network design benefits from the intrinsic characteristics of the input data: images have an array-like structure [124], and local groups of values are correlated (motifs or patterns) and invariant to spatial location [59, 14]. Furthermore, when compared to fully connected networks, CNNs are superior due to 4 key features: 1) shared weights between the same features in different locations reduce the number of parameters [63], 2) sparse connections [3], 3) pooling layers and 4) automatically identifies the relevant features without any human supervision [3, 63].

In the CNN category itself there are different variants, but they all abide the fundamental structure of a feedforward hierarchical multi-layer network (Figure 1). Feedforward because the information only flows in a singular direction without cycling [129], hierarchical because the higher complexity internal representations are learned from lower ones [59, 142] and multi-layer because it is composed of a series of stages, blocks or layers. The raw data is fed to an input layer, forwarded to a sequence of intercalating convolutional and pooling layers, transmitted to a stage of one or more fully-connected layers [59, 34, 3].

Convolutional Layer

The convolutional layer aims at extracting feature representations from the inputs, and is formed by a set of learnable filters called kernels and an activation

function [34, 124].

-1	0	+1
-2	0	+2
-1	0	+1

G_x

+1	+2	+1
0	0	0
-1	-2	-1

G_y

Figure 2: 3x3 Kernels of the Sobel-Feldman operator used for edge detection [96].

A kernel (Figure 2), is a grid-like structure of fixed dimensions [WxHxD], where W is the width, H is the height and D is the depth (number of channels). Each of its elements is a learnable weight that is adjusted during training to extract significant features [3]. With a predetermined stride, the kernel scans its receptive field [50], horizontally and vertically, through the input data, and produces the feature map [59, 3] by performing an element-wise product, called convolution, that can be described as follows [50]:

$$f_l^k(p, q) = \sum_c \sum_{x,y} i_c(x, y) \cdot w_l^k(u, v) \quad (2.1)$$

where $f_l^k(p, q)$ is an element at line p and column q in the feature map from the k -th kernel in the l -th layer, $i_c(x, y)$ is the element at line x and row y in the input data, and $w_l^k(u, v)$ is the weight at line u and column v from the k -th kernel of the l -th layer.

Input	Kernel	Output																																													
<table border="1" style="border-collapse: collapse; width: 100%;"> <tr><td>0</td><td>0</td><td>0</td><td>0</td><td>0</td></tr> <tr><td>0</td><td>0</td><td>1</td><td>2</td><td>0</td></tr> <tr><td>0</td><td>3</td><td>4</td><td>5</td><td>0</td></tr> <tr><td>0</td><td>6</td><td>7</td><td>8</td><td>0</td></tr> <tr><td>0</td><td>0</td><td>0</td><td>0</td><td>0</td></tr> </table>	0	0	0	0	0	0	0	1	2	0	0	3	4	5	0	0	6	7	8	0	0	0	0	0	0	\ast <table border="1" style="border-collapse: collapse; width: 100%;"> <tr><td>0</td><td>1</td></tr> <tr><td>2</td><td>3</td></tr> </table>	0	1	2	3	$=$ <table border="1" style="border-collapse: collapse; width: 100%;"> <tr><td>0</td><td>3</td><td>8</td><td>4</td></tr> <tr><td>9</td><td>19</td><td>25</td><td>10</td></tr> <tr><td>21</td><td>37</td><td>43</td><td>16</td></tr> <tr><td>6</td><td>7</td><td>8</td><td>0</td></tr> </table>	0	3	8	4	9	19	25	10	21	37	43	16	6	7	8	0
0	0	0	0	0																																											
0	0	1	2	0																																											
0	3	4	5	0																																											
0	6	7	8	0																																											
0	0	0	0	0																																											
0	1																																														
2	3																																														
0	3	8	4																																												
9	19	25	10																																												
21	37	43	16																																												
6	7	8	0																																												

Figure 3: Convolution operation using a 2×2 kernel.

The overall architecture of CNNs are inspired by the visual perception [46], so a direct parallelism can be made to better define the activation function. The kernels can be seen as receptors, or artificial neurons, that respond to different features, whereas the activation function is a simulation of the threshold function that dictates if the next neuron is activated or not. Additionally, the convolution operation is linear, consequently, if no nonlinear activation function was used, the input of the next layer would be a linear output of the previous layer. The introduction of nonlinearity through activation functions, such as ReLU (Rectified Linear Unit) and its variations (Leaky, Parametric, Randomized, Concatenated, Bounded, etc) or others like Sigmoid or Tanh [27], allows deep neural networks to approximate any function, enhancing the ability to fit to any data [63].

Pooling Layer

After the features are extracted, their spatial location becomes less relevant for the following layers. Introducing a pooling layer that reduces the spatial size of the feature maps by joining identical features [59, 34], keeps only the dominant information. This downsampling operation has two important advantages that help reduce the overfitting problem [2, 63]. First, it reduces the number of learnable features, which requires less memory to train the network. Second, it enhances feature extraction invariance to shifts and rotations by emphasizing only the relevant features.

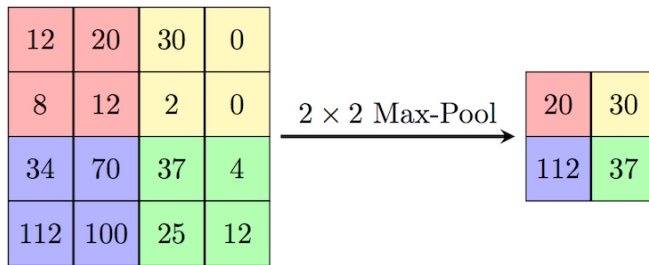


Figure 4: Max pool, an example of a pooling operation.

There are many ways of downsampling the feature map through pooling such as min pooling, average pooling or stochastic pooling. However max pooling is by far the most popular one. As pictured in (Figure 4), this operation divides the feature map in sections and computes the maximum value in each while discarding the other ones.

Fully Connected Layer

The fully connected (FC) layer is located at the end of the network. It is a dense, feedforward neural network in which every neuron is connected to all other neurons [124, 3]. The final feature map is flattened and transformed in a one-dimensional feature vector and the purpose of the FC layer is using this vector as an input, and act as the CNN classifier by performing high logic reasoning [34].

2.2.2 Training

Training a network in the context of CNNs is the process of finding the optimal kernel weights' values. The training data is passed through the model, the predictions asserted and the distance between them and the expected ones is measured by a loss function. LeCun *et al.* [60] presents the problem as follows:

$$E^p = \mathcal{D}(D^p, Y^p) \quad (2.2)$$

The loss function, E^p , is a measure of error. It computes the difference between the expected result, D^p , and the predicted result Y^p , where $Y^p = F(Z^p, W)$ is a function of the p -th training example, Z^p , for a determined weight W . Additionally, $E_{train}(W)$, is the average of all the errors calculated in a training set $\{(Z^x, D^x), \dots (Z^p, D^p)\}$. Training the network is nothing more than a function minimization problem, and for that there are several techniques, the optimizers.

Optimizers

By computing the gradient of the loss function in respect to the learnable parameters it allows studying how said parameters influence the loss function and how it can be more efficiently minimized. This algorithm is called gradient descent [87], and is the simplest minimization technique. By definition, the gradient of a function is the direction of the steepest ascent, henceforth, the learnable parameters are updated once every epoch in the opposite direction to reduce the error:

$$W_k = W_{k-1} - \epsilon \frac{\delta E(W)}{\delta W} \quad (2.3)$$

where ϵ is a constant called **learning rate** that controls how much the parameters are updated and has an immense impact in the performance of a neural network. According to Goodfellow *et al.* [33], if the learning rate is set too low, training will be much slower and can become permanently stuck with a high training error. On the other hand, if the learning rate is too high, the gradient descent can increase the training error instead of reducing it.

Stochastic Gradient Descent (SGD) [3] is an efficient algorithm in terms of memory usage, and is the algorithm of choice to optimize the loss function but others such as mini-batch gradient descent or Adam (Adaptive moment estimation) [52] are also common.

Backpropagation

Regardless of the optimizer selected, computing an analytical expression for the gradient is trivial, but evaluating it is a computational heavy task when the aim is to find a minimum with respect to all the parameters in the network. To this extent, the backpropagation algorithm is a solution to do so efficiently [58] by computing the gradient using an application of the *Chain Rule of Calculus* $\left(\frac{dz}{dx} = \frac{dz}{dy} \frac{dy}{dx}\right)$, that starts at the final layer, and proceeds backwards [33].

Transfer Learning

Developing a Deep Learning system requires data in large scale [81], specially labeled one. In a general sense, gathering information can be very difficult, but if the domain of study is too specific or not widespread enough, that poses an even greater challenge. To overcome this solution, based on the psychologist C.H. Judd's theory, a technique called Transfer Learning takes place. This is defined by Zhuang *et al.* [144] as: given a source and target domain, transfer learning is the act of utilizing the knowledge acquired in the source to further improve the performance of the learned decision functions on the target domain. A classic example is the case of learning how to ride a motorcycle. It will be easier for someone who has already learned how to ride a bicycle than it is to someone starting from scratch.

In the context of CNNs, there are 2 ways of approaching the aforesaid problem. By taking a pre-trained CNN and either use it as a fixed feature extractor or fine-tuning it. In the first case, an already trained CNN is used, however, the final few layers or the fully connected one is discarded and retrained to a specific task, while the rest of the network is frozen and used as the feature extractor. The second approach is referred to as fine-tuning a network and, as the name suggests, the source network's parameters are used as a starting point and is retrained using the desired data. That can be achieved by updating the whole network or through freezing the layers. The first ones are the more common since they are responsible for extracting the more general, universal features (edges or patterns).

2.3 A Face Recognition System

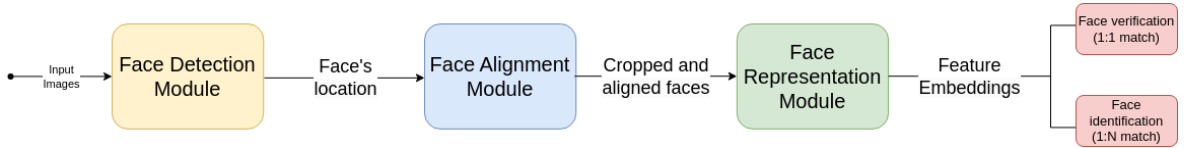


Figure 5: A typical learning-based face recognition pipeline, guided by the approach in [113].

According to Ranjan *et al.* [85], the goal of a face recognition system is to find, process and learn from a face, gathering as much information as possible. As a result, it is one of the most widely implemented biometric system solutions in light of its versatility when facing real world application [26].

All end-to-end automatic face recognition systems follow a sequential and modular¹ pipeline (Figure 5) composed of three pillar stages [113]: face detection, face alignment and face representation. First an image or frame from a video is used as an input then, as the name suggests, the **face detection** module is responsible for finding a face. Next, the **face alignment** phase applies spatial transformations to the data in order to normalize the faces’ pictures to a standardized view. Finally, the **face representation** stage, makes use of deep learning techniques to learn and further extract discriminative features that will allow the recognition *per se*. A feature is nothing more than a characteristic inherent to the input image that has been measured or processed, and presented as a result [33].

All three stages have their individual importance and methods of implementation. **Face detection** is achievable through classical approaches [108, 11] or deep methods, among them is RetinaFace [25] and MTCNN [133]. **Face alignment**, once again, can be accomplished through traditional measures [22, 69] or more modern ones, namely PropagationNet [44] or, yet again, MTCNN [133] which

¹ Sequential because each stage relies on the output from the previous ones, and modular in the sense that each stage employs its own method which can be modified or shaped to better adapt to specific tasks.

concurrently performs detection and alignment. To conclude, the **face representation** module is no exception, and can also be divided in two groups, regarding the methodology used. Some conventional systems were already mentioned, such as Eigenfaces [80, 106], and the deep learning ones are the object of discussion of this dissertation and will be reviewed along the following sections. As such, the focus will be on describing, with particular interest, the face representation stage. For a deeper and extensive study, please refer to: [128] in the case of classic face detection approaches and [74] for deep learning based methods; [115] addresses traditional face alignment methods and is complemented with [26] for more up-to-date techniques; and [57] tackles classic face representation.

2.3.1 Face Detection

Face detection is the first step in any automatic facial recognition system. Given an input image to a face detector module, it is in charge of detecting every face in the picture and returning bounding-boxes coordinates, for each one, with a certain confidence score [26, 85].

Previously employed traditional face detectors are incapable of detecting facial information when faced with challenges such as variants in image resolution, age, pose, illumination, race, occlusions or accessories (masks, glasses, makeup) [26, 85]. The progress in deep learning and increasing GPU power led Deep CNNs (DCNNs) to become a viable and reliable option that solves said problems in face detection. Methods such as CenterFace [123], MTCNN [133] or RetinaFace[25] are examples of the more commonly adopted state-of-the-art approaches.

These techniques can be included in different categories depending on the method's characteristics. A more analytical perspective [26] distributes the methods, depending upon their architecture or purpose of application, over seven categories: multi-stage, single-stage, anchor-based, anchor-free, multi-task learning, CPU real-time and, finally, problem-oriented. To an in depth review of each category, refer to the Appendix - Face Detection Classes.

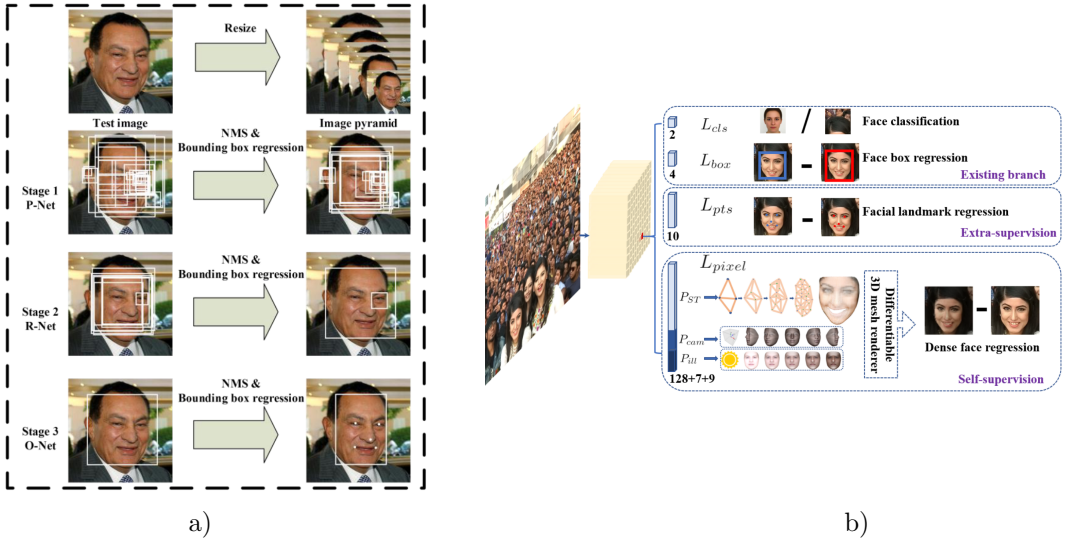


Figure 6: Comparison between **a)** MTCNN: multi-stage, CPU real-time and multi-task learning, and **b)** RetinaFace: single-stage, anchor-based, CPU real-time and multi-task learning. MTCNN [133] proposes a series of bounding boxes then, through a series of refinement stages, the best solution and landmarks are found. RetinaFace [25] accomplishes, in a single-stage, face classification and bounding box regression by evaluating anchors, landmark localization and dense 3D projection for facial correspondence.

2.3.2 Face Alignment

Face Alignment, or facial landmark detection [15], is the second stage of the face recognition pipeline, and has the objective of calibrating the detected face to a canonical layout, through landmark-based or landmark-free approaches, in order to leverage the core final stage of face representation [26].

Despite the fact that traditional face alignment methods are very accurate, that only occurs in constrained circumstances. Therefore, once again, to address that issue, deep learning-based methods are the solution to perform an accurate facial landmark localization that realistically scales to real world scenarios [31].

Furthermore, face alignment, can be accomplished through two categories of methods: landmark-based and landmark-free. Landmark-based alignment leverages facial landmarks (eyes, mouth, nose, etc.) to normalize the image to a layout

through spatial transformations [26]. Methods like Wing loss [31], Kernel Density Deep Neural Network [16] or the Recurrent Dual Refinement (RDR) proposed in [122] integrate this category. Landmark-free alignment, as the name obviously suggests, is the category of methods that align the face without points of reference, namely RDCFace [138] or the one proposed by Hayat *et al.* [36]. The Appendix - Face Alignment Classes presents more details regarding the aforementioned.

As can be seen from the previous section, this step in the face recognition process can be accomplished, very sporadically, through standalone methods that process the detected face from the previous stage, but generally joint detection and alignment methods, such as RetinaFace [25], are the optimal choice [15].

2.3.3 Face Representation

Finally, Face Representation is the last stage of the Face Recognition process. It is responsible for processing the aligned face from the previous stage and mapping the produced feature representation to a feature space, in which features from the same person are closer together and those that are different stand further apart from each other [26].

According to the literature [26, 62, 85, 92, 113], there is a consensus about how Face Recognition can be performed in two settings of operation: face verification and face identification. This distinction is only made possible due to the approaches available in the Face Representation stage that can leverage one, the other or both. Face verification, is a one-to-one, pair-wise match, and it is the action of verifying if the query face matches the identity that is being claimed. These principles are used in biometric systems such as self-service immigration clearance using E-passport [62]. Face identification, is a one-to-many correlation process that compares a query face to a database of faces and associates it to the corresponding match (or matches). A typical use case is to identify someone in a watchlist or surveillance videos [62].

The overall pipeline comes to a conclusion in this module. However, as can be seen in (Figure 5), due to its importance for the face recognition problem, it is highlighted the inherent pipeline of the Face Representation stage is discussed in depth in the next section.

2.4 Face Representation Pipeline

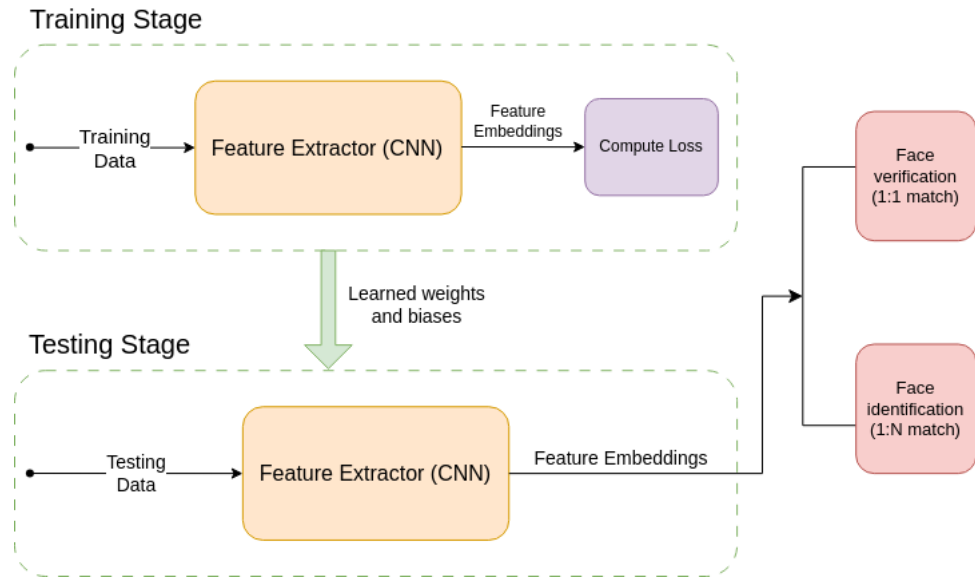


Figure 7: Face Representation pipeline, guided by the approach in [113].

As shown in (Figure 7), Face Representation is a two-step module composed of a training and testing stage. So as to be capable of performing face recognition, in either a verification or identification manner, a face representation system needs to learn robust, invariant and discriminative features that can distinguish identities [85].

To meet these requirements, the feature extractor must first be trained properly by taking data from previous stages and outputting a feature representation that is compared to the desired value using a loss function [59, 113]. After that, everything is ready for the testing stage, where the face recognition *per se* occurs

by calculating a similarity score for the feature representation produced by the trained feature extractor, and dictating if the identity belongs to the same person (face verification) or if it matches any identity (face identification) [85].

2.4.1 Datasets: Training and Testing Data

As been discussed throughout this dissertation, Deep Learning techniques can solve the problem of handling unconstrained scenarios, where there are variations in pose, illumination, occlusion, and so forth. To support this, in the past few years, datasets have been developed with this in mind so to be able to provide a large and diverse set of both training data, allowing for adequate regularization to unseen circumstances, and testing data that benchmarks the face recognition system in, as similar as possible, unconstrained real world scenarios [26].

In the following pages, a mix of training datasets, of overall relevance and more geared towards the purpose of this dissertation, will be reviewed.

Training Data

When developing a deep face recognition system it is essential to keep in mind its necessity to adapt, and that is where the dataset used for training comes at play. Large training datasets are essential for face recognition [81], but large-scale is not enough. There must be a balance between the depth (number of unique identities) and the breadth (or width) (number of images per identity) [7, 13], and it will lead to different effects. On one hand, a training dataset that is deep will help the face recognition system to produce more discriminative feature representations, since it will have a great number of identities to learn from. On the other hand, a wider set will have more images per identity, therefore, variations in pose, expressions, illuminations, occlusions, background clutter, image quality, accessories, and so forth [6] can be introduced and ultimately lead to more robust

feature representations.

Table 1: Comparison of the training datasets. ✓- Datasets that are still available to the public. ✗- Datasets that have been removed from distribution.

Dataset	Year	Availability	Images/videos	Depth	Avg. Breadth	Distribution	Description
CASIA-WebFace [126]	2014	✗	494,414/-	10,575	46.7	Public	First public face recognition dataset.
Facebook [101]	2015	✗	500M/-	10M	50	Private	<i>Facebook</i> 's private dataset used to test different properties in face identification.
Google [92]	2015	✗	200M/-	8M	25	Private	Private dataset used to train the FaceNet method.
VGGFace [81]	2015	✗	2.6M/-	2,622	991.6	Public	High width public dataset released alongside VGGFace method.
MS-Celeb-1M [35]	2016	✗	10M/-	100k	100	Public	Large-scale celebrities dataset.
MegaFace [77]	2016	✗	4,753,320/-	672,057	7.1	Public	Non-celebrity dataset.
VGGFace2 [13]	2017	✗	3.31M/-	9131	362.5	Public	High characteristics variation dataset.
UMDFaces-Videos [7]	2017	✗	-/22,075	3,107	7.1	Public	Video-based dataset with great variations.
Celeb-500k [12]	2018	✓	50M/-	500k	100	Public	Noisy celebrities dataset.
Celeb-500k-2R [12]	2018	✓	25M/-	245k	102	Public	Cleaned version.
IMDb-Face [109]	2018	✓	1.7M/-	59k	28.8	Public	Manually cleaned revision of MS-Celeb-1M and MegaFace.
MS1MV2 [23]	2019	✓	5.8M/-	85k	68.2	Public	Semi-automatic cleaned version of MS-Celeb-1M.
RMFRD [116]	2020	✓	95k/-	525	180.9	Public	Dataset of masked and unmasked celebrities.
Clint360k [4]	2021	✓	17M/-	360k	47.2	Public	Cleaned version of the Celeb-500k AND MS1MV2 datasets.
WebFace260M [143]	2021	✓	260M/-	4M	65	Public	Largest publicly available dataset of celebrities faces (noisy).
WebFace42M [143]	2021	✓	42M/-	2M	21	Public	Cleaned and smaller version.
WebFace4M [143]	2021	✓	4.2M/-	200k	21	Public	Smaller version.
DigiFace-1M [6]	2022	✓	1.22M/-	110k	11.1	Public	Large-scale, fully synthetic dataset.

Table 1 showcases large scale datasets that are the usual source of training data. Some noteworthy examples: CASIA-WebFace [126] that was the first public one of this kind; MS-Celeb-1M [35] that gathers 10 million images from 100 thousand celebrities; MS1MV2 [23], the semi-automatic cleaned version of MS-Celeb-1M; MegaFace [77], which introduces close to 5 million images from 670 thousand non-celebrity identities; WebFace260M [143] revolutionizes the dataset space with 260 million faces from 4 million identities; DigiFace-1M [6], a synthetic dataset that addresses privacy violations, lack of informed consent and exploitation of distribution licenses and vague terms (such as "celebrities") to gather data are some of the criticisms that raised enough concerns that lead to revoking the distribution of several datasets.

Testing Data

After the training is completed the performance of the system needs to be evaluated on different challenges to properly access if it scales (or generalizes) to real-world scenarios. The way of doing so is by employing test datasets, where their evaluation protocols are designed to perform pair matching, that is, face verification.

Table 2: Comparison of the test datasets. ✓ - Datasets that are still available to the public. ✗ - Datasets that have been removed from distribution.

Dataset	Year	Availability	Images/videos	Depth	Avg. Breadth	Description
LFW [42]	2007	✗	13,233/-	5,749	2.3	The most well known face verification public dataset.
YTF [120]	2011	✓	-/3,425	1595	2.1	Face verification video dataset inspired on the LFW
IJB-A [53]	2015	✗	5,712/2,085	500	11.4/4.2	Benchmark that aims at straying from accuracy saturation by proposing a more challenging dataset.
CFP [93]	2016	✗	7,000/-	500	14	Studies the effect of extreme pose variations on face verification.
CPLFW [140]	2017	✓	13,233/-	5,749	2.3	Variation of the LFW for different poses with refined verification pairs.
CALFW [141]	2017	✓	13,233/-	5,749	2.3	Same principles of CPLFW but applied to age related tests.
AgeDB [76]	2017	✓	16,488/-	568	29.0	Similar to CALFW but promotes noise free labelling by doing it manually.
IJB-B [118]	2017	✗	21,798/7,011	1,845	11.8/3.8	Improvement over the IJB-B dataset (more data and more possible pairs).
TinyFace [18]	2018	✓	15,975 (153,428)/-	5,139	3.1	Genuine low resolution face recognition benchmark.
IJB-C [70]	2018	✗	31,334/11,779	3,531	8.9/3.3	IJB-B refinement (more protocols and increased individuals diversity).
IJB-S [48]	2018	✗	5,656/350 (202)	202	28/2.7	Very challenging manually annotated benchmark.
RFW [114]	2018	✓	40,607/-	11,429	3.5	Benchmarks the racial bias of face verification methods.
QMUL-SurvFace [19]	2018	✓	463,507/-	15,573	Public	Dataset collected in uncooperative surveillance scenarios, presenting high variance of characteristics.
MDMFR [107]	2021	✓	2,896/-	226	12.8	Large scale dataset for masked face recognition.
XQLFW [54]	2021	✓	13,233/-	5,749	2.3	LFW variation to study the effect of resolution on face verification.
CAFR [139]	2022	✓	1,446,500/-	25,000	57.9	Large scale dataset to study the impact of individual's age.
FaVCI2D [82]	2022	✓	64,879/-	52,411	1.2	Face verification dataset that addresses easy pairs, demographic bias and ethical concerns.

One of the most well known test data set is LFW [42], but with the evolution of face recognition methods, it quickly became saturated in terms of accuracy reports. This motivated investigations to develop more challenging datasets, like A, B, C and S IJB benchmarks [53, 118, 70, 48], QMUL-SurvFace [19] and YTF (for video tests) [120], or for specific hurdles [26], for instance, CPLFW [140] or CFP [93] for cross-pose, CALFW [141] or AgeDB30 [76] for cross-age, RFW [48] for racial variations, XQLFW [54] for quality assessment or MDMFR [107] for masked reognition. Although some of the previously referenced datasets do have a benchmarking component and are described as such, they can also be generally employed to train or fine-tune algorithms for specific challenges.

For a better description of all the datasets see the Appendix - Train Data and Appendix - Test Data.

2.4.2 Feature Extractor

A feature extractor is present in both the training and testing stage of the Face Representation process, as it allows the visual data to be processed for evaluation by transforming the input into low dimensional representations [60]. It is also what distinguishes a Conventional Machine Learning approach from a Deep Learning one.

The following methods are all based in deep learning, therefore the *modus operandi* abides by the same principles and can be outlined as follows: 1) the feature extractor is a deep neural network, more specifically a Convolutional Neural Network (CNN), that is trained with a loss function, 2) the trained feature extractor contains prior knowledge and is applied on unseen test data and 3) the results are used to compute 1:N similarity (face identification - “who is this person?”) or 1:1 similarity (face verification - “are these persons the same?”).

Over the years, the architecture of CNNs evolved and became of great importance to all image related tasks. Other than the already mentioned revolutionary AlexNet [55], there are other designs that significantly contributed to breakthroughs and broken benchmark records. There can be general architectures, like VGGNet [95], GoogLeNet [99], ResNet [37], iResNet [28], or specialized architectures. For example, lightweight face recognition implementations such as MobileFaceNet [17], VarGFaceNet [125], MixFaceNet [10] and ConvFaceNeXt [39].

→ **VGGNet** [95] took inspiration from AlexNet and improved its accuracy in image classification by studying the effect of the network’s depth. It accomplished that by substituting the 11x11 convolution kernel with stride 4 for a stack of very small 3x3 receptive field with stride 1. The final best performing model was 19 layers deep (16 convolutional and 3 fully-connected) and had 144 million parameters.

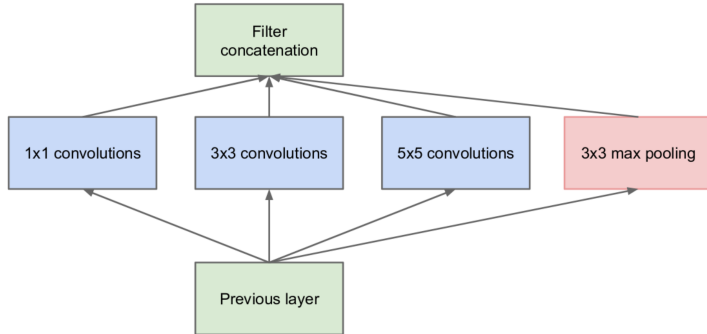


Figure 8: GoogLeNet’s inception block from the original paper [99].

→ **GoogLeNet** [99], also known as Inception-V1, aimed at reducing the computational cost associated with training and employing a network, while retaining highly accurate results. That was accomplished by introducing sparse connectivity (not all feature maps are shared with the forward layers), an inception block Figure 8, consisting of multi-scale convolutional layers with small blocks of different sized kernels (1×1 , 3×3 and 5×5), and replacing the last fully connected layer with a global averaging pooling one and adding a dimension lowering bottleneck layer of 1×1 convolution before large kernels. These changes helped to achieve a low number of 4 million parameters (12x fewer than the revolutionary AlexNet and 36x less than VGGNet)

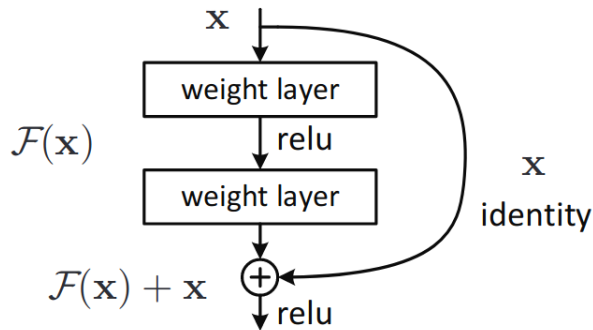


Figure 9: ResNet’s residual block from the original paper [37].

→ **ResNet** [37] is one of the most resourced architecture of feature extractors when applied to face recognition and its main objective is to efficiently train deep neural networks. By reformulating the layers as residual learning functions, it supports deeper architectures while being easier to optimize while improving performance. It also solves the accuracy degradation and the vanishing gradient problems verified when the depth of the network is increased. The main contribution is the introduction of the residual block (Figure 9). It consists of convolutional layers, followed by element-wise addition between the output and the input of the block. This addition performs an identity mapping by creating a direct “shortcut connection” that skips the input directly to the output, allowing the network to learn the difference between the input and the output, i.e., the residual. Enabling the flow of information from earlier layers directly to later layers, facilitates the gradient flow during training and makes it easier for the network to learn. Depending on the depth, there are different variations of the ResNet architecture: ResNet-18 (11.7 million parameters), ResNet-34 (21.8 million parameters), ResNet-50 (25.6 million parameters), ResNet-101(44.6 million parameters), ResNet-152 (60.2 million parameters).

→ **iResNet** [28] further improves the ResNet architecture. It proposes separating the network into stages, providing a better path of information flow through the network’s layers. Also, it introduces an enhanced version of the residual learning block with 4 times more spatial channels that focuses on the spatial convolution, and an improved projection shortcut (used when the dimensions of the previous blocks does not match the ones of the next) that includes an additional 3x3 max pooling. A major advantage is that all the improvements above do not increase the original model’s parameters and, consequently, overall complexity.

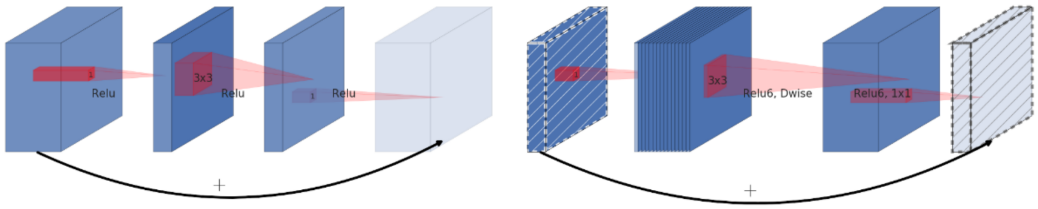


Figure 10: Comparison between ResNet’s residual block (left) [17] with the inverted residual block proposed by MobileNetV2 (right) [89] and used by MobileFaceNet. Image taken from MovileNetV2’s paper [89].

→ **MobileFaceNet** [17] is a set of face verification CNN models designed to perform in real time and with high accuracy on mobile and embedded devices. It is built upon the inverted residual bottlenecks (Figure 10) proposed in the general architecture lightweight CNN MobileNetV2 [89] that have the purpose of reducing the number of parameters of the network. The general residual bottleneck block [37] is composed of an input, followed by bottlenecks to reduce dimension and finished with an expansion to restore it, and the shortcut connects the high dimension layers. On the other hand, in the inverted residual architecture, it is considered that the information is stored in the bottleneck layers and the expansion is a mere implementation detail, therefore, a shortcut is placed directly between the bottlenecks. To solve the accuracy problem of face recognition CNNs that have a global average pooling layer, MobileFaceNets replaces it by a global depthwise convolution layer with kernel of size $7 \times 7 \times 1280$ followed by a 1×1 convolution as the feature output layer. The primary MobileFaceNet architecture has 0.99 million parameters, but there is also the MobileFaceNet-M (the final 1×1 convolution is removed) and the MobileFaceNet-S (the 1×1 linear convolution before the global depthwise convolution is also removed).

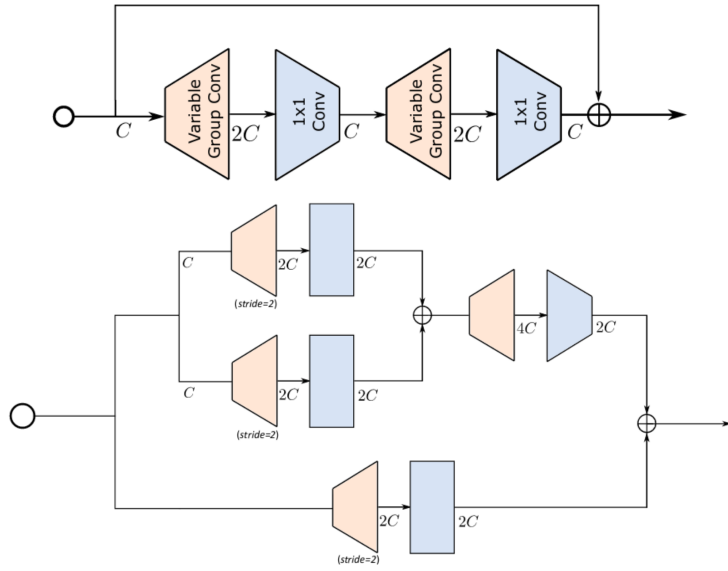


Figure 11: VargNet’s normal block (top) and downsampling block (bottom) [134] used by VargFaceNet. Image from VargNet’s paper [134].

→ **VarGFaceNet** [125] is a lightweight face recognition CNN implementation based on the VarGNet architecture [134] [17] that introduced a variable group convolution to solve unbalance of computational intensity due to hardware and compilers optimization. VarGFaceNet will use the normal and downsampling blocks from the VarGNet CNN (Figure 11), but will add a Squeeze and Excitation (SE) block [40] and replace the usual ReLU activation function by the PReLU [38] one, since it is better for face recognition tasks. Other than that, the head setting is also changed without losing discriminative ability. The network is started with a 3×3 convolution with stride 1 that preserves the input size, instead of the down-sampling 3×3 one with stride 2 from VarGNet. Finally, the embedding setting is also modified by performing variable group convolution and pointwise convolution to shrink the feature map to a 512-dimensional feature vector that is fed to the fully connected layer. In conclusion, the VarGFaceNet network is capable of performing accurate face recognition while maintaining a low amount of 5 million parameters.

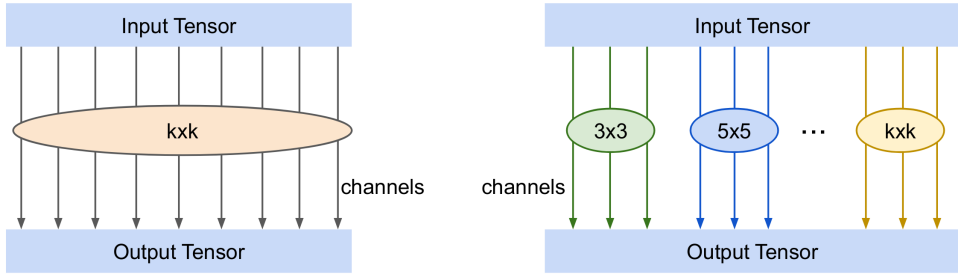


Figure 12: A normal convolution block that uses a single kernel (left) and the Mixed Depthwise Convolution proposed by MixNet [102].

→ **MixFaceNet** [10] is a lightweight implementation of MixNet [102] tailored for face verification. MixNet introduced Mixed Depthwise Convolution Kernels (Figure 12) that extends the theory behind depthwise convolution, but employs multiple kernel sizes in a single convolution, promoting the capturing of different patterns from distinct resolutions while reducing the number of parameters needed. The main differences proposed by the MixFaceNet design compared to MixNet resides in the head and embedding settings. For the network head set-up, fast downsampling in the first convolution layer with a 3×3 kernel and stride of 2, and PReLU [38] activation function are used. Regarding the embedding settings, the global average pooling layer used by the MixNet architecture is replaced by a global depthwise convolution, in the same manner as the previously described MobileFaceNet.

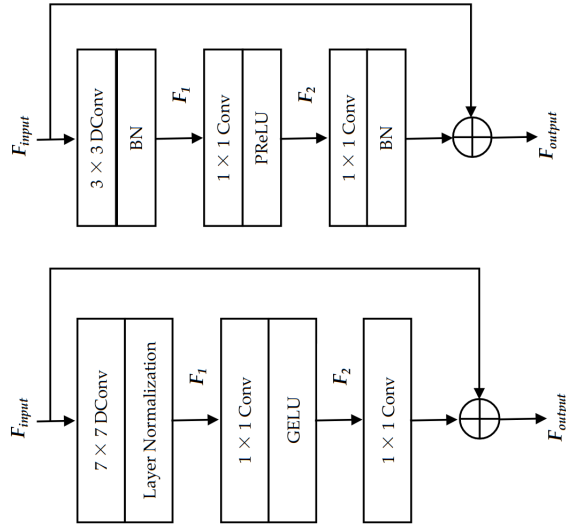


Figure 13: Convolutional block proposed by ConvNeXt [68] (top) and the one by ConvFaceNeXt [39] (bottom). Image from the ConvFaceNeXt work [39].

→ **ConvFaceNeXt** [39] is a family of lightweight face recognition models, based on the ConvNeXt [68] and MobileFaceNet architectures (Figure 13). The original ConvNeXt block is modified to better adapt to face recognition tasks and optimized to reduce the number of parameters. Accordingly, the Enhanced ConvNext (ECN) block is designed by adopting a smaller 3x3 kernel during the depthwise convolution, instead of the original 7x7 one. Adopting the principles studied in the MobileFaceNets implementation, rather than the usual layer of normalization and GeLU in the ConvNeXt model, batch normalization and PReLU [38] are employed.

2.4.3 Loss

The initial face recognition proposals inherited principles from successful object classification implementations, henceforth, the most common loss function utilized was the well-known softmax loss. Unfortunately, it soon proved to be inefficient for face recognition applications since intra-variations (age gap between pictures of the same identity, for example) can be larger than inter-ones (Figure 14). Thus, the investigation interest shifted towards developing loss functions that had a better

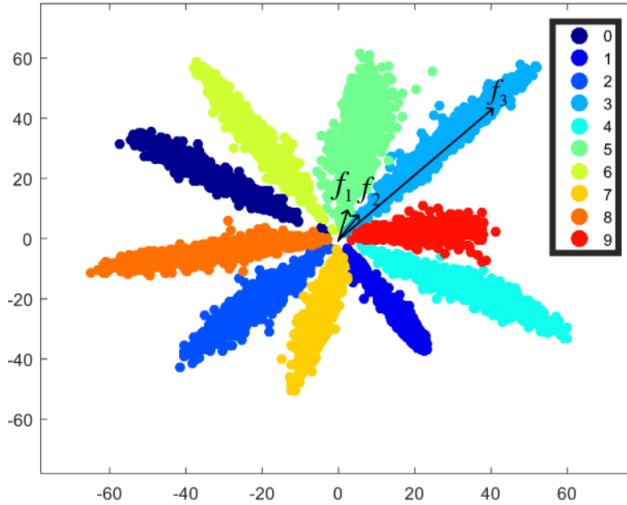


Figure 14: Intra- and Inter-class challenge [111]. Eventhough features f_2 and f_3 belong to the same class, the euclidean distance between f_1 and f_2 is much smaller, proving the ineffectiveness of the softmax loss regarding inter-class compactness and inter-class separateness.

generalization ability and promoted more separable (to distinguish between an identity) and discriminative (to distinguish between identities) features [113].

Face recognition can be achieved using either metric learning loss functions that learn a feature embedding to compute similarity or softmax-based loss functions that treat the problem as a classification task. Some works merge the two concepts.

Classification-based loss functions

Classification-based loss functions, derived from the general object classification task, aim at learn an N-way classification of all the classes, where each class relates to an identity composed of several faces [26].

Because the methods are classification-based, the pioneers such as DeepFace or DeepID [98], utilized the most widely implemented loss function for classification, i.e. the softmax loss. It consists of a fully connected layer, the softmax function

and cross-entropy loss, and can be formulated as follows:

$$\mathcal{L} = -\frac{1}{N} \sum_{i=1}^N \log \frac{e^{W_{y_i}^T x_i + b_{y_i}}}{\sum_{j=1}^c e^{W_j^T x_i + b_j}}, \quad (2.4)$$

where N is the number of images, c is the number of identities, y_i is the x_i 's ground-truth label, W_{y_i} is the ground-truth weight from x_i in the fully connected layer and b_j is a bias term. The term inside the logarithm represents the probability on the ground-truth class and the training objective is to maximize this probability.

Taking the aforementioned principles and the drawbacks of lackluster generalization, and separable/discriminative abilities, the following loss functions proposed improving the softmax loss to better serve face recognition tasks.

→ **NormFace** [111] improves the classic softmax loss by studying the effect of L_2 normalization to the features and weights during the training stage. Because introducing this constraint resulted in the network not converging, a scale factor is also adopted that resizes the cosine similarity's scale between features and weights. This normalized softmax loss function can be reformulated as

$$\mathcal{L}_{norm} = -\frac{1}{N} \sum_{i=1}^N \log \frac{e^{s \cos(\theta_{y_i})}}{e^{s \cos(\theta_{y_i})} + \sum_{j=1, j \neq y_i}^c s \cos(\theta_j)}, \quad (2.5)$$

where s is the scale parameter and $\cos(\theta_j)$ results from the inner product between the L_2 normalized weights W_j and features x_i , i.e., $\cos(\theta_j) = \frac{\langle x_i, W_j \rangle}{\|W_j\|_2 \|x_i\|_2}$

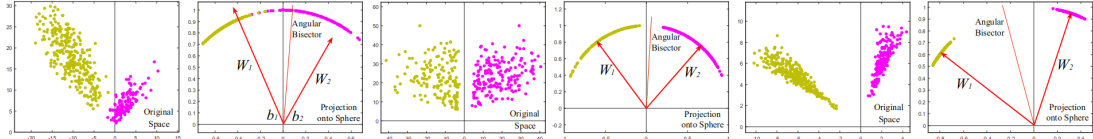


Figure 15: Comparison between the classic softmax loss, modified softmax loss (NormFace) [111] and SphereFace [66].

→ **SphereFace** [66] improved the intra-class compactness and inter-class distance by introducing a very important concept of angular margin that contrasts with

the usual Euclidean margin. As proven by Liu *et al.*, features learned by softmax loss adopt an intrinsic angular distribution, therefore, euclidean margins are not compatible with softmax loss (Figure 15). The decision boundary for a classic softmax loss function is $(W_1 - W_2)x + b_1 - b_2 = 0$, and by normalizing the weights and zeroing the bias, it becomes $\|x\|(\cos(\theta_1) - \cos(\theta_2)) = 0$, where x is a feature vector and the decision will only depend on the angles between class 1 and 2. SphereFace introduces the hyperparameter m ($m \geq 1 \in \mathbb{Z}$) that will, effectively, control the margin size between class 1 and 2 respectively as such $\|x\|(\cos(m\theta_1) - \cos(\theta_2)) = 0$ and $\|x\|(\cos(\theta_1) - \cos(m\theta_2)) = 0$.

→ **AM-Softmax** and **CosFace** both improved SphereFace’s main problem: the potential unstable training convergence due to the multiplicative angular margin. Thus, an additive cosine margin $\cos\theta_{y_i} + m$ is proposed to facilitate the convergence.

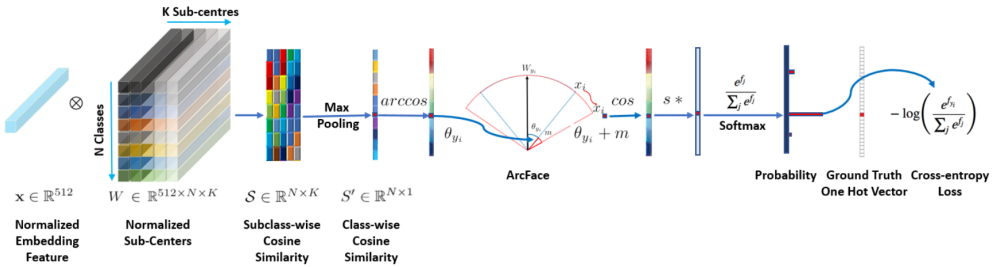


Figure 16: ArcFace training process as described in the original paper [23].

→ **ArcFace** [23] aims at optimizing the geodesic distance margin since there is a mathematical correspondence between the angle and the arc in the normalized hypersphere. The concept behind this is described in (Figure 16). First, the cosine distance among features is obtained by the dot product between the feature produced by the CNN and the fully connected layer. After that, the arc-cosine is used to calculate the angle between the feature and the target one. Finally, the authors took the principles from AM-softmax [110] and SphereFace [66], and introduced an additive angular margin directly to the angle $\cos(\theta_{y_i} + m)$, getting

the target logit back by the cosine function and further stabilizing the training process and improving the discriminative power of the overall system. The loss function is reformulated by: 1) zeroing the bias and transforming the softmax loss logit $W_j^T x_i = \|W_j\| \|x_i\| \cos(\theta_j)$, as suggested in [66], where θ_j is the angle between the weight W_j and the feature x_i , 2) following [111, 66, 112] the weights are normalized by L_2 , 3) the features x are also normalized in L_2 per [84, 111, 110, 112] suggestion. This normalization insures that there is only an angular dependence between weights and features, and the learned features are distributed along a hypersphere with radius s . To conclude, ArcFace can be described as follows:

$$\mathcal{L} = -\log \left(\frac{e^{s(\cos(\theta_{y_i} + m))}}{e^{s(\cos(\theta_{y_i} + m))} + \sum_{j=1, j \neq y_i}^N e^{s \cos(\theta_j)}} \right), \quad (2.6)$$

where m is the employed additive angular margin penalty between the feature x_i and the ground truth center W_{y_i} to promote the intra-class compactness and inter-class distance (Figure 17).

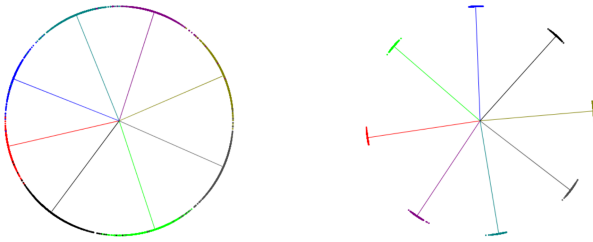


Figure 17: Demonstration of the intra-class compactness and inter-class distance of ArcFace (right) compared to Norm-Softmax (left) for 8 identities. The distance margin between classes is clear for ArcFace. Image from ArcFace’s paper [23].

To this day, ArcFace is still the state-of-the-art regarding face recognition, and one of the most implemented loss functions of this category, and it is usual to see other novel losses to use it as a starting point. The accuracy saturation of more common benchmarks like LFW [42] lead to the appearance of harder ones, which will lead to loss functions aimed at more specific challenges, namely CurricularFace [45], MagFace [73], AdaFace [51] or QMagFace [104].

Metric learning loss functions

Metric learning loss functions include the methods that aim optimizing the distance between feature embeddings. That is, increase the distance between negative embeddings and minimize the distance for those that are positive.

One classic example is the contrastive loss, but this category's attention mainly pends over the triplet loss first implemented by Schroff *et al.* in FaceNet [92].

→ **Contrastive Loss** [26] has the objective of optimizing the distance between identity pairs: positive pairs are encouraged to be closer and negative ones to be further apart. The loss function to be minimized is

$$\mathcal{L}_{contrastive} = \begin{cases} \frac{1}{2} \|f(x_i) - f(x_j)\|_2^2, & \text{if } y_i = y_j \\ \frac{1}{2} \max(0, m_d - \|f(x_i) - f(x_j)\|_2^2), & \text{if } y_i \neq y_j \end{cases} \quad (2.7)$$

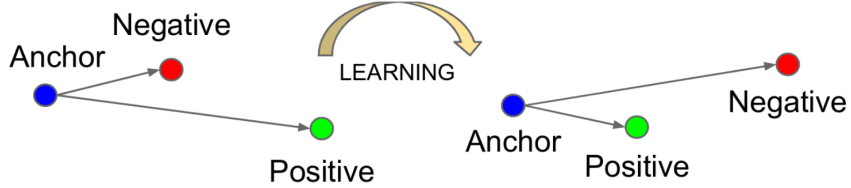


Figure 18: Representation of training using triplet loss. Image from Facenet's paper [92].

→ **Triplet Loss (2014)** [92] embeds an image to a d-dimensional feature vector in an Euclidean space. The motivation is to guarantee that, for every individual i , the squared distance between an image x_i^a (anchor) of an identity and its corresponding true identities x_i^p (positive) is smaller than the distance between non-identities, x_i^n (negative). This structure is called a triplet (Figure 18). The aforesaid can be described in mathematical terms as:

$$\|f(x_i^a) - f(x_i^p)\|_2^2 + \alpha < \|f(x_i^a) - f(x_i^n)\|_2^2, \quad (2.8)$$

where $f(\cdot)$ are the feature embeddings from all the possible triplets, and α is a margin between positive and negative pairs. Therefore, the loss function to be

optimized is:

$$\mathcal{L}_{triplet} = \sum_i^N [\|f(x_i^a) - f(x_i^p)\|_2^2 - \|f(x_i^a) - f(x_i^n)\|_2^2 + \alpha] \quad (2.9)$$

However, there is a major drawback associated with this methodology. The selection of the triplets has a significant impact on the results and there is a combinatorial explosion regarding the number of possible triplets, specially for large-scale datasets, leading to a slower convergence and computational overhead if all the possible triplets are to be used. The only way to address this problem is through the development of efficient mining strategies that select both hard and representative triplets.

2.5 Related work

The development of solutions for student monitoring, specially image-based, has encompassed a plethora of possibilities that can face several challenges, specially not being capable of controlling the capturing conditions or the computational power of the device where the system is executed. Depending on the application, they can be intended for commercial purposes or developed as part of academic research. Commercial solutions such as Kryterion, ProctorExam, ProctorU, Proctororio, ProctorFree, or SMOWL [83] are available; however, with the exception of SMOWL, due to their proprietary nature, their methods of implementation are not disclosed, not allowing to study them adequately. Therefore, all the methods analyzed, except SMOWL, will fall under the second category.

→ **Zhang et al. [136] (2016)** studied a system based on facial features exclusively. The faces are first detected and extracted using the OpenCV pretrained classifier based on the Viola-Jones/Haar Cascades algorithm. Subsequently, recognition is carried out utilizing the Eigenfaces algorithm, which incorporates Principal Component Analysis (PCA). The main disadvantage of this solution is lacking

the flexibility to adverse visual conditions that Deep Learning techniques have.

→ **Atoum *et al.* [5] (2017)** proposed a solution that employs Viola-Jones/Haar Cascades face detector and Minimum Average Correlation Energy (MACE) filter for face verification. Once again, the methodologies utilized are too sensitive to image variations, such as illumination, pose, expressions, etc.

→ **Zhang *et al.* [137] (2018)** latter proposed another solution. In a similar fashion to Zhang *et al.* [136] and Atoum *et al.* [5], the face detection is achieved through the same OpenCV pretrained module. On the other hand, the detected and cropped faces are now processed by a modification of the Stereo Matching algorithm. Because this method extracts information from pairs of stereo images, it is subject to occlusions, ambiguities, textures, etc.

→ **Sawhney *et al.* [90] (2019)** introduced an approach where the face detection is accomplished in two stages: 1) bounding box regression with the Viola-Jones/Haar Cascades algorithm and 2) facial landmark generation with a Local Model-based algorithm. After the faces are extracted, the face recognition stage, in similarity with Zhang *et al.* [136], applies simultaneously Eigenfaces with PCA, therefore, the drawbacks coincide.

→ **Ganidisastra and Bandung [32] (2021)** introduced a Deep Learning-based approach that employs two models for face detection and recognition: YOLO-face for face detection and Facenet for face recognition. Notably, Facenet is continuously trained with data collected at the end of each user session. This training process causes the system to overfit to each individual identity, leading to reduced adaptability in handling new scenarios due to limited data availability. Furthermore, the training of Facenet utilizes the triplet loss, which can be computationally challenging, especially on less powerful hardware. This is primarily due to the exponential increase in possible combinations when mining triplets during the

training process.

→ **SMOWL [56] (2021)** is a multi-modal tool that analyzes voice, face and key-strokes data. For this dissertation, the interest resides only on the facial aspect of it. For face detection, it utilizes a combination of FaceBoxes with MobileNet-SSD for occlusion detection. The face recognition is accomplished with a Facenet model trained with triplet loss on the MS-Celeb-1M dataset. Anew, the triplet loss training can be considered a drawback.

→ **TrustID [29] (2023)** is our solution, designed and developed at ISR - UC. It utilizes as a face detection a linear detector conjointly with a Histogram of Oriented Gradients and pyramidal image search. After the faces are detected and aligned, they are cropped to a Region of Interest (RoI) of 150×150 pixels. Finally, the faces are passed to a face recognition module that uses a CNN with 29 layers based on the ResNet-34, trained with triplet loss on a dataset of, approximately, 3 million faces derived from the Visual Geometry Group Face [81] and FaceScrub [79] datasets.

The primary focus of this work revolves around the selection of the architecture for the face recognition module, which, as previously mentioned, will exclusively center on image-based Deep Learning approaches. In pursuit of this goal, the monitoring system must proactively address potential, previously mentioned, challenges that may arise during data acquisition. Deep Learning methods have shown remarkable capabilities in tackling such challenges effectively.

In particular, the face recognition module must exhibit robustness in handling variations in illumination, pose, and image quality, especially in scenarios where precise control over these factors is unattainable. Furthermore, we need to consider the computational resources available to users, as students may access the system using smartphones or less powerful computing devices. Consequently, our choice of framework must be resilient to these variations and resource constraints.

Chapter 3

Methodology

From the previously described systems in Section 2.5, two methods must be picked: one for face detection and one for face representation (that include the feature extracting backbone neural network and the loss function necessary for training¹). The next sections describe these choices and the reasons behind them, as well as the implementation and necessary steps.

3.1 Face detection

Following the proposed pipeline for a Face Recognition system, the initial design choice pertains to the Face Detection module, responsible for detecting, selecting and standardizing the faces. A comprehensive study of solutions was presented in Section 2.3.1, wherein RetinaFace emerged as the best overall solution for a student monitoring context for the following, therefore, it will be method used in this work. This approach accepts an image as input and produces multiple outputs, including a bounding box, five key facial landmarks (representing the center of the eyes, nose, and corners of the mouth), and a confidence score that reflects the likelihood of the detection accurately identifying a face. The selection of this method

¹ As this dissertation specifically focuses on the face recognition domain, the loss function pertains exclusively to the training of that stage.

was predominantly influenced by three critical factors: 1) adaptability to changes in light, pose, facial expressions, etc., facilitated by the DCNN backbone, 2) incorporation of a single-stage approach and leveraging multi-task learning, enabling efficient real-time detection of facial landmarks using just a single CPU core (for VGA resolution), and 3) availability of readily implemented solutions with ample support.

The solution of choice is a Pytorch implementation² of the original method that offers both a MobileNet-0.25 or ResNet-50 as backbones pre-trained on ImageNet. To better suit our application, further development over the original implementation was required. RetinaFace is distributed as a general face detection algorithm that is deployed on data with multiple faces to be handled, therefore, there is no built-in method for face selection or transformations, like alignment and resizing. However, on a student’s monitoring scenario, only one face is relevant, and as consequence of that, the face recognition systems are to be trained and validated on single face pictures normalized to a canonical view.

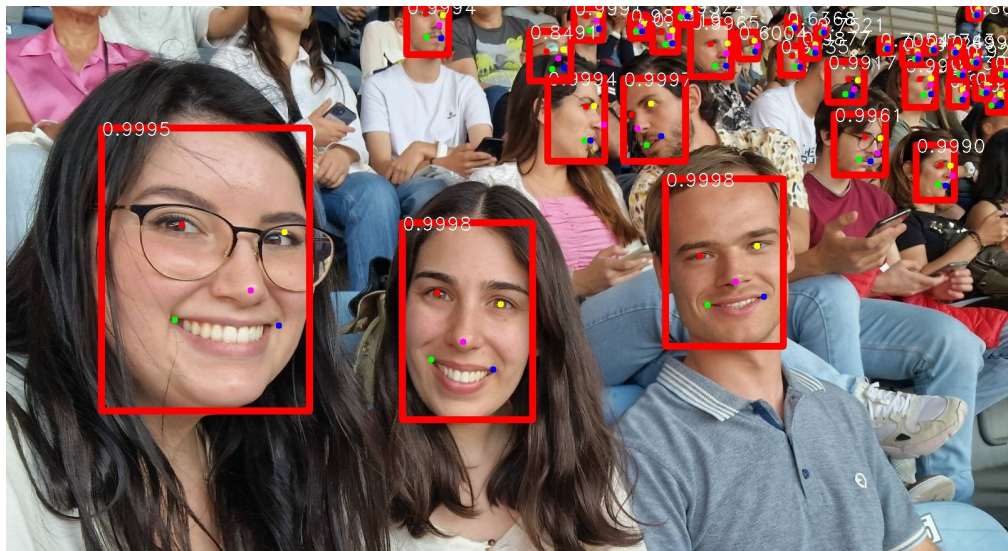


Figure 19: Results produced by the RetinaFace method over a test photo. Represented are the bounding boxes, respective confidence scores and the five facial landmarks.

² https://github.com/biubug6/Pytorch_Retinaface

Instantiating the model with default threshold parameters and Resnet-50 as the backbone, it produces the results seen in (Figure 19). From all the bounding boxes available, one must be picked, and one way of doing so is by assuming that the more relevant face is closer to the camera, hence the area of its bounding box will be greater.

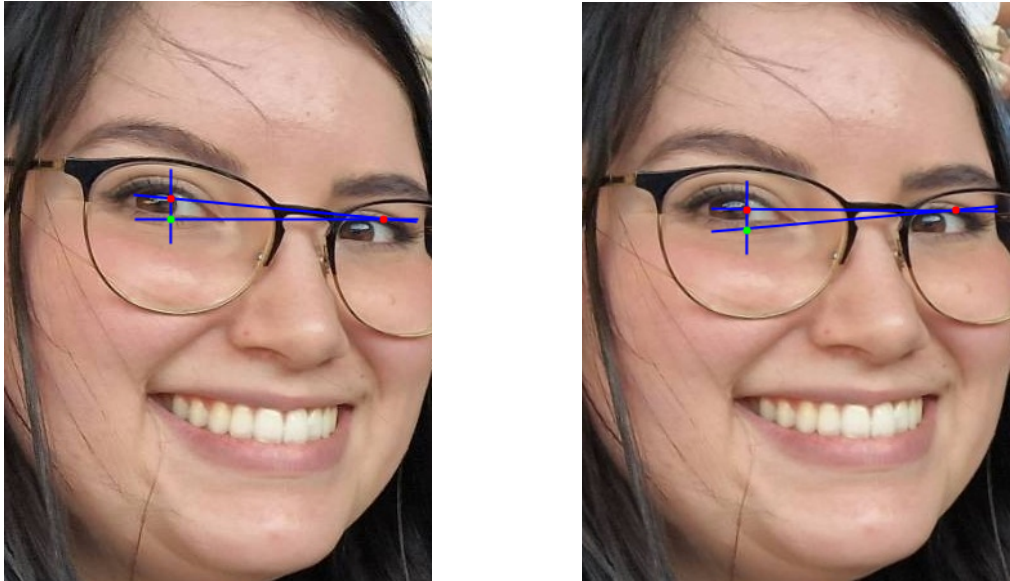


Figure 20: Landmark based alignment. The green dot serves as an auxiliary point, resulting from the intersection of a horizontal line originating at the pivot eye and a vertical line projected from the other eye. Subsequently, the rotation angle is determined by computing the arctangent of two distances: the distance between the higher eye and the auxiliary point, and the distance from the auxiliary point to the pivot eye.

The alignment is done with the help of the eyes landmarks as seen in (Figure 20). The eye lower relative to the other is declared as the pivot and starting point of a horizontal line that acts as the reference to calculate the angle of rotation. Following the selection, cropping, and alignment of the face, it is resized to fit the required dimensions for the subsequent phase.

3.2 Face Representation

The Face Representation stage addresses handling the features of each face and includes a feature extractor and a loss function. Following the review on related works in Section 2.5 Ganidisastra and Bandung [32] and SMOWL [56] both utilize Facenet trained with triplet loss for face recognition. This naturally prompts an investigation into the potential effects on performance when utilizing a more modern network (ResNet variations), as well as a lightweight network with fewer parameters (MobileFaceNet). Furthermore, considering the drawbacks associated with triplet loss training, examining the impact of a well-established loss function, like ArcFace would also be noteworthy, as it encourages intra-class compactness and inter-class distance. Due to time constraints, the methods of choice are all pretrained and subsequently fine-tuned on datasets appropriate to the model’s scenario deployment.

3.2.1 FaceNet

For this method, we utilize a highly regarded PyTorch implementation³ that offers pretrained models in either the CASIA-WebFace or VGGFace2 dataset. The images’ faces are cropped and aligned (but not rotated) using MTCNN, and resized to $160 \times 160 \times 3$. However, this implementation has differences compared to the Facenet described in the original paper [92]. Firstly, differing from the original adopted GoogLeNet-style Inception model, the backbone network employed here is the Inception Resnet V1, which integrates residual blocks into the Inception architecture. As highlighted in Section 2.4.2, this modification streamlines the training process by addressing issues such as accuracy degradation and gradient vanishing. Secondly, adhering to the recommendations by Parkhi *et al.* [81], the network was trained as a classifier using softmax loss, departing from the original’s triplet loss metric learning approach. Finally, the method’s output is a

³ <https://github.com/timesler/facenet-pytorch>

512-dimensional embedding, differing from the 128-dimensional output reported in the original paper.

3.2.2 ResNet

The choices for this architecture were designed to cover a range of neural network depth, complexity and trainable parameters. Henceforth, there are 3 objects of study, ranging from less to deeper ones: iResnet-18⁴, a 29 layer version of Resnet-34⁵ (used in the TrustID project) and iResnet-50 (with Squeeze and Excitation blocks)⁶. Both the iResnet-18 and iResnet-50 were trained on $112 \times 112 \times 3$ faces from the MS1MV2 dataset, using ArcFace as the loss function, and output 512-dimensional feature embeddings. Regarding the Resnet-34, it was trained with triplet loss on a custom dataset comprised of 3 million $150 \times 150 \times 3$ images from the Visual Geometry Group Face [81] and FaceScrub [79], and outputs a 128-dimensional feature embedding.

3.2.3 MobileFaceNet

MobileFaceNet⁶ is a lightscale approach to face recognition that will further aid the study of the computational cost and model's performance trade-off. Since is made available by the same author as the iResnet-50, it has technical similarities. Once again, it is trained with ArcFace loss on $112 \times 112 \times 3$ images from the MS1MV2 dataset and outputs the usual 512-dimensional embedding.

3.3 Finetuning data

Considering that the intended application of the face recognition systems is to monitor students, it is not unreasonable to assume that, due to the nature of the

⁴ <https://github.com/deepinsight/insightface>

⁵ http://dlib.net/face_recognition.py.html

⁶ https://github.com/TreB1eN/InsightFace_Pytorch

capture device (webcam or smartphone) or its positioning, that will be reflected on the quality of the data. For instance, one potential scenario involves a student with one monitor and a laptop placed to the side of it, accompanied by a lamp on the opposite side. This will configuration will result in face captures with very different resolutions, poses and lightning compared to another student using a laptop, in a well lit room, facing the subject.



Figure 21: Different face capturing scenarios. The top row corresponds to 1280×720 files captured by a webcam, while the bottom row are 2309×3072 pictures from a smartphone’s front facing camera.

As can be seen in (Figure 21), for faces captured in the same exact scenarios and conditions there is a huge discrepancy between the webcam and smartphone pictures, ranging from resolution, detail, color and hue, and illumination. Therefore, it is crucial to have a robust system that is capable of being insensitive to these variations, hence the possible need to finetune pretrained models for that. In this regard, we will examine two distinct datasets: DigiFace-1M and QMUL-SurvFace.

Amidst the controversies surrounding the methods of data acquisition for some publicly distributed datasets, including MS-Celeb-1M, MegaFace, FaceScrub, IJB-C or VGGFace, Bae *et al.* developed DigiFace-1M [6] with those concerns in mind. This fully synthetic dataset emulates different scenarios with variant poses,

light, expression and accessories (hats, masks, makeup, etc.), and it serves as an interesting object of study of the potential of this type of datasets to diminish the reliance over real face data to finetune a model for more adverse scenarios.

The second dataset used to finetune our models of choice is QMUL-SurvFace [19] by Cheng *et al.*. Initially described as a benchmarking dataset, its unconstrained way of capturing resulted on faces with very high variance in resolution, capturing angles, poses, light or accessories, poses as a perfect source to further adapt the models to said scenarios. Another noteworthy benefit of this dataset is that the images were collected with the consent of the individuals, meaning that ethical and privacy dilemmas are not at play.

3.4 Benchmarks

The evaluation will be conducted with 10-fold cross validation on the processed dataset to match the size of the training data for each model. First with the original pretrained model and then with the fine-tuned version of the selected one. The model will produce the feature embeddings and pairwise cosine similarity, and if it is above a certain threshold the pair is considered as a match.

To comprehensively assess the performance of the chosen models, we will subject them to testing across eight diverse datasets: VGGFace2, AgeDB30, two CFP variations (CFP-FF for frontal-frontal pairs and CFP-FP for frontal-profile pairs), CALFW, CPLFW, XQLFW and LFW. This approach is designed to capture a wide array of characteristics, closely resembling real-world scenarios for a thorough evaluation, therefore, four dataset groups Table 3 based on their characteristics are defined: frontal, age, pose and hard.

Table 3: Benchmarks' groups, their difficulty and intended evaluation purpose. * - Very easy.
***** - Very difficult.

	Dataset	Difficulty	Evaluation purpose
Frontal	CFP-FF	***	Frontal view performance.
	LFW	*	
Age	AgeDB30	***	Sensitivity to age variations.
	CALFW	***	
Pose	CFP-FP	****	Performance for a range of poses.
	CPLFW	***	
Hard	VGGFace2	*****	Great variation in pose, age, illumination, etc.
	XQLFW	*****	Performance for very low image quality.

The chosen evaluation metrics are based on biometric systems of verification and encompass Accuracy, the Receiver Operating Characteristic (ROC) and Detection Error Trade-off (DET) plots obtained by sweeping an interval of thresholds and calculating the True Acceptance Rate (TAR), False Acceptance Rate (FAR) and the False Reject Rate (FRR), and the Equal Error Rate (EER). The $Accuracy = \frac{TP+TN}{TP+TN+FP+FN}$ is a measure for the number of correct predictions, $TAR = \frac{TP}{TP+FN}$ indicates the proportion of genuine face pairs correctly classified and $FAR = \frac{FP}{FP+TN}$ indicates the quantity of imposter face pairs incorrectly classified as matches, where TP is True Positive, TN is True Negative, FP is False Positive and FN is False Negative. With the previous metrics is possible to obtain the ROC plot and study the trade-off between the TAR and FAR at different thresholds and evaluate the performance of different models (Figure 22). $FRR = 1 - TAR$ calculates the ratio of genuine matches that are classified as a non-match and allows to generate the DET curve which serves a similar purpose to the ROC curves, but with a better performance visualization due to the axis' logarithmic scale. Finally, the EER is the point where $FRR = FAR$ and the lower it is, the better performing the system is.

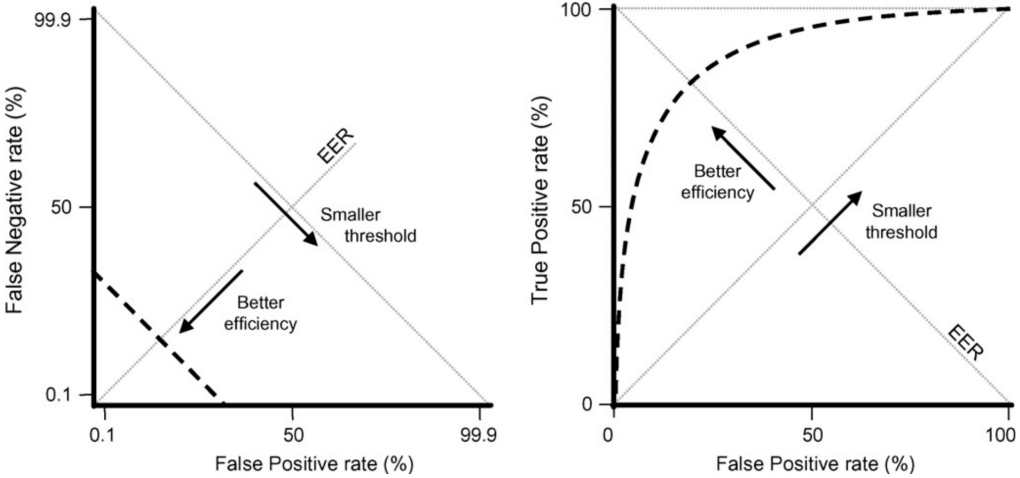


Figure 22: DET (left) and ROC (right) curves. The y-axis represents the True Positive Rate (or TAR) for the ROC curves and False Negative Rate (or FRR) for the DET curves. The x-axis represents the False Positive Rate (or FAR) for both plots. Image from [88]

(Figure 22) highlights the performance visualization for both the curves' plots. The closer the ROC curve is to the top left corner, the better performance the model has, since that means that it is able of correctly identify more genuine face matches (TAR) while minimizing the wrong identities incorrectly classified as matches (FAR). For DET, a curve closer to the origin represents a better model, since it minimizes the amount of genuine identities matches classified wrongly classified as imposters (FRR) for a more strict FAR threshold.

3.5 Implementation details

All the training, processing, and benchmarking was developed in a Docker environment to ensure reproducibility. The code was written using Python 3.8.10 and relies on PyTorch 1.14.0 and Torchvision 0.15.0, along with their corresponding required libraries. The training process is conducted exclusively on a single GPU, specifically NVIDIA's GeForce RTX 3080 Ti 12GB.

Regarding the implementation, all development was done with modularity in

mind. First, the data is processed with the customized RetinaFace detection and alignment algorithm and saved. Then, it is proceeded forward to the neural network that produces a feature embedding for each image. If the model is being trained, the embedding will be passed on to the ArcFace module, which will output the feature’s logits. Following the the original paper [23], the logits are turned to probabilities by applying the softmax activation function and then contributing to the final step, i.e, the cross entropy loss. Because ArcFace is a separate structure that does not integrate the backbone networks as a custom layer, the neural networks can be quickly and easily changed.

3.6 Discussion

Considering the possible challenging scenarios described allied to the incapability of guaranteeing robust computational power or quality capture devices, due to the image-based student monitoring application, it prompts a selection of the methods of face detection, recognition methods and training datasets with that in mind.

RetinaFace’s backbone DCNN assures adaptability to image variations resulting from the capture device, and its multi-task, real-time and single CPU core data processing eliminates the need for powerful execution machines. After being processed by the customized RetinaFace implementation, the datasets (QMUL-SurvFace and DigiFace-1M) will serve as a fine-tuning source. Their increased depth, width and varied image characteristics (accessories, illumination, poses, quality, etc.) constitute a theoretical robust source of diverse information to improve a model. Finally, Section 2.5 highlighted FaceNet, iResnet-18, iResnet-SE-50 and MobileFaceNet as possible substitutes to TrustID’s face recognition method. Since they are all deep learning approaches, they all have an inherent flexibility to adapt to information, but the data where they were trained has great influence on their performance. Regarding the computational power, these methods

also differ in the overhead they generate, wherein iResnet-SE-50 is the heaviest and MobileFaceNet is the lightest. Hence, because they are trained on different datasets and have different complexity, each one must be benchmarked in order to pick the model to be fine-tuned that shows a better performance/resource utilization trade-off. Furthermore, it's important to acknowledge that achieving perfect accuracy may not be an absolute requirement. This is because the monitoring process involves face verifications occurring over an extended period, during which a large quantity of verifications can compensate for lower accuracy values.

Chapter 4

Results

The main purpose of the following chapter is to select a better approach to TrustID’s facial recognition solution that encapsulates a good trade-off between performance and computational cost. To achieve that, first the pre-trained models are benchmarked. These results, combined with the models’ complexity and resources cost related specifications, will allow the choice of the best model to be fine-tuned. After training, the tests are repeated in order to evaluate if the model improved or not, and a final choice for the main objective is made.

4.1 Models’ specifications

We will compare the following four models against the TrustID Resnet-34 based solution, which comprises 29 layers, an average inference time of 7.28 seconds (over the entirity of all benchmark datasets) and has been trained on the VGG Face and Facescrub ensemble dataset using triplet loss. Relevant specifications to assist the identification of a superior model are presented in Table 4.

Table 4: Model’s characteristics. “# Parameter” refers to the trainable parameters, “# Mult-Adds” to the number of multiplication and addition operations, “# Layers” denotes the quantity of convolutional and linear layers present in the model, “Embedding” signifies the dimensionality of the feature embedding produced by the model’s output, “Inference time (s)” represents the average time taken for inference of all images from all the benchmark datasets, “Loss” is the loss function used to train the model, and “Dataset” are the training images.

	# Parameters	# Mult-Adds (G)	# Layers	Embedding	Inference time (s)	Loss	Dataset
MobileFaceNet	1,200,512	56.62	17	512	2.79	ArcFace	MS1MV2
iResnet-18	24,025,600	668.15	18	512	5.01	ArcFace	MS1MV2
FaceNet	28,907,599	152.21	63	512	5.89	Softmax	CASIA-WebFace
iResnet-SE-50	43,797,696	1610.00	50	512	9.78	ArcFace	MS1MV2

This initial analysis suggests that MobileFaceNet has promising characteristics. It is the least complex model, therefore, is less prone to overfitting to new data and, most importantly, the amount of computational overhead created and inference times are much inferior to the others at study. This is supported by the fewer number of convolutional and linear layers, trainable parameters and mult-adds. Albeit the similar depth to that of iResnet-18, MobileFaceNet has, approximately, 95% fewer parameters, which is reflected on the number of total mult-adds. However, further investigation is required to determine whether the aforementioned characteristics might pose a bottleneck, potentially leading to a less robust solution with subpar performance. The ideal solution should strike a balance between adapting to new data and necessary computational costs.

4.2 Benchmarking Results

4.2.1 Accuracy

After performing 10-fold cross validation on all the benchmark datasets with the pretrained models, the mean accuracy is presented on the following table.

Table 5: Model’s face verification accuracy.

Datasets Models	Frontal		Age		Pose		Hard	
	CFP-FF	LFW	AgeDB30	CALFW	CFP-FP	CPLFW	VGGFace2	XQLFW
MobileFaceNet	0.9884	0.9912	0.9308	0.9362	0.8957	0.8642	0.9050	0.5063
iResnet-18	0.9960	0.9960	0.9728	0.9555	0.9414	0.8943	0.9198	0.4943
FaceNet	0.8909	0.9038	0.7147	0.7470	0.7664	0.6738	0.7748	0.5000
TrustID	0.8807	0.9906	0.7153	0.7198	0.7030	0.6235	0.7400	0.6135
iResnet-SE-50	0.9959	0.9953	0.9263	0.9543	0.9457	0.9047	0.9396	0.5137

From Table 5, we can see that iResnet-18 and iResnet-SE-50 have comparable performance. iResnet-18 achieves higher accuracy values on more datasets than any other model, however, iResnet-SE-50 performs better on the datasets where iResnet-18 does not, but only by a very small margin. Additionally, concerning the datasets where iResnet-SE-50 exhibited slightly lower performance, the accuracy scores are also very close. Specifically, between the two models, CFP-FF, LFW, CALFW, CFP-FP, CPLFW and VGGFace2 are all within a margin of error that can be attributed to non-deterministic behaviors in PyTorch, the libraries used, hardware, and/or CUDA. It is also important to note that, even though MobileFaceNet did not achieve the higher accuracy on any benchmark, the scores are the third best and considering its lightweight specifications highlighted in Table 4, the results are very promising and present a good example of accuracy and computational cost trade-off without a compromising accuracy for student monitoring. Regarding the results from the extremely hard XQLFW, they are exceedingly low, approaching 0.5 or worse, for almost all the methods. This suggests that the model is producing outputs that resemble random guesses, which is exactly what occurs with FaceNet. The only exception is TrustID, which can be probably justified by the method of training. By resizing smaller training images to 150×150 there is a degradation in quality that leads to a model more prepared to handle these situations.

4.2.2 ROC Curves

The previous table indicates that the three methods with superior performance, based exclusively on the accuracy at the best similarity threshold for each model and dataset, are the iResnet-SE-50, iResnet-18 and MobileFaceNet. To conduct a more thorough investigation allowing us to select the most appropriate model to be fine-tuned, the TAR values are computed for a range of FAR values and the ROC curves are generated. By inspecting how close the ROC curve is to the top left corner, the prime models can be determined since those are able to correctly identify more genuine matches while keeping the impostor matches low.

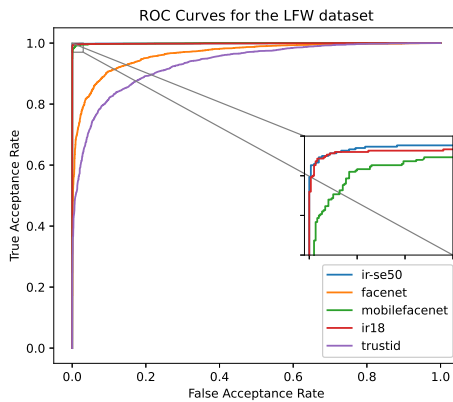


Figure 23: ROC Curves for the LFW benchmark from the F1

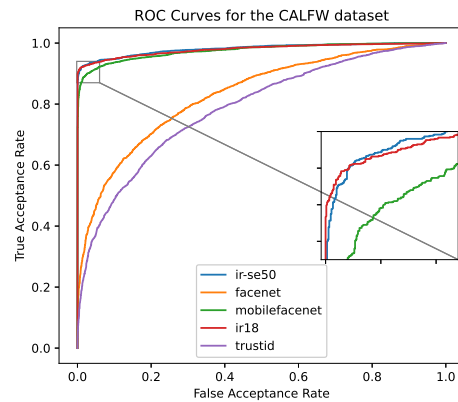


Figure 24: ROC Curves for the CALFW benchmark from the A

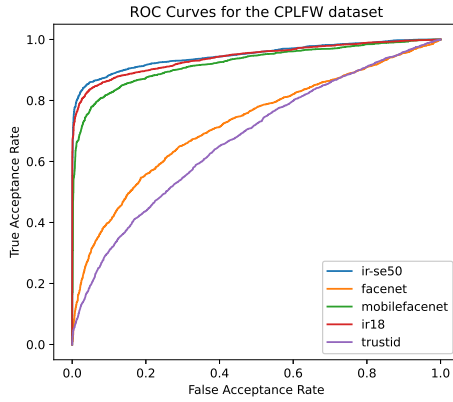


Figure 25: ROC Curves for the CPLFW benchmark from the Pose group.

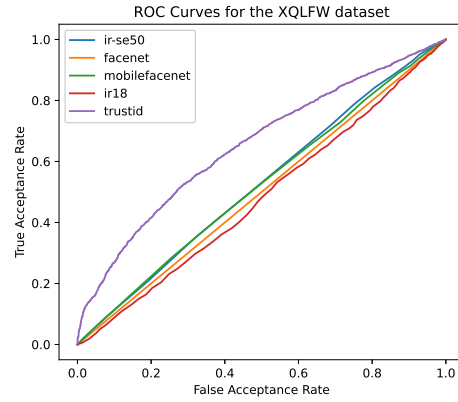


Figure 26: ROC Curves for the XQLFW benchmark from the Hard group.

The selected ROC curves support our initial assumptions¹. It is evident that, across the entire FAR range, the three top-performing models are iResnet-SE-50, iResnet-18, and MobileFacenet. With the exception of XQLFW in (Figure 34), where all models, except TrustID, perform poorly and are close to random guessing, the remaining seven datasets consistently position these three models near the top-left corner. This pattern indicates strong model performance. In scenarios with low FAR values, where the model is less tolerant of incorrectly identifying impostors as matches, the number of correctly classified pairs (TAR) is higher.

Table 6: TAR@FAR for all the models and benchmarks.

		iResnet-SE-50			iResnet-18		MobileFacenet			FaceNet		TrustID	
		1e - 4	1e - 3	1e-2	1e - 3	1e - 2	1e - 4	1e - 3	1e - 2	1e - 3	1e - 2	1e - 3	1e - 2
Frontal	CFP-FF	0.10000	0.10000	0.99771	0.09886	0.99743	0.09057	0.09600	0.98657	0.02886	0.55257	0.03314	0.58114
	LFW	0.99067	0.99333	0.99700	0.99100	0.99600	0.91467	0.96933	0.99167	0.39900	0.68800	0.26967	0.50567
Age	AgeDB30	0.68267	0.81700	0.92600	0.91533	0.95300	0.4950	0.59500	0.80267	0.02900	0.14867	0.03467	0.11100
	CALFW	0.86633	0.88233	0.91733	0.90167	0.91933	0.68100	0.75900	0.87100	0.07867	0.26767	0.05300	0.18267
Pose	CFP-FP	0.07600	0.07971	0.87371	0.07628	0.87400	0.04200	0.05171	0.69857	0.00857	0.22171	0.00686	0.12629
	CPLFW	0.37533	0.58833	0.7900	0.66767	0.75400	0.06467	0.17200	0.64400	0.00967	0.12433	0.01567	0.07300
Hard	VGGFace2	0.06000	0.77280	0.86280	0.70320	0.81840	0.05240	0.53880	0.72160	0.17000	0.31720	0.06640	0.19400
	XQLFW	0.00001	0.00033	0.00800	0.00033	0.00433	0.00001	0.00100	0.00433	0.02000	0.40433	0.02167	0.07867

The aforementioned three highest-achieving models distance themselves from FaceNet and TrustID on the ROC plots, although there is some overlap. As such, Table 6 allows us to analyze their performance at lower FAR values, where this overlap occurs.

For $FAR = 1e - 4$, all models fail on more demanding datasets, but for less intricate ones, iResnet-SE-50 achieves suitable performance on LFW and CALFW, and MobileFaceNet on LFW. Reducing the strictness and increasing the FAR to $1e - 3$, leads to an improvement on the results, as expected. The iResnet models produce high TAR values on all datasets apart from the more challenging CFP variations and XQLFW datasets. MobileFacenet starts to improve but still performs poorly on the pose group, hard group, CFP pair and AgeDB30 dataset.

¹ Please refer to Appendix - ROC Curves for the remaining from each benchmark group

Finally, at $1e - 2$ is the threshold at which all models excel without compromising the security of the system, since increasing the FAR to $1e - 1$ would lead to too much falsely matched pairs. iResnet-SE-50 and iResnet-18 have comparable performance with high scores on the same benchmarks and both failing XQLFW. MobileFaceNet approaches iResnet levels of capability aside from slightly lower scores on the age and pose groups and the XQLFW dataset.

4.2.3 DET Curves

To finalize the selection of the most appropriate model, the FRRs are calculated and plotted against the previous FAR values to obtain the DET curves. The intersection between the identity line that divides the graph and the DETs, i.e., the EER points can be extracted. These curves also allow to make a better distinction between models due to the more expansive logarithmic scale in which they are generated. In this case, contrary to the ROC curves, the better performing models are closer to the lower left corner, since that will minimize both the amount of impostors matched as true identities (FAR) and true identities classified as impostors (FRR).

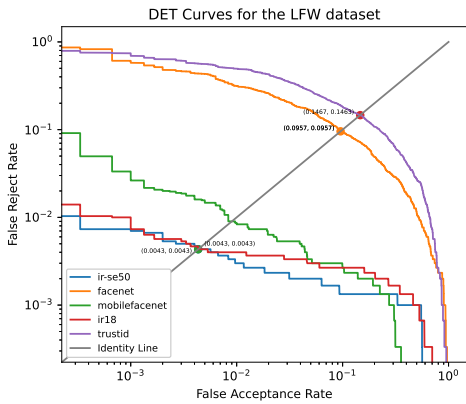


Figure 27: DET Curves for the LFW benchmark from the Frontal group.

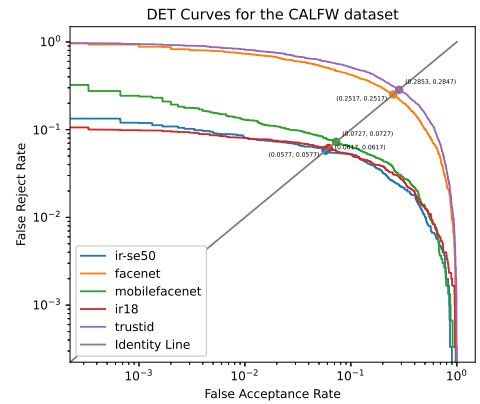


Figure 28: DET Curves for the CALFW benchmark from the Age group.

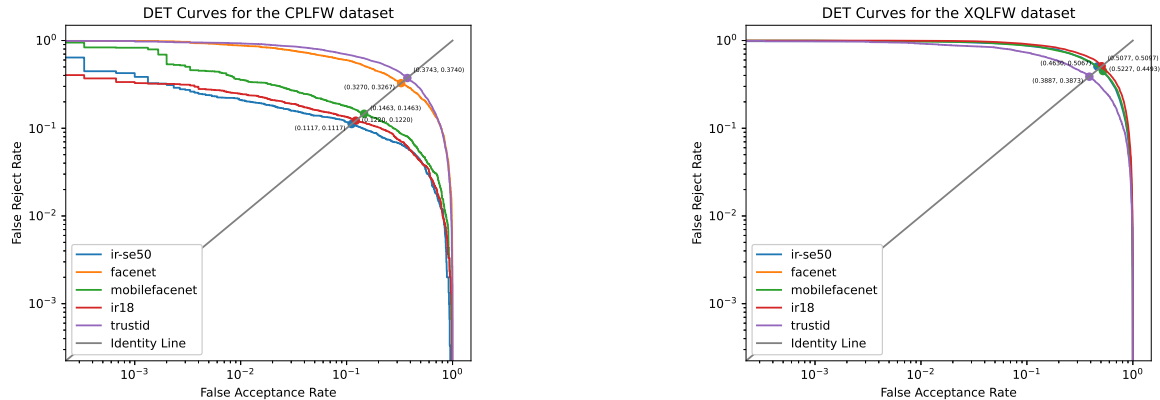


Figure 29: DET Curves for the CPLFW benchmark from the Pose group.

Figure 30: DET Curves for the XQLFW benchmark from the Hard group.

Table 7: EER values for all the models and respective benchmarks.

	Frontal		Age		Pose		Hard	
	CFP-FF	LFW	AgeDB30	CALFW	CFP-FP	CPLFW	VGGFace2	XQLFW
MobileFaceNet	0.0126	0.0090	0.0723	0.0727	0.1069	0.1463	0.1020	0.4849
iResnet-18	0.0043	0.0045	0.0297	0.0617	0.0609	0.1220	0.0882	0.5094
FaceNet	0.1111	0.0957	0.2900	0.2517	0.2326	0.3270	0.2276	-
TrustID	0.1210	0.1465	0.2827	0.2850	0.2951	0.3742	0.2594	0.3880
iResnet-SE-50	0.0040	0.0043	0.0723	0.0577	0.0554	0.1117	0.0708	0.4854

As a final analysis, the DET plots² and the EER values support what has been previously discussed: iResnet-SE-50, iResnet-18 and MobileFaceNet are the best performing models. To no surprise, this group is always close to each other and close to the ideal corner of the DET graphs. Additionally, XQLFW reveals once again to be too much of a challenge. Regarding the EER scores, the results and conclusions are similar to the ones from Table 5. iResnet-SE-50, the more complex model, has the lower scores, with iResnet-18 a close second and MobileFaceNet as the third.

² Please refer to Appendix - DET Curves for the remaining from each benchmark group

4.2.4 Discussion

At this stage, we are capable of assuring, based on the previous tests, that there are more adequate solutions to TrustID’s facial verification framework. The three top performing methods proved their robustness to extreme variation in pose (CFP-FP and CPLFW), age (AgeDB30 and CALFW) or illumination (CFP-FF, VGGFace2). That being said, the benchmark concerning quality and image degradation (XQLFW) proved to be a major hurdle to most of the models aside from TrustID.

Considering the benchmarks’ results, the much lower amount of trainable parameters, mult-adds and inference time, MobileFaceNet is the best balance between performance and computational cost. As discussed in section 3.6, due to the monitoring context, achieving perfect accuracy is not the main concern. This is due to the fact that, as the monitoring occurs over a time span it allows the system to perform more face verifications, compensating for lower accuracy values. Furthermore, although it is true that MobileFacenet’s accuracy is high in the pose group and VGGFace2, there is room for improvement in the TAR at low FAR values, hence the fine-tuning. The objective of further training the model first with QMUL-SurvFace is to try and improve its scores in both the hard group, but specially XQLFW, and pose group benchmarks. On the other hand, DigiFace-1M enables the study of the impact of fully-synthetic ethically collected data on the scores throughout the benchmarks, with a special attention to the pose group benchmarks.

4.3 Training Details

By leveraging Optuna’s hyperparameter searching capabilities³, we observe that the optimal combination is to train over batches of size 32 for 10 epochs with a $1e - 4$ learning rate that decays according to a Cosine Annealing scheduler

³ <https://optuna.org/>

with warm up restarts. Additionally, because the model has Batch Normalization layers, they need to be explicitly set to evaluation mode during training. If this step is overlooked, the mean and variance used will be the ones from the batch and not the values achieved during the pre-training, leading to incorrect evaluation values. Following the original ArcFace work [23], the optimizer of choice is Stochastic Gradient Descent with momentum 0.9 and weight decay $5e - 4$, scale $s = 64$ and margin $m = 0.5$. Manual early stopping is performed to ensure the most favorable achievable results, by evaluating on XQLFW and CPLFW during training and saving the model’s training checkpoint with the highest performing accuracy. These validation datasets are selected accordingly to the areas where the models showed potential for improvement based on the benchmarks performed.

4.4 Training Results

Fine-tuning all the layers

The first approach is to update the whole network, since both QMUL-SurvFace and DigiFace-1M are large datasets with a high number of images and identities, there are less chances of quickly overfitting to the training data. Table 8 and Table 9 summarize the accuracy results for QMUL-SurvFace and DigiFace-1M, respectively.

Table 8: MobileFaceNet accuracy scores before and after fine-tuning the whole network on QMUL-SurvFace with different ArcFace margins.

Benchmarks		Original	$m = 0.5$	$m = 0.4$	$m = 0.3$
Frontal	CFP-FF	0.9884	0.7957 (↓)	0.7916 (↓)	0.7916 (↓)
	LFW	0.9912	0.7957 (↓)	0.7915 (↓)	0.7913 (↓)
Age	AgeDB30	0.9308	0.6165 (↓)	0.6112 (↓)	0.6362 (↓)
	CALFW	0.9362	0.6593 (↓)	0.6235 (↓)	0.6472 (↓)
Pose	CFP-FP	0.8957	0.6447 (↓)	0.6381 (↓)	0.6556 (↓)
	CPLFW	0.8642	0.6048 (↓)	0.5843 (↓)	0.5992 (↓)
Hard	VGGFace2	0.9050	0.6516 (↓)	0.6188 (↓)	0.6314 (↓)
	XQLFW	0.5063	0.5325 (↑)	0.5355 (↑)	0.5215 (↑)
Stopping Epoch			6	7	7

According to Table 8, fine-tuning with QMUL-SurvFace improves, as intended, the XQLFW benchmark performance by 5.17%. However, the verified increase is moderate and disadvantageous when the accuracy degradation verified on the remaining benchmarks is taken into account. Hence, in an effort to improve the results, the margin is reduced in order to generate a less penalizing training with a more lax distance between classes. The results from these settings are shown in Table 8, and when fine-tuned with QMUL-SurvFace, it occurs the same behavior as in $m = 0.5$. The XQLFW results are also better than the original pre-trained model, increasing 5.77% for $m = 0.4$ and 3.00% for $m = 0.3$, while the other scores worsen.

Table 9: MobileFaceNet accuracy scores before and after fine-tuning the whole network on DigiFace-1M with different ArcFace margins.

Benchmarks		Original	$m = 0.5$	$m = 0.4$	$m = 0.3$
Frontal	CFP-FF	0.9884	0.8011 (↓)	0.8231 (↓)	0.8157 (↓)
	LFW	0.9912	0.8011 (↓)	0.8231 (↓)	0.8157 (↓)
Age	AgeDB30	0.9308	0.6732 (↓)	0.6733 (↓)	0.6723 (↓)
	CALFW	0.9362	0.6755 (↓)	0.7010 (↓)	0.7010 (↓)
Pose	CFP-FP	0.8957	0.6191 (↓)	0.6483 (↓)	0.6609 (↓)
	CPLFW	0.8642	0.5945 (↓)	0.6078 (↓)	0.6170 (↓)
Hard	VGGFace2	0.9050	0.6520 (↓)	0.6744 (↓)	0.6758 (↓)
	XQLFW	0.5063	0.4965 (↓)	0.5003 (↓)	0.4975 (↓)
Stopping Epoch			6	5	6

In the case of DigiFace-1M in Table 9, no discernible improvements were observed, and reducing the margin size did not yield any positive changes. Instead, the model appears to struggle in adapting to the dataset, resulting in adjustments to the weights that ultimately led to a deterioration in benchmark performance.

When comparing directly with the paper’s suggested margin ($m = 0.5$), some conclusions can be drawn. The model fine-tuned with QMUL-SurvFace produces inferior results in the frontal and age groups for $m = 0.4$ and $m = 0.3$, the pose group is superior for both margins and the hard group is mixed, where VGGFace2 has lower performance for $m = 0.4$ and $m = 0.3$, and XQLFW improves for $m = 0.4$ and not for $m = 0.3$. On the other hand, when $m = 0.4$ and $m = 0.3$, the DigiFace-1M training saw a marginal improvement throughout the tests but still performs poorly. All in all, reducing the margin size does not have a meaningful impact on the accuracy results, aside from the XQLFW when tuned with QMUL-SurvFace.

To achieve a more profound understanding of how the model reacts to the data, Table 10 and Table 11 present the TAR at very low FAR.

Table 10: TAR@FAR after fine-tuning the model with QMUL-SurvFace.

		$m = 0.5$			$m = 0.4$			$m = 0.3$		
Benchmarks		$1e - 4$	$1e - 3$	$1e - 2$	$1e - 4$	$1e - 3$	$1e - 2$	$1e - 4$	$1e - 3$	$1e - 2$
Frontal	CFP-FF	0.0140 (↓)	0.0209 (↓)	0.3486 (↓)	0.0063 (↓)	0.0154 (↓)	0.2940 (↓)	0.0091 (↓)	0.0169 (↓)	0.3097 (↓)
	LFW	0.3099 (↓)	0.3263 (↓)	0.4760 (↓)	0.1267 (↓)	0.1680 (↓)	0.3940 (↓)	0.1927 (↓)	0.2310 (↓)	0.4697 (↓)
Age	AgeDB30	0.0050 (↓)	0.0083 (↓)	0.0867 (↓)	0.0027 (↓)	0.0053 (↓)	0.0730 (↓)	0.0093 (↓)	0.0240 (↓)	0.0860 (↓)
	CALFW	0.0313 (↓)	0.8053 (↑)	0.8053 (↓)	0.0070 (↓)	0.0323 (↓)	0.0827 (↓)	0.0283 (↓)	0.0340 (↓)	0.0920 (↓)
Pose	CFP-FF	0.0006 (↓)	0.9380 (↑)	0.9380 (↑)	0.0003 (↓)	0.0003 (↓)	0.0666 (↓)	0.0000 (↓)	0.0003 (↓)	0.0626 (↓)
	CPLFW	0.0060 (↓)	0.9664 (↑)	0.9664 (↑)	0.0050 (↓)	0.0067 (↓)	0.0397 (↓)	0.0073 (↓)	0.0147 (↓)	0.0613 (↓)
Hard	VGGFace2	0.0040 (↓)	0.0536 (↓)	0.1060 (↓)	0.0036 (↓)	0.0376 (↓)	0.0880 (↓)	0.0040 (↓)	0.0364 (↓)	0.1216 (↓)
	XQLFW	0.0000 (↓)	0.0023 (↑)	0.0173 (↑)	0.0000 (↓)	0.0000 (↓)	0.0000 (↓)	0.0000 (↓)	0.0000 (↓)	0.0000 (↓)

The reduced margins $m = 0.4$ and $m = 0.3$ produce lower TAR scores at any FAR, including the very relevant frontal group. However, when $m = 0.5$, there are some improvements. At $FAR = 1e - 3$ and $FAR = 1e - 2$, the pose group suffers a significant improvement and XQLFW increases slightly.

Table 11: TAR@FAR after fine-tuning the model with DigiFace-1M.

		$m = 0.5$			$m = 0.4$			$m = 0.3$		
Benchmarks		$1e - 4$	$1e - 3$	$1e - 2$	$1e - 4$	$1e - 3$	$1e - 2$	$1e - 4$	$1e - 3$	$1e - 2$
Frontal	CFP-FF	0.0020 (↓)	0.0069 (↓)	0.1906 (↓)	0.0026 (↓)	0.0111 (↓)	0.3580 (↓)	0.0057 (↓)	0.0109 (↓)	0.3606 (↓)
	LFW	0.1633 (↓)	0.2810 (↓)	0.5520 (↓)	0.2300 (↓)	0.3403 (↓)	0.6310 (↓)	0.2320 (↓)	0.3743 (↓)	0.6113 (↓)
Age	AgeDB30	0.0013 (↓)	0.0083 (↓)	0.0530 (↓)	0.0010 (↓)	0.0153 (↓)	0.0747 (↓)	0.0003 (↓)	0.0250 (↓)	0.0790 (↓)
	CALFW	0.0017 (↓)	0.0043 (↓)	0.0780 (↓)	0.0013 (↓)	0.0300 (↓)	0.1207 (↓)	0.0050 (↓)	0.0170 (↓)	0.1223 (↓)
Pose	CFP-FF	0.0000 (↓)	0.0000 (↓)	0.0149 (↓)	0.0000 (↓)	0.0000 (↓)	0.0194 (↓)	0.0000 (↓)	0.0003 (↓)	0.0226 (↓)
	CPLFW	0.0013 (↓)	0.0017 (↓)	0.0190 (↓)	0.0007 (↓)	0.0016 (↓)	0.0263 (↓)	0.0007 (↓)	0.0033 (↓)	0.0287 (↓)
Hard	VGGFace2	0.0000 (↓)	0.0008 (↓)	0.0220 (↓)	0.0000 (↓)	0.0020 (↓)	0.0404 (↓)	0.0000 (↓)	0.0028 (↓)	0.0440 (↓)
	XQLFW	0.0000 (↓)	0.0000 (↓)	0.0083 (↓)	0.0003 (↑)	0.0013 (↑)	0.0087 (↑)	0.0000 (↓)	0.0010 (—)	0.0073 (↑)

Once again, the model trained with DigiFace-1M, does not perform and loses discriminative power at any margin and FAR value with the exception of a few outliers values that increase minimally, which can be seen as a mere fluctuation.

In the context of general CNN architectures, it is well-established that the initial layers are primarily responsible for learning fundamental features such as edges, basic shapes, and patterns that constitute objects or faces. Therefore, with the intention of improving the previous results, by preserving the weights

associated with these earlier layers and avoiding introducing noise during further training, two other approaches are followed: 1) freeze the first 5 layers and 2) train only the 2 final layers. Additionally, based on the previous experiences, different ArcFace margins are also studied.

Fine-tuning with 5 initial frozen layers

Table 12 and Table 13 present the accuracy scores after fine-tuning MobileFaceNet without updating the first five layers' weights. By freezing only 5 layers, the model still keeps its ability to learn more complex information associated with final stages of the network.

Table 12: MobileFaceNet accuracy scores before and after fine-tuning the network, with the first five layers frozen, on QMUL-SurvFace with different ArcFace margins.

Benchmarks		Original	$m = 0.5$	$m = 0.4$	$m = 0.3$
Frontal	CFP-FF	0.9884	0.7821 (↓)	0.8414 (↓)	0.8155 (↓)
	LFW	0.9912	0.7820 (↓)	0.8415 (↓)	0.8156 (↓)
Age	AgeDB30	0.9308	0.5985 (↓)	0.6373 (↓)	0.6382 (↓)
	CALFW	0.9362	0.6506 (↓)	0.6962 (↓)	0.6765 (↓)
Pose	CFP-FP	0.8957	0.6477 (↓)	0.6627 (↓)	0.6499 (↓)
	CPLFW	0.8642	0.5943 (↓)	0.6195 (↓)	0.5872 (↓)
Hard	VGGFace2	0.9050	0.6442 (↓)	0.6822 (↓)	0.6610 (↓)
	XQLFW	0.5063	0.4925 (↓)	0.5020 (↓)	0.5127 (↑)
Stopping Epoch			8	5	6

Table 13: MobileFaceNet accuracies before and after fine-tuning the network, with the first five layers frozen, on DigiFace-1M with different ArcFace margins.

Benchmarks		Original	$m = 0.5$	$m = 0.4$	$m = 0.3$
Frontal	CFP-FF	0.9884	0.8840 (↓)	0.8806 (↓)	0.8788 (↓)
	LFW	0.9912	0.8840 (↓)	0.8805 (↓)	0.8789 (↓)
Age	AgeDB30	0.9308	0.7265 (↓)	0.7125 (↓)	0.7303 (↓)
	CALFW	0.9362	0.7400 (↓)	0.7478 (↓)	0.7398 (↓)
Pose	CFP-FP	0.8957	0.7219 (↓)	0.7039 (↓)	0.7223 (↓)
	CPLFW	0.8642	0.6423 (↓)	0.6335 (↓)	0.6435 (↓)
Hard	VGGFace2	0.9050	0.7220 (↓)	0.7122 (↓)	0.7080 (↓)
	XQLFW	0.5063	0.4997 (↓)	0.4967 (↓)	0.5033 (↓)
Stopping Epoch			6	6	6

As expected, the weights are less updated, hence the majority of the accuracy scores are higher than when training the whole network. Also, for QMUL-SurvFace (Table 12), if $m = 0.3$ there is even an improvement in the XQLFW benchmark. Finally, DigiFace-1M (Table 13) at any m value, shows no positive developments against the pre-trained model.

Table 14: TAR@FAR after fine-tuning the model, with the first five layers frozen, on QMUL-SurvFace.

		m=0.5			m=0.4			m=0.3		
Benchmarks		1e-4	1e-3	1e-2	1e-4	1e-3	1e-2	1e-4	1e-3	1e-2
Frontal	CFP-FF	0.0117 (↓)	0.0149 (↓)	0.2769 (↓)	0.0174 (↓)	0.0303 (↓)	0.4786 (↓)	0.0163 (↓)	0.0286 (↓)	0.3897 (↓)
	LFW	0.2033 (↓)	0.2277 (↓)	0.5047 (↓)	0.2907 (↓)	0.3473 (↓)	0.5870 (↓)	0.2597 (↓)	0.2743 (↓)	0.5533 (↓)
Age	AgeDB30	0.0137 (↓)	0.0207 (↓)	0.0597 (↓)	0.0087 (↓)	0.0180 (↓)	0.0643 (↓)	0.0063 (↓)	0.0177 (↓)	0.0777 (↓)
	CALFW	0.018 (↓)	0.0210 (↓)	0.0877 (↓)	0.0667 (↓)	0.0737 (↓)	0.1510 (↓)	0.0267 (↓)	0.0570 (↓)	0.1450 (↓)
Pose	CFP-FP	0.0000 (↓)	0.0009 (↓)	0.0617 (↓)	0.0011 (↓)	0.0029 (↓)	0.0871 (↓)	0.0009 (↓)	0.0020 (↓)	0.0694 (↓)
	CPLFW	0.0070 (↓)	0.0170 (↓)	0.0570 (↓)	0.0100 (↓)	0.0183 (↓)	0.0870 (↓)	0.0093 (↓)	0.0187 (↓)	0.0633 (↓)
Hard	VGGFace2	0.0032 (↓)	0.0352 (↓)	0.1112 (↓)	0.0056 (↓)	0.0712 (↓)	0.1516 (↓)	0.0040 (↓)	0.0528 (↓)	0.1304 (↓)
	XQLFW	0.0000 (↓)	0.0000 (↓)	0.0000 (↓)	0.0000 (↓)	0.0000 (↓)	0.0040 (↓)	0.0000 (↓)	0.0003 (↓)	0.0037 (↓)

Table 15: TAR@FAR after fine-tuning the model, with the first five layers frozen, on DigiFace-1M.

		m=0.5			m=0.4			m=0.3		
Benchmarks		1e-4	1e-3	1e-2	1e-4	1e-3	1e-2	1e-4	1e-3	1e-2
Frontal	CFP-FF	0.0189 (↓)	0.0354 (↓)	0.5574 (↓)	0.0183 (↓)	0.0303 (↓)	0.5200 (↓)	0.0294 (↓)	0.0346 (↓)	0.5539 (↓)
	LFW	0.3207 (↓)	0.5577 (↓)	0.7440 (↓)	0.2677 (↓)	0.5180 (↓)	0.7360 (↓)	0.4420 (↓)	0.5980 (↓)	0.7497 (↓)
Age	AgeDB30	0.0083 (↓)	0.0363 (↓)	0.1450 (↓)	0.0027 (↓)	0.0203 (↓)	0.1407 (↓)	0.0047 (↓)	0.0253 (↓)	0.1353 (↓)
	CALFW	0.0407 (↓)	0.0813 (↓)	0.2690 (↓)	0.0100 (↓)	0.0593 (↓)	0.2423 (↓)	0.0150 (↓)	0.0393 (↓)	0.2590 (↓)
Pose	CFP-FP	0.0006 (↓)	0.0026 (↓)	0.1231 (↓)	0.0003 (↓)	0.0029 (↓)	0.0880 (↓)	0.0003 (↓)	0.0017 (↓)	0.1106 (↓)
	CPLFW	0.0003 (↓)	0.0017 (↓)	0.0383 (↓)	0.0007 (↓)	0.0023 (↓)	0.0247 (↓)	0.0003 (↓)	0.0017 (↓)	0.0407 (↓)
Hard	VGGFace2	0.0000 (↓)	0.0176 (↓)	0.1732 (↓)	0.0000 (↓)	0.0056 (↓)	0.1392 (↓)	0.0000 (↓)	0.0040 (↓)	0.1468 (↓)
	XQLFW	0.0000 (↓)	0.0010 (—)	0.0100 (↑)	0.0003 (↑)	0.0007 (↓)	0.0067 (↑)	0.0000 (↓)	0.0010 (—)	0.0093 (↑)

Finally, Table 14 and Table 15 highlight that training with less layers does not improve the performance at any FAR or margin. Moreover, the previous enhancements verified when the complete model is trained with QMUL-SurvFace with $m = 0.5$, and $FAR = 1e-3$ and $FAR = 1e-2$ are lost with this configuration.

Fine-tuning the last 2 layers

To finalize, we conducted additional tests by training only the last two layers (one convolutional and linear). This allows us to investigate in which direction the model evolves in terms of results when even less stages are trained.

Table 16: MobileFaceNet accuracy scores before and after fine-tuning the network, with all the layers frozen aside the last two, on QMUL-SurvFace with different ArcFace margins.

Benchmarks		Original	$m = 0.5$	$m = 0.4$	$m = 0.3$
Frontal	CFP-FF	0.9884	0.8751 (↓)	0.8821 (↓)	0.8786 (↓)
	LFW	0.9912	0.8751 (↓)	0.8821 (↓)	0.8785 (↓)
Age	AgeDB30	0.9308	0.7097 (↓)	0.7220 (↓)	0.7080 (↓)
	CALFW	0.9362	0.7762 (↓)	0.7833 (↓)	0.7752 (↓)
Pose	CFP-FP	0.8957	0.6729 (↓)	0.6714 (↓)	0.6719 (↓)
	CPLFW	0.8642	0.6585 (↓)	0.6635 (↓)	0.6635 (↓)
Hard	VGGFace2	0.9050	0.6992 (↓)	0.7014 (↓)	0.7006 (↓)
	XQLFW	0.5063	0.4975 (↓)	0.4993 (↓)	0.5010 (↓)
Stopping Epoch			6	3	6

Table 17: MobileFaceNet accuracies before and after fine-tuning the network, with all the layers frozen aside the last two, on DigiFace-1M with different ArcFace margins.

Benchmarks		Original	$m = 0.5$	$m = 0.4$	$m = 0.3$
Frontal	CFP-FF	0.9884	0.9568 (↓)	0.9630 (↓)	0.9574 (↓)
	LFW	0.9912	0.9569 (↓)	0.9629 (↓)	0.9574 (↓)
Age	AgeDB30	0.9308	0.8420 (↓)	0.8533 (↓)	0.8403 (↓)
	CALFW	0.9362	0.8672 (↓)	0.8795 (↓)	0.8643 (↓)
Pose	CFP-FP	0.8957	0.8133 (↓)	0.8199 (↓)	0.8171 (↓)
	CPLFW	0.8642	0.7650 (↓)	0.7830 (↓)	0.7697 (↓)
Hard	VGGFace2	0.9050	0.8158 (↓)	0.8290 (↓)	0.8134 (↓)
	XQLFW	0.5063	0.4923 (↓)	0.4995 (↓)	0.4993 (↓)
Stopping Epoch			5	3	4

Table 16 and Table 17 follows the pattern seen in the previous experiment. On one hand, training less layers produces results closer to the pre-trained model, on the other, the network does not improve in any meaningful way.

Table 18: TAR@FAR after fine-tuning the model, with all the layers frozen except the last two, on QMUL-SurvFace.

		m=0.5			m=0.4			m=0.3		
Benchmarks		1e-4	1e-3	1e-2	1e-4	1e-3	1e-2	1e-4	1e-3	1e-2
Frontal	CFP-FF	0.038 (↓)	0.0394 (↓)	0.6503 (↓)	0.0280 (↓)	0.0369 (↓)	0.6237 (↓)	0.0306 (↓)	0.0411 (↓)	0.6483 (↓)
	LFW	0.1793 (↓)	0.5243 (↓)	0.7050 (↓)	0.1727 (↓)	0.5347 (↓)	0.6920 (↓)	0.1863 (↓)	0.5210 (↓)	0.6910 (↓)
Age	AgeDB30	0.0210 (↓)	0.0283 (↓)	0.1320 (↓)	0.0373 (↓)	0.0390 (↓)	0.1457 (↓)	0.0213 (↓)	0.0327 (↓)	0.1243 (↓)
	CALFW	0.0477 (↓)	0.0977 (↓)	0.3130 (↓)	0.0653 (↓)	0.1137 (↓)	0.3323 (↓)	0.0500 (↓)	0.1073 (↓)	0.3047 (↓)
Pose	CFP-FP	0.0020 (↓)	0.0034 (↓)	0.1323 (↓)	0.0020 (↓)	0.0043 (↓)	0.1346 (↓)	0.0017 (↓)	0.0031 (↓)	0.1146 (↓)
	CPLFW	0.0170 (↓)	0.0453 (↓)	0.1567 (↓)	0.0207 (↓)	0.0503 (↓)	0.1607 (↓)	0.0213 (↓)	0.0457 (↓)	0.1683 (↓)
Hard	VGGFace2	0.0040 (↓)	0.0508 (↓)	0.2036 (↓)	0.0052 (↓)	0.0544 (↓)	0.2160 (↓)	0.0044 (↓)	0.0488 (↓)	0.1996 (↓)
	XQLFW	0.0003 (↑)	0.0003 (↓)	0.0080 (↓)	0.0003 (↓)	0.0007 (↓)	0.0110 (↑)	0.0003 (↓)	0.0013 (↑)	0.0123 (↑)

Table 19: TAR@FAR after fine-tuning the model, with all the layers frozen except the last two, on DigiFace-1M.

		m=0.5			m=0.4			m=0.3		
Benchmarks		1e-4	1e-3	1e-2	1e-4	1e-3	1e-2	1e-4	1e-3	1e-2
Frontal	CFP-FF	0.0734 (↓)	0.0794 (↓)	0.8874 (↓)	0.0743 (↓)	0.0817 (↓)	0.9245 (↓)	0.0734 (↓)	0.0794 (↓)	0.9009 (↓)
	LFW	0.8316 (↓)	0.8880 (↓)	0.9516 (↓)	0.8516 (↓)	0.8923 (↓)	0.9503 (↓)	0.8417 (↓)	0.8840 (↓)	0.9517 (↓)
Age	AgeDB30	0.1307 (↓)	0.1707 (↓)	0.4283 (↓)	0.2260 (↓)	0.2390 (↓)	0.4747 (↓)	0.1303 (↓)	0.1893 (↓)	0.4237 (↓)
	CALFW	0.3793 (↓)	0.4287 (↓)	0.6457 (↓)	0.4913 (↓)	0.5370 (↓)	0.6933 (↓)	0.4120 (↓)	0.4683 (↓)	0.6550 (↓)
Pose	CFP-FF	0.0137 (↓)	0.0300 (↓)	0.4074 (↓)	0.0194 (↓)	0.0251 (↓)	0.4469 (↓)	0.0120 (↓)	0.0217 (↓)	0.4206 (↓)
	CPLFW	0.1050 (↑)	0.2400 (↑)	0.3673 (↓)	0.0830 (↑)	0.2007 (↑)	0.3977 (↓)	0.0713 (↑)	0.1890 (↑)	0.3780 (↓)
Hard	VGGFace2	0.0192 (↓)	0.2220 (↓)	0.4572 (↓)	0.0192 (↓)	0.2620 (↓)	0.5116 (↓)	0.0152 (↓)	0.2328 (↓)	0.4632 (↓)
	XQLFW	0.0000 (↓)	0.0000 (↓)	0.0047 (↑)	0.0000 (↓)	0.0000 (↓)	0.0057 (↑)	0.0000 (↓)	0.0000 (↓)	0.0040 (↓)

To conclude, the TAR values continue to be worse than the original model, for both QMUL-SurvFace (Table 18) and DigiFace-1M (Table 19), with the usual outliers values that are slightly higher but do not highlight any pattern of improvement.

4.4.1 Discussion

Taking into consideration the previous experiments, it can be inferred that the most adequate solution is the pre-trained model. Further training on any of the selected datasets does not improve the overall performance. Although fine-tuning the whole network with QMUL-SurvFace leads to higher accuracy on the XQLFW benchmark, the scores for the other tests are worse. Moreover, when $m = 0.5$ the model is more discriminative for $FAR = 1e - 3$ and $1e - 2$ on the pose group and XQLFW, but once again, on the other benchmarks the model is less discriminative. Since the intended application is to monitor students, it is highly required for the model to adapt to any quality and pose, that is, profile and frontal. Therefore, improvement on one benchmark at a cost of having negative impact on the others is less than idealized. The initial pre-trained model outperforms TrustID’s method, with low computational cost and respectable scores on all the tests and benchmarks. Despite the fact that it did not respond well to the fine-tuning on

the selected datasets, it still is the most competent approach to the student monitoring problem as it performs appropriately considering the possible challenges of pose, illumination, expressions, etc. while maintaining a light resource utilization.

Chapter 5

Conclusion

5.1 Main Outcomes

This work studied different neural networks models in order to propose a better approach to TrustID’s facial verification module. The main objective was to find a good compromise between the maximum accurate performance and the minimum computational cost possible without compromising safety. To that extent, four different sized models were suggested: MobileFaceNet, FaceNet, iResnet-18 and iResnet-SE-50. First they were compared in terms of their specifications: number of trainable parameters, mult-adds, number of trainable layers, embedding size, inference time, loss function and training dataset. Because the system is to be applied on a student monitoring scenario, the capturing device will induce high data variations, hence the model must be invariant to poses, illumination, quality, etc. With that in mind, appropriate benchmarks were designed to test the methods in a wide range of possible scenarios.

Initial tests, studied the pre-trained models in order to pick the best one to then verify if it can be refined. Analyzing the accuracies on all benchmarks, the ROC curves, TAR at different FAR values, DET curves and EER points, clearly showcased the best three models that could substitute TrustID0s solution: iResnet-

SE-50, iResnet-18 and MobileFaceNet. iResnet-SE-50 and iResnet-18 are two contenders that performed very similarly and MobileFaceNet consistently placed third place, but is very close. Balancing MobileFaceNet’s performance with its inherent lightweight characteristics, it was selected as the best starting point for fine-tuning, since it has much less trainable parameters, number of mult-adds operations and inference time for a small performance trade-off.

Two datasets were picked to fine-tune, each one with an objective in mind. QMUL-SurvFace was proposed as a way of improving the performance on the very difficult XQLFW benchmark. Then DigiFace-1M served as an experiment to test how the model would react to fully synthetic ethically sourced data, and if it would improve the performance on pose related benchmarks. First all the layers of the network, aside from the batch norm ones, were trained for three different ArcFace margins (0.5, 0.4 and 0.3). This approach revealed to be successful in increasing the XQLFW accuracy performance and discriminative power at lower FAR ($1e-3$ and $1e-2$ for $m = 0.5$) for the pose group and XQLFW when trained with QMUL-SurvFace. However, that came along with worse results on the other benchmarks. On the same experiment, DigiFace-1M didn’t produce any results worth mentioning, since it only deteriorated the model’s results.

With the performance degradation verified on the benchmarks for both datasets, two new training approaches that envolved freezing layers were employed. First, five initial layers were frozen, and the reamining were trained. Then, all the layers aside from the last two were frozen. The main intention would be to update less the weights responsible for capturing more general information and train only more detail specific layers, ultimately leading to the improvements verified on whole network training approach with results closer to the original model where they became worse. These tests proved that to not be the case. We concluded that, as would be theoretically expected, the lesser layers were trained, the closer the results are to the pre-trained model, but the XQLFW performance didn’t improve, and again DigiFace-1M didn’t show any enhancement whatsoever. This behaviour

also leads us to believe that, because the model trained with less layers still shows performs degradation while not improving in the same domains where the model trained through all the layers does, that cand indicate that the model needs to be more complex in order to be able to adapt to the dataset's intricacies without tuning it over all the layers.

All in all, MobileFaceNet is a good trade-off between computational overhead and accurate results that performs better than TrustID on the designed benchmarks.

5.2 Future work

After this work has been concluded, a better solution was suggested. However, there are some experiments that are worth investigating. Following the ethically sourced data philosophy, it would be interesting to train MobileFaceNet from scratch using only DigiFace-1M or an ensemble of datasets of synthetic data and consensual images to evaluate how the model would perform on the same benchmarks geared toward student monitoring scenarios.

Bibliography

- [1] T. Ahonen, A. Hadid, and M. Pietikäinen. “Face Description with Local Binary Patterns: Application to Face Recognition”. In: *IEEE Transactions on Pattern Analysis and Machine Intelligence* 28.12 (2006). Cited By :4611, pp. 2037–2041. ISSN: 0162-8828. DOI: 10.1109/TPAMI.2006.244 (cit. on p. 6).
- [2] Arohan Ajit, Koustav Acharya, and Abhishek Samanta. “A Review of Convolutional Neural Networks”. In: *2020 International Conference on Emerging Trends in Information Technology and Engineering (Ic-ETITE)*. Feb. 2020, pp. 1–5. DOI: 10.1109/ic-ETITE47903.2020.049 (cit. on p. 9).
- [3] Laith Alzubaidi et al. “Review of Deep Learning: Concepts, CNN Architectures, Challenges, Applications, Future Directions”. In: *Journal of Big Data* 8.1 (Mar. 2021), p. 53. ISSN: 2196-1115. DOI: 10.1186/s40537-021-00444-8. (Visited on 02/09/2023) (cit. on pp. 7, 8, 10, 11).
- [4] Xiang An et al. *Partial FC: Training 10 Million Identities on a Single Machine*. Comment: 8 pages, 9 figures. Jan. 2021. arXiv: 2010.05222 [cs]. (Visited on 04/28/2023) (cit. on pp. 19, 94).
- [5] Yousef Atoum et al. “Automated Online Exam Proctoring”. In: *IEEE Transactions on Multimedia* 19.7 (July 2017), pp. 1609–1624. ISSN: 1941-0077. DOI: 10.1109/TMM.2017.2656064 (cit. on p. 34).
- [6] Gwangbin Bae et al. “DigiFace-1M: 1 Million Digital Face Images for Face Recognition”. In: *2023 IEEE/CVF Winter Conference on Applications of*

Computer Vision (WACV). Datasets. Waikoloa, HI, USA: IEEE, Jan. 2023, pp. 3515–3524. ISBN: 978-1-66549-346-8. DOI: 10.1109/WACV56688.2023.00352. (Visited on 02/28/2023) (cit. on pp. 18, 19, 41, 94).

- [7] Ankan Bansal et al. *The Do's and Don'ts for CNN-based Face Verification*. Comment: 10 pages including references, added more experiments on deeper vs wider dataset (section 3.2). Sept. 2017. arXiv: 1705.07426 [cs]. (Visited on 04/28/2023) (cit. on pp. 18, 19, 93).
- [8] Maria Barron Rodriguez et al. *Remote Learning During the Global School Lockdown: Multi-Country Lessons*. World Bank, Aug. 2021. DOI: 10.1596/36141. (Visited on 03/13/2023) (cit. on p. 1).
- [9] Chandrasekhar Bhagavatula et al. *Faster Than Real-time Facial Alignment: A 3D Spatial Transformer Network Approach in Unconstrained Poses*. Comment: International Conference on Computer Vision (ICCV) 2017. Sept. 2017. arXiv: 1707.05653 [cs]. (Visited on 04/15/2023) (cit. on p. 91).
- [10] Fadi Boutros et al. “MixFaceNets: Extremely Efficient Face Recognition Networks”. In: *2021 IEEE International Joint Conference on Biometrics (IJCB)*. Aug. 2021, pp. 1–8. DOI: 10.1109/IJCB52358.2021.9484374 (cit. on pp. 21, 26).
- [11] S. Charles Brubaker et al. “On the Design of Cascades of Boosted Ensembles for Face Detection”. In: *International Journal of Computer Vision* 77.1 (May 2008), pp. 65–86. ISSN: 1573-1405. DOI: 10.1007/s11263-007-0060-1 (cit. on p. 13).
- [12] Jiajiong Cao, Yingming Li, and Zhongfei Zhang. “Celeb-500K: A Large Training Dataset for Face Recognition”. In: *2018 25th IEEE International Conference on Image Processing (ICIP)*. Oct. 2018, pp. 2406–2410. DOI: 10.1109/ICIP.2018.8451704 (cit. on pp. 19, 93).

- [13] Qiong Cao et al. *VGGFace2: A Dataset for Recognising Faces across Pose and Age*. Comment: This paper has been accepted by IEEE Conference on Automatic Face and Gesture Recognition (F&G), 2018. (Oral). May 2018. arXiv: 1710.08092 [cs]. (Visited on 04/27/2023) (cit. on pp. 18, 19, 92).
- [14] Weipeng Cao et al. “A Review on Neural Networks with Random Weights”. In: *Neurocomputing* 275 (Jan. 2018), pp. 278–287. ISSN: 0925-2312. DOI: 10.1016/j.neucom.2017.08.040. (Visited on 02/09/2023) (cit. on p. 7).
- [15] Fengju Chang et al. *FacePoseNet: Making a Case for Landmark-Free Face Alignment*. Aug. 2017. arXiv: 1708.07517 [cs]. (Visited on 04/15/2023) (cit. on pp. 15, 16, 91).
- [16] Lisha Chen, Hui Su, and Qiang Ji. “Face Alignment With Kernel Density Deep Neural Network”. In: *2019 IEEE/CVF International Conference on Computer Vision (ICCV)*. Seoul, Korea (South): IEEE, Oct. 2019, pp. 6991–7001. ISBN: 978-1-72814-803-8. DOI: 10.1109/ICCV.2019.00709. (Visited on 04/15/2023) (cit. on pp. 16, 91).
- [17] Sheng Chen et al. *MobileFaceNets: Efficient CNNs for Accurate Real-Time Face Verification on Mobile Devices*. Comment: Accepted as a conference paper at CCBR 2018. Camera-ready version. June 2018. arXiv: 1804.07573 [cs]. (Visited on 02/27/2023) (cit. on pp. 21, 24, 25).
- [18] Zhiyi Cheng, Xiatian Zhu, and Shaogang Gong. “Low-Resolution Face Recognition”. In: *Computer Vision – ACCV 2018*. Ed. by C. V. Jawahar et al. Vol. 11363. Cham: Springer International Publishing, 2019, pp. 605–621. ISBN: 978-3-030-20892-9 978-3-030-20893-6. DOI: 10.1007/978-3-030-20893-6_38. (Visited on 05/04/2023) (cit. on pp. 20, 97).
- [19] Zhiyi Cheng, Xiatian Zhu, and Shaogang Gong. *Surveillance Face Recognition Challenge*. Comment: The QMUL-SurvFace challenge is publicly available at <https://qmul-survface.github.io/>. Aug. 2018. arXiv: 1804.09691 [cs]. (Visited on 04/28/2023) (cit. on pp. 20, 42, 98).

- [20] Chengjun Liu and H. Wechsler. “Gabor Feature Based Classification Using the Enhanced Fisher Linear Discriminant Model for Face Recognition”. In: *IEEE Transactions on Image Processing* 11.4 (Apr. 2002), pp. 467–476. ISSN: 1941-0042. DOI: 10.1109/TIP.2002.999679 (cit. on p. 6).
- [21] Dan Cireşan et al. “A Committee of Neural Networks for Traffic Sign Classification”. In: *The 2011 International Joint Conference on Neural Networks*. July 2011, pp. 1918–1921. DOI: 10.1109/IJCNN.2011.6033458 (cit. on p. 5).
- [22] T.F Cootes et al. “View-Based Active Appearance Models”. In: *Image and Vision Computing* 20.9 (Aug. 2002), pp. 657–664. ISSN: 0262-8856. DOI: 10.1016/S0262-8856(02)00055-0 (cit. on p. 13).
- [23] Jiankang Deng et al. “ArcFace: Additive Angular Margin Loss for Deep Face Recognition”. In: () (cit. on pp. 19, 30, 31, 45, 55, 93).
- [24] Jiankang Deng et al. *Joint Multi-view Face Alignment in the Wild*. Comment: submit to IEEE Transactions on Image Processing. Aug. 2017. arXiv: 1708.06023 [cs]. (Visited on 04/15/2023) (cit. on p. 91).
- [25] Jiankang Deng et al. *RetinaFace: Single-stage Dense Face Localisation in the Wild*. May 2019. arXiv: 1905.00641 [cs]. (Visited on 04/13/2023) (cit. on pp. 13–16, 89, 90).
- [26] Hang Du et al. “The Elements of End-to-end Deep Face Recognition: A Survey of Recent Advances”. In: *ACM Computing Surveys* 54.10s (Jan. 2022), pp. 1–42. ISSN: 0360-0300, 1557-7341. DOI: 10.1145/3507902. (Visited on 03/07/2023) (cit. on pp. 13–16, 18, 20, 28, 32, 90, 91).
- [27] Shiv Ram Dubey, Satish Kumar Singh, and Bidyut Baran Chaudhuri. *Activation Functions in Deep Learning: A Comprehensive Survey and Benchmark*. Comment: Accepted in Neurocomputing, Elsevier. June 2022. arXiv: 2109.14545 [cs]. (Visited on 07/26/2023) (cit. on p. 9).

- [28] Ionut Cosmin Duta et al. “Improved Residual Networks for Image and Video Recognition”. In: *2020 25th International Conference on Pattern Recognition (ICPR)*. Milan, Italy: IEEE, Jan. 2021, pp. 9415–9422. ISBN: 978-1-72818-808-9. DOI: [10.1109/ICPR48806.2021.9412193](https://doi.org/10.1109/ICPR48806.2021.9412193). (Visited on 05/16/2023) (cit. on pp. 21, 23).
- [29] José Nuno Faria et al. “Image-Based Face Verification for Student Identity Management — the TRUSTID Case Study”. In: *Adjunct Proceedings of the 31st ACM Conference on User Modeling, Adaptation and Personalization*. UMAP ’23 Adjunct. New York, NY, USA: Association for Computing Machinery, June 2023, pp. 66–71. ISBN: 978-1-4503-9891-6. DOI: [10.1145/3563359.3597397](https://doi.org/10.1145/3563359.3597397). (Visited on 07/25/2023) (cit. on pp. 1, 35).
- [30] B. Farley and W. Clark. “Simulation of Self-Organizing Systems by Digital Computer”. In: *Transactions of the IRE Professional Group on Information Theory* 4.4 (1954), pp. 76–84. DOI: [10.1109/TIT.1954.1057468](https://doi.org/10.1109/TIT.1954.1057468) (cit. on p. 4).
- [31] Zhen-Hua Feng et al. *Wing Loss for Robust Facial Landmark Localisation with Convolutional Neural Networks*. Comment: 11 pages, 6 figures, 6 tables. Oct. 2018. arXiv: [1711.06753 \[cs\]](https://arxiv.org/abs/1711.06753). (Visited on 04/14/2023) (cit. on pp. 15, 16, 90, 91).
- [32] Asep Hadian Sudrajat Ganidisastra and Yoanes Bandung. “An Incremental Training on Deep Learning Face Recognition for M-Learning Online Exam Proctoring”. In: *2021 IEEE Asia Pacific Conference on Wireless and Mobile (APWiMob)*. Apr. 2021, pp. 213–219. DOI: [10.1109/APWiMob51111.2021.9435232](https://doi.org/10.1109/APWiMob51111.2021.9435232) (cit. on pp. 34, 39).
- [33] Ian Goodfellow, Yoshua Bengio, and Aaron Courville. *Deep Learning*. <http://www.deeplearningbook.org> MIT Press, 2016 (cit. on pp. 11, 13).
- [34] Jiuxiang Gu et al. “Recent Advances in Convolutional Neural Networks”. In: *Pattern Recognition* 77 (May 2018), pp. 354–377. ISSN: 0031-3203. DOI:

- 10.1016/j.patcog.2017.10.013. (Visited on 02/09/2023) (cit. on pp. 7–10).
- [35] Yandong Guo et al. *MS-Celeb-1M: A Dataset and Benchmark for Large-Scale Face Recognition*. July 2016. arXiv: 1607 . 08221 [cs]. (Visited on 04/25/2023) (cit. on pp. 19, 92).
- [36] Munawar Hayat et al. “Joint Registration and Representation Learning for Unconstrained Face Identification”. In: *2017 IEEE Conference on Computer Vision and Pattern Recognition (CVPR)*. Honolulu, HI: IEEE, July 2017, pp. 1551–1560. ISBN: 978-1-5386-0457-1. DOI: 10 . 1109/CVPR . 2017 . 169. (Visited on 04/15/2023) (cit. on pp. 16, 91).
- [37] Kaiming He et al. “Deep Residual Learning for Image Recognition”. In: *2016 IEEE Conference on Computer Vision and Pattern Recognition (CVPR)*. Las Vegas, NV, USA: IEEE, June 2016, pp. 770–778. ISBN: 978-1-4673-8851-1. DOI: 10 . 1109/CVPR . 2016 . 90. (Visited on 05/16/2023) (cit. on pp. 21–24).
- [38] Kaiming He et al. *Delving Deep into Rectifiers: Surpassing Human-Level Performance on ImageNet Classification*. Feb. 2015. arXiv: 1502 . 01852 [cs]. (Visited on 05/16/2023) (cit. on pp. 25–27).
- [39] Seng Chun Hoo, Haidi Ibrahim, and Shahrel Azmin Suandi. “ConvFaceNeXt: Lightweight Networks for Face Recognition”. In: *Mathematics* 10.19 (Jan. 2022), p. 3592. ISSN: 2227-7390. DOI: 10 . 3390/math10193592. (Visited on 05/16/2023) (cit. on pp. 21, 27).
- [40] Jie Hu et al. *Squeeze-and-Excitation Networks*. Comment: journal version of the CVPR 2018 paper, accepted by TPAMI. May 2019. arXiv: 1709 . 01507 [cs]. (Visited on 05/16/2023) (cit. on p. 25).
- [41] Peiyun Hu and Deva Ramanan. “Finding Tiny Faces”. In: *2017 IEEE Conference on Computer Vision and Pattern Recognition (CVPR)*. Honolulu,

- HI: IEEE, July 2017, pp. 1522–1530. ISBN: 978-1-5386-0457-1. DOI: 10 . 1109/CVPR.2017.166. (Visited on 04/14/2023) (cit. on p. 90).
- [42] Gary B Huang et al. “Labeled Faces in the Wild: A Database for Studying Face Recognition in Unconstrained Environments”. In: () (cit. on pp. 20, 31, 94).
- [43] Lichao Huang et al. *DenseBox: Unifying Landmark Localization with End to End Object Detection*. Sept. 2015. arXiv: 1509.04874 [cs]. (Visited on 04/13/2023) (cit. on p. 90).
- [44] Xiehe Huang et al. *PropagationNet: Propagate Points to Curve to Learn Structure Information*. Comment: 10 pages, 8 figures, 8 tables, CVPR2020. June 2020. arXiv: 2006.14308 [cs]. (Visited on 04/08/2023) (cit. on p. 13).
- [45] Yuge Huang et al. “CurricularFace: Adaptive Curriculum Learning Loss for Deep Face Recognition”. In: *2020 IEEE/CVF Conference on Computer Vision and Pattern Recognition (CVPR)*. Seattle, WA, USA: IEEE, June 2020, pp. 5900–5909. ISBN: 978-1-72817-168-5. DOI: 10 . 1109/CVPR42600 . 2020 . 00594. (Visited on 02/28/2023) (cit. on p. 31).
- [46] D. H. HUBEL and T. N. WIESEL. “Receptive Fields, Binocular Interaction and Functional Architecture in the Cat’s Visual Cortex.” In: *The Journal of physiology* 160.1 (Jan. 1962), pp. 106–154. ISSN: 0022-3751 1469-7793. DOI: 10 . 1113/jphysiol . 1962 . sp006837 (cit. on p. 9).
- [47] A G Ivakhnenko and V G Lapa. “Cybernetic Predicting Devices”. In: () (cit. on p. 5).
- [48] Nathan D. Kalka et al. “IJB-S: IARPA Janus Surveillance Video Benchmark”. In: *2018 IEEE 9th International Conference on Biometrics Theory, Applications and Systems (BTAS)*. Oct. 2018, pp. 1–9. DOI: 10 . 1109/BTAS . 2018 . 8698584 (cit. on pp. 6, 20, 97).

- [49] Xu Kang, Bin Song, and Fengyao Sun. “A Deep Similarity Metric Method Based on Incomplete Data for Traffic Anomaly Detection in IoT”. In: *Applied Sciences* 9 (Jan. 2019), p. 135. doi: 10.3390/app9010135 (cit. on p. 7).
- [50] Asifullah Khan et al. “A Survey of the Recent Architectures of Deep Convolutional Neural Networks”. In: *Artificial Intelligence Review* 53.8 (Dec. 2020), pp. 5455–5516. ISSN: 1573-7462. doi: 10.1007/s10462-020-09825-6. (Visited on 02/09/2023) (cit. on p. 8).
- [51] Minchul Kim, Anil K. Jain, and Xiaoming Liu. “AdaFace: Quality Adaptive Margin for Face Recognition”. In: *2022 IEEE/CVF Conference on Computer Vision and Pattern Recognition (CVPR)*. New Orleans, LA, USA: IEEE, June 2022, pp. 18729–18738. ISBN: 978-1-66546-946-3. doi: 10.1109/CVPR52688.2022.01819. (Visited on 02/27/2023) (cit. on p. 31).
- [52] Diederik P Kingma and Jimmy Lei. “Adam: A Method for Stochastic Optimization”. In: (2015) (cit. on p. 11).
- [53] Brendan F. Klare et al. “Pushing the Frontiers of Unconstrained Face Detection and Recognition: IARPA Janus Benchmark A”. In: *2015 IEEE Conference on Computer Vision and Pattern Recognition (CVPR)*. Boston, MA, USA: IEEE, June 2015, pp. 1931–1939. ISBN: 978-1-4673-6964-0. doi: 10.1109/CVPR.2015.7298803. (Visited on 02/28/2023) (cit. on pp. 20, 95).
- [54] Martin Knoche, Stefan Hormann, and Gerhard Rigoll. “Cross-Quality LFW: A Database for Analyzing Cross- Resolution Image Face Recognition in Unconstrained Environments”. In: *2021 16th IEEE International Conference on Automatic Face and Gesture Recognition (FG 2021)*. Dec. 2021, pp. 1–5. doi: 10.1109/FG52635.2021.9666960 (cit. on pp. 20, 98).
- [55] Alex Krizhevsky, Ilya Sutskever, and Geoffrey E Hinton. “ImageNet Classification with Deep Convolutional Neural Networks”. In: *Advances in Neu-*

- ral Information Processing Systems*. Vol. 25. Curran Associates, Inc., 2012. (Visited on 01/26/2023) (cit. on pp. 5, 6, 21).
- [56] Mikel Labayen et al. “Online Student Authentication and Proctoring System Based on Multimodal Biometrics Technology”. In: *IEEE Access* 9 (2021), pp. 72398–72411. ISSN: 2169-3536. DOI: 10.1109/ACCESS.2021.3079375 (cit. on pp. 35, 39).
- [57] Erik Learned-Miller et al. “Labeled Faces in the Wild: A Survey”. In: *Advances in Face Detection and Facial Image Analysis*. Ed. by Michal Kawulok, M. Emre Celebi, and Bogdan Smolka. Cham: Springer International Publishing, 2016, pp. 189–248. ISBN: 978-3-319-25956-7 978-3-319-25958-1. DOI: 10.1007/978-3-319-25958-1_8. (Visited on 03/09/2023) (cit. on pp. 6, 14).
- [58] Y. LeCun et al. “Backpropagation Applied to Handwritten Zip Code Recognition”. In: *Neural Computation* 1.4 (1989), pp. 541–551. DOI: 10.1162/neco.1989.1.4.541 (cit. on pp. 5, 11).
- [59] Yann LeCun, Yoshua Bengio, and Geoffrey Hinton. “Deep Learning”. In: *Nature* 521.7553 (May 2015), pp. 436–444. ISSN: 0028-0836, 1476-4687. DOI: 10.1038/nature14539 (cit. on pp. 7–9, 17).
- [60] Yann LeCun et al. “Gradient-Based Learning Applied to Document Recognition”. In: (1998) (cit. on pp. 5, 6, 10, 21).
- [61] Z. Lei, M. Pietikainen, and S.Z. Li. “Learning Discriminant Face Descriptor”. In: *IEEE Transactions on Pattern Analysis and Machine Intelligence* 36.2 (2014). Cited By :287, pp. 289–302. ISSN: 0162-8828. DOI: 10.1109/TPAMI.2013.112 (cit. on p. 6).
- [62] Stan Z. Li and Anil K. Jain, eds. *Handbook of Face Recognition*. London: Springer, 2011. ISBN: 978-0-85729-931-4 978-0-85729-932-1. DOI: 10.1007/978-0-85729-932-1. (Visited on 02/14/2023) (cit. on p. 16).

- [63] Zewen Li et al. “A Survey of Convolutional Neural Networks: Analysis, Applications, and Prospects”. In: *IEEE Transactions on Neural Networks and Learning Systems* 33.12 (Dec. 2022), pp. 6999–7019. ISSN: 2162-2388. DOI: 10.1109/TNNLS.2021.3084827 (cit. on pp. 6, 7, 9).
- [64] Hao Liu et al. “Two-Stream Transformer Networks for Video-Based Face Alignment”. In: *IEEE Transactions on Pattern Analysis and Machine Intelligence* 40.11 (Nov. 2018), pp. 2546–2554. ISSN: 1939-3539. DOI: 10.1109/TPAMI.2017.2734779 (cit. on p. 91).
- [65] Wei Liu et al. “SSD: Single Shot MultiBox Detector”. In: vol. 9905. Comment: ECCV 2016. 2016, pp. 21–37. DOI: 10.1007/978-3-319-46448-0_2. arXiv: 1512.02325 [cs]. (Visited on 04/13/2023) (cit. on p. 89).
- [66] Weiyang Liu et al. *SphereFace: Deep Hypersphere Embedding for Face Recognition*. Comment: CVPR 2017 (v4: updated the Appendix). Jan. 2018. arXiv: 1704.08063 [cs]. (Visited on 02/28/2023) (cit. on pp. 29–31).
- [67] Yang Liu et al. *HAMBox: Delving into Online High-quality Anchors Mining for Detecting Outer Faces*. Comment: 9 pages, 6 figures. arXiv admin note: text overlap with 1802.09058 by other authors. Dec. 2019. arXiv: 1912.09231 [cs]. (Visited on 04/13/2023) (cit. on p. 89).
- [68] Zhuang Liu et al. *A ConvNet for the 2020s*. Comment: CVPR 2022; Code: <https://github.com/facebookresearch/ConvNeXt>. Mar. 2022. arXiv: 2201.03545 [cs]. (Visited on 09/12/2023) (cit. on p. 27).
- [69] Brais Martinez et al. “Local Evidence Aggregation for Regression-Based Facial Point Detection”. In: *IEEE Transactions on Pattern Analysis and Machine Intelligence* 35.5 (May 2013), pp. 1149–1163. ISSN: 1939-3539. DOI: 10.1109/TPAMI.2012.205 (cit. on p. 13).
- [70] Brianna Maze et al. “IARPA Janus Benchmark - C: Face Dataset and Protocol”. In: *2018 International Conference on Biometrics (ICB)*. Feb.

- 2018, pp. 158–165. DOI: [10.1109/ICB2018.2018.00033](https://doi.org/10.1109/ICB2018.2018.00033) (cit. on pp. 20, 97).
- [71] J McCarthy et al. “A PROPOSAL FOR THE DARTMOUTH SUMMER RESEARCH PROJECT ON ARTIFICIAL INTELLIGENCE”. In: () (cit. on p. 4).
- [72] Warren S McCulloch and Walter Pitts. “A LOGICAL CALCULUS OF THE IDEAS IMMANENT IN NERVOUS ACTIVITY”. In: () (cit. on p. 4).
- [73] Qiang Meng et al. “MagFace: A Universal Representation for Face Recognition and Quality Assessment”. In: *2021 IEEE/CVF Conference on Computer Vision and Pattern Recognition (CVPR)*. Nashville, TN, USA: IEEE, June 2021, pp. 14220–14229. ISBN: 978-1-66544-509-2. DOI: [10.1109/CVPR46437.2021.01400](https://doi.org/10.1109/CVPR46437.2021.01400). (Visited on 02/28/2023) (cit. on p. 31).
- [74] Shervin Minaee et al. *Going Deeper Into Face Detection: A Survey*. Mar. 2021 (cit. on p. 14).
- [75] Marvin Minsky and Seymour Papert. *Perceptrons: An Introduction to Computational Geometry*. Cambridge, MA, USA: MIT Press, 1969 (cit. on pp. 5, 6).
- [76] Stylianos Moschoglou et al. “AgeDB: The First Manually Collected, In-the-Wild Age Database”. In: *2017 IEEE Conference on Computer Vision and Pattern Recognition Workshops (CVPRW)*. Honolulu, HI, USA: IEEE, July 2017, pp. 1997–2005. ISBN: 978-1-5386-0733-6. DOI: [10.1109/CVPRW.2017.250](https://doi.org/10.1109/CVPRW.2017.250). (Visited on 05/02/2023) (cit. on pp. 20, 96).
- [77] Aaron Nech and Ira Kemelmacher-Shlizerman. “Level Playing Field for Million Scale Face Recognition”. In: *2017 IEEE Conference on Computer Vision and Pattern Recognition (CVPR)*. Datasets. Honolulu, HI: IEEE, July 2017, pp. 3406–3415. ISBN: 978-1-5386-0457-1. DOI: [10.1109/CVPR.2017.363](https://doi.org/10.1109/CVPR.2017.363). (Visited on 02/28/2023) (cit. on pp. 19, 92).

- [78] Allen Newell, John C Shaw, and Herbert A Simon. “Report on a General Problem Solving Program”. In: *IFIP Congress*. Vol. 256. Pittsburgh, PA. 1959, p. 64 (cit. on p. 4).
- [79] Hong-Wei Ng and Stefan Winkler. “A Data-Driven Approach to Cleaning Large Face Datasets”. In: *2014 IEEE International Conference on Image Processing (ICIP)*. Oct. 2014, pp. 343–347. DOI: [10.1109/ICIP.2014.7025068](https://doi.org/10.1109/ICIP.2014.7025068) (cit. on pp. 35, 40).
- [80] P. N. Belhumeur, J. P. Hespanha, and D. J. Kriegman. “Eigenfaces vs. Fisherfaces: Recognition Using Class Specific Linear Projection”. In: *IEEE Transactions on Pattern Analysis and Machine Intelligence* 19.7 (July 1997), pp. 711–720. ISSN: 1939-3539. DOI: [10.1109/34.598228](https://doi.org/10.1109/34.598228) (cit. on pp. 5, 14).
- [81] Omkar M. Parkhi, Andrea Vedaldi, and Andrew Zisserman. “Deep Face Recognition”. In: *Proceedings of the British Machine Vision Conference 2015*. VGG-Face. Swansea: British Machine Vision Association, 2015, pp. 41.1–41.12. ISBN: 978-1-901725-53-7. DOI: [10.5244/C.29.41](https://doi.org/10.5244/C.29.41). (Visited on 02/27/2023) (cit. on pp. 12, 18, 19, 35, 39, 40, 92).
- [82] Adrian Popescu et al. “Face Verification with Challenging Imposters and Diversified Demographics”. In: *2022 IEEE/CVF Winter Conference on Applications of Computer Vision (WACV)*. Datasets. Waikoloa, HI, USA: IEEE, Jan. 2022, pp. 1151–1160. ISBN: 978-1-66540-915-5. DOI: [10.1109/WACV51458.2022.00122](https://doi.org/10.1109/WACV51458.2022.00122). (Visited on 02/28/2023) (cit. on pp. 20, 99).
- [83] David Portugal et al. “Continuous User Identification in Distance Learning: A Recent Technology Perspective”. In: *Smart Learning Environments* 10.1 (July 2023), p. 38. ISSN: 2196-7091. DOI: [10.1186/s40561-023-00255-9](https://doi.org/10.1186/s40561-023-00255-9). (Visited on 09/12/2023) (cit. on p. 33).
- [84] Rajeev Ranjan, Carlos D. Castillo, and Rama Chellappa. *L₂-Constrained Softmax Loss for Discriminative Face Verification*. L2-softmax

Loss functions. June 2017. arXiv: 1703.09507 [cs]. (Visited on 02/28/2023) (cit. on p. 31).

- [85] Rajeev Ranjan et al. “Deep Learning for Understanding Faces: Machines May Be Just as Good, or Better, than Humans”. In: *IEEE Signal Processing Magazine* 35.1 (Jan. 2018), pp. 66–83. ISSN: 1558-0792. DOI: 10.1109/MSP.2017.2764116 (cit. on pp. 5, 6, 13, 14, 16–18).
- [86] Shaoqing Ren et al. *Faster R-CNN: Towards Real-Time Object Detection with Region Proposal Networks*. Comment: Extended tech report. Jan. 2016. arXiv: 1506.01497 [cs]. (Visited on 04/13/2023) (cit. on p. 89).
- [87] Sebastian Ruder. “An Overview of Gradient Descent Optimization Algorithms”. In: () (cit. on p. 11).
- [88] Nicolas Saenz-Lechon et al. “Methodological Issues in the Development of Automatic Systems for Voice Pathology Detection”. In: *Biomedical Signal Processing and Control* 1 (Apr. 2006), pp. 120–128. DOI: 10.1016/j.bspc.2006.06.003 (cit. on p. 44).
- [89] Mark Sandler et al. *MobileNetV2: Inverted Residuals and Linear Bottlenecks*. Mar. 2019. arXiv: 1801.04381 [cs]. (Visited on 05/16/2023) (cit. on p. 24).
- [90] Shreyak Sawhney et al. “Real-Time Smart Attendance System Using Face Recognition Techniques”. In: *2019 9th International Conference on Cloud Computing, Data Science & Engineering (Confluence)*. Jan. 2019, pp. 522–525. DOI: 10.1109/CONFLUENCE.2019.8776934 (cit. on p. 34).
- [91] Jürgen Schmidhuber. “Deep Learning in Neural Networks: An Overview”. In: *Neural Networks* 61 (Jan. 2015), pp. 85–117. ISSN: 08936080. DOI: 10.1016/j.neunet.2014.09.003. (Visited on 01/24/2023) (cit. on p. 5).

- [92] Florian Schroff, Dmitry Kalenichenko, and James Philbin. “FaceNet: A Unified Embedding for Face Recognition and Clustering”. In: *2015 IEEE Conference on Computer Vision and Pattern Recognition (CVPR)*. June 2015, pp. 815–823. DOI: [10.1109/CVPR.2015.7298682](https://doi.org/10.1109/CVPR.2015.7298682). arXiv: [1503.03832](https://arxiv.org/abs/1503.03832) [cs]. (Visited on 02/16/2023) (cit. on pp. 16, 19, 32, 39).
- [93] Soumyadip Sengupta et al. “Frontal to Profile Face Verification in the Wild”. In: *2016 IEEE Winter Conference on Applications of Computer Vision (WACV)*. Celebrities in Frontal Profile (CFP) Datasets. Mar. 2016, pp. 1–9. DOI: [10.1109/WACV.2016.7477558](https://doi.org/10.1109/WACV.2016.7477558) (cit. on pp. 20, 96).
- [94] P.Y. Simard, D. Steinkraus, and J.C. Platt. “Best Practices for Convolutional Neural Networks Applied to Visual Document Analysis”. In: *Seventh International Conference on Document Analysis and Recognition, 2003. Proceedings*. Vol. 1. Edinburgh, UK: IEEE Comput. Soc, 2003, pp. 958–963. ISBN: 978-0-7695-1960-9. DOI: [10.1109/ICDAR.2003.1227801](https://doi.org/10.1109/ICDAR.2003.1227801). (Visited on 01/25/2023) (cit. on p. 5).
- [95] Karen Simonyan and Andrew Zisserman. “VERY DEEP CONVOLUTIONAL NETWORKS FOR LARGE-SCALE IMAGE RECOGNITION”. In: (2015) (cit. on p. 21).
- [96] Irwin Sobel and Gary Feldman. “A 3×3 Isotropic Gradient Operator for Image Processing”. In: *Pattern Classification and Scene Analysis* (Jan. 1973), pp. 271–272 (cit. on p. 8).
- [97] J. Stallkamp et al. “Man vs. Computer: Benchmarking Machine Learning Algorithms for Traffic Sign Recognition”. In: *Neural Networks. Selected Papers from IJCNN 2011* 32 (Aug. 2012), pp. 323–332. ISSN: 0893-6080. DOI: [10.1016/j.neunet.2012.02.016](https://doi.org/10.1016/j.neunet.2012.02.016). (Visited on 01/25/2023) (cit. on p. 5).
- [98] Yi Sun, Xiaogang Wang, and Xiaoou Tang. “Deep Learning Face Representation from Predicting 10,000 Classes”. In: *2014 IEEE Conference on*

- Computer Vision and Pattern Recognition*. DeepID. June 2014, pp. 1891–1898. DOI: [10.1109/CVPR.2014.244](https://doi.org/10.1109/CVPR.2014.244) (cit. on p. 28).
- [99] Christian Szegedy et al. *Going Deeper with Convolutions*. Sept. 2014. arXiv: [1409.4842 \[cs\]](https://arxiv.org/abs/1409.4842). (Visited on 05/16/2023) (cit. on pp. 21, 22).
- [100] Yaniv Taigman et al. “DeepFace: Closing the Gap to Human-Level Performance in Face Verification”. In: *2014 IEEE Conference on Computer Vision and Pattern Recognition*. Columbus, OH, USA: IEEE, June 2014, pp. 1701–1708. ISBN: 978-1-4799-5118-5. DOI: [10.1109/CVPR.2014.220](https://doi.org/10.1109/CVPR.2014.220). (Visited on 02/13/2023) (cit. on p. 6).
- [101] Yaniv Taigman et al. “Web-Scale Training for Face Identification”. In: *2015 IEEE Conference on Computer Vision and Pattern Recognition (CVPR)*. Boston, MA, USA: IEEE, June 2015, pp. 2746–2754. ISBN: 978-1-4673-6964-0. DOI: [10.1109/CVPR.2015.7298891](https://doi.org/10.1109/CVPR.2015.7298891). (Visited on 02/28/2023) (cit. on p. 19).
- [102] Mingxing Tan. “MixConv: Mixed Depthwise Convolutional Kernels”. In: () (cit. on p. 26).
- [103] Xu Tang et al. *PyramidBox: A Context-assisted Single Shot Face Detector*. Comment: 21 pages, 12 figures. Aug. 2018. arXiv: [1803.07737 \[cs\]](https://arxiv.org/abs/1803.07737). (Visited on 04/14/2023) (cit. on p. 90).
- [104] Philipp Terhorst et al. “QMagFace: Simple and Accurate Quality-Aware Face Recognition”. In: *2023 IEEE/CVF Winter Conference on Applications of Computer Vision (WACV)*. Waikoloa, HI, USA: IEEE, Jan. 2023, pp. 3473–3483. ISBN: 978-1-66549-346-8. DOI: [10.1109/WACV56688.2023.00348](https://doi.org/10.1109/WACV56688.2023.00348). (Visited on 02/28/2023) (cit. on p. 31).
- [105] Jonathan Tompson et al. *Efficient Object Localization Using Convolutional Networks*. Comment: 8 pages with 1 page of citations. June 2015. arXiv: [1411.4280 \[cs\]](https://arxiv.org/abs/1411.4280). (Visited on 02/13/2023) (cit. on p. 6).

- [106] Matthew Turk and Alex Pentland. “Eigenfaces for Recognition”. In: *Journal of Cognitive Neuroscience* 3.1 (Jan. 1991), pp. 71–86. ISSN: 0898-929X. DOI: 10.1162/jocn.1991.3.1.71. (Visited on 03/07/2023) (cit. on pp. 5, 14).
- [107] Naeem Ullah et al. “A Novel DeepMaskNet Model for Face Mask Detection and Masked Facial Recognition”. In: *Journal of King Saud University - Computer and Information Sciences* 34.10, Part B (Nov. 2022), pp. 9905–9914. ISSN: 1319-1578. DOI: 10.1016/j.jksuci.2021.12.017. (Visited on 02/27/2023) (cit. on pp. 20, 98).
- [108] P. Viola and M. Jones. “Rapid Object Detection Using a Boosted Cascade of Simple Features”. In: *Proceedings of the 2001 IEEE Computer Society Conference on Computer Vision and Pattern Recognition. CVPR 2001.* Vol. 1. Dec. 2001, pp. I–I. DOI: 10.1109/CVPR.2001.990517 (cit. on p. 13).
- [109] Fei Wang et al. *The Devil of Face Recognition Is in the Noise*. Comment: accepted to ECCV’18. July 2018. arXiv: 1807 . 11649 [cs]. (Visited on 04/28/2023) (cit. on pp. 19, 93).
- [110] Feng Wang et al. “Additive Margin Softmax for Face Verification”. In: *IEEE Signal Processing Letters* 25.7 (July 2018). AMS Loss, pp. 926–930. ISSN: 1070-9908, 1558-2361. DOI: 10 . 1109 / LSP . 2018 . 2822810. arXiv: 1801 . 05599 [cs]. (Visited on 02/28/2023) (cit. on pp. 30, 31).
- [111] Feng Wang et al. “NormFace: L2 Hypersphere Embedding for Face Verification”. In: *Proceedings of the 25th ACM International Conference on Multimedia*. Comment: camera-ready version. Oct. 2017, pp. 1041–1049. DOI: 10 . 1145 / 3123266 . 3123359. arXiv: 1704 . 06369 [cs]. (Visited on 02/27/2023) (cit. on pp. 28, 29, 31).
- [112] Hao Wang et al. *CosFace: Large Margin Cosine Loss for Deep Face Recognition*. Comment: Accepted by CVPR 2018. Apr. 2018. arXiv: 1801 . 09414 [cs]. (Visited on 02/28/2023) (cit. on p. 31).

- [113] Mei Wang and Weihong Deng. “Deep Face Recognition: A Survey”. In: *Neurocomputing* 429 (Mar. 2021), pp. 215–244. ISSN: 0925-2312. DOI: 10.1016/j.neucom.2020.10.081. (Visited on 02/27/2023) (cit. on pp. 6, 13, 16, 17, 28).
- [114] Mei Wang et al. “Racial Faces in the Wild: Reducing Racial Bias by Information Maximization Adaptation Network”. In: *2019 IEEE/CVF International Conference on Computer Vision (ICCV)*. Seoul, Korea (South): IEEE, Oct. 2019, pp. 692–702. ISBN: 978-1-72814-803-8. DOI: 10.1109/ICCV.2019.00078. (Visited on 05/05/2023) (cit. on pp. 20, 97).
- [115] Nannan Wang et al. “Facial Feature Point Detection: A Comprehensive Survey”. In: *Neurocomputing* 275 (Jan. 2018), pp. 50–65. ISSN: 0925-2312. DOI: 10.1016/j.neucom.2017.05.013 (cit. on p. 14).
- [116] Zhongyuan Wang et al. *Masked Face Recognition Dataset and Application*. Mar. 2020. arXiv: 2003.09093 [cs]. (Visited on 05/01/2023) (cit. on pp. 19, 94).
- [117] Joseph Weizenbaum. “ELIZA—a Computer Program for the Study of Natural Language Communication between Man and Machine”. In: *Communications of the ACM* 9.1 (Jan. 1966), pp. 36–45. ISSN: 0001-0782. DOI: 10.1145/365153.365168. (Visited on 01/18/2023) (cit. on p. 5).
- [118] Cameron Whitelam et al. “IARPA Janus Benchmark-B Face Dataset”. In: *2017 IEEE Conference on Computer Vision and Pattern Recognition Workshops (CVPRW)*. July 2017, pp. 592–600. DOI: 10.1109/CVPRW.2017.87 (cit. on pp. 20, 96).
- [119] Chris J Winstead. “Remote Microelectronics Laboratory Education in the COVID-19 Pandemic”. In: *2022 Intermountain Engineering, Technology and Computing (IETC)*. May 2022, pp. 1–6. DOI: 10.1109/IETC54973.2022.9796805 (cit. on p. 1).

- [120] Lior Wolf, Tal Hassner, and Itay Maoz. “Face Recognition in Unconstrained Videos with Matched Background Similarity”. In: *CVPR 2011*. June 2011, pp. 529–534. doi: 10.1109/CVPR.2011.5995566 (cit. on pp. 20, 95).
- [121] Wayne Wu et al. *Look at Boundary: A Boundary-Aware Face Alignment Algorithm*. Comment: Accepted to CVPR 2018. Project page: <https://wywu.github.io/projects/> May 2018. arXiv: 1805.10483 [cs]. (Visited on 04/15/2023) (cit. on p. 91).
- [122] Shengtao Xiao et al. “Recurrent 3D-2D Dual Learning for Large-Pose Facial Landmark Detection”. In: *2017 IEEE International Conference on Computer Vision (ICCV)*. Venice: IEEE, Oct. 2017, pp. 1642–1651. ISBN: 978-1-5386-1032-9. doi: 10.1109/ICCV.2017.181. (Visited on 04/15/2023) (cit. on pp. 16, 91).
- [123] Yuanyuan Xu et al. *CenterFace: Joint Face Detection and Alignment Using Face as Point*. Comment: 11 pages, 3 figures. A demo of CenterFace can be available at <https://github.com/Star-Clouds/CenterFace>. Nov. 2019. arXiv: 1911.03599 [cs]. (Visited on 04/13/2023) (cit. on pp. 14, 89, 90).
- [124] Rikiya Yamashita et al. “Convolutional Neural Networks: An Overview and Application in Radiology”. In: *Insights into Imaging* 9.4 (Aug. 2018), pp. 611–629. ISSN: 1869-4101. doi: 10.1007/s13244-018-0639-9. (Visited on 02/09/2023) (cit. on pp. 6–8, 10).
- [125] Mengjia Yan et al. *VarGFaceNet: An Efficient Variable Group Convolutional Neural Network for Lightweight Face Recognition*. Comment: 8 pages, 2 figures. In Proceedings of the IEEE International Conference on Computer Vision Workshop, 2019. Nov. 2019. arXiv: 1910.04985 [cs]. (Visited on 02/27/2023) (cit. on pp. 21, 25).
- [126] Dong Yi et al. *Learning Face Representation from Scratch*. Nov. 2014. arXiv: 1411.7923 [cs]. (Visited on 04/25/2023) (cit. on pp. 19, 92).

- [127] Z. Cao et al. “Face Recognition with Learning-Based Descriptor”. In: *2010 IEEE Computer Society Conference on Computer Vision and Pattern Recognition*. June 2010, pp. 2707–2714. ISBN: 1063-6919. DOI: 10.1109/CVPR.2010.5539992 (cit. on p. 6).
- [128] Stefanos Zafeiriou, Cha Zhang, and Zhengyou Zhang. “A Survey on Face Detection in the Wild: Past, Present and Future”. In: *Computer Vision and Image Understanding* 138 (Sept. 2015), pp. 1–24. ISSN: 1077-3142. DOI: 10.1016/j.cviu.2015.03.015 (cit. on p. 14).
- [129] Andreas Zell. “Simulation Neuronaler Netze”. In: 1994 (cit. on p. 7).
- [130] Caiming Zhang and Yang Lu. “Study on Artificial Intelligence: The State of the Art and Future Prospects”. In: *Journal of Industrial Information Integration* 23 (Sept. 2021), p. 100224. ISSN: 2452414X. DOI: 10.1016/j.jii.2021.100224. (Visited on 01/11/2023) (cit. on p. 4).
- [131] Changzheng Zhang, Xiang Xu, and Dandan Tu. *Face Detection Using Improved Faster RCNN*. Feb. 2018. arXiv: 1802.02142 [cs]. (Visited on 04/13/2023) (cit. on p. 89).
- [132] Yu-Dong Zhang et al. “Improved Breast Cancer Classification Through Combining Graph Convolutional Network and Convolutional Neural Network”. In: *Information Processing & Management* 58.2 (Mar. 2021), p. 102439. ISSN: 0306-4573. DOI: 10.1016/j.ipm.2020.102439 (cit. on p. 6).
- [133] Kaipeng Zhang et al. “Joint Face Detection and Alignment Using Multi-task Cascaded Convolutional Networks”. In: *IEEE Signal Processing Letters* 23.10 (Oct. 2016). Comment: Submitted to IEEE Signal Processing Letters, pp. 1499–1503. ISSN: 1070-9908, 1558-2361. DOI: 10.1109/LSP.2016.2603342. arXiv: 1604.02878 [cs]. (Visited on 04/13/2023) (cit. on pp. 13–15, 90, 91).

- [134] Qian Zhang et al. *VarGNet: Variable Group Convolutional Neural Network for Efficient Embedded Computing*. Comment: Technical report. Apr. 2020. arXiv: 1907.05653 [cs]. (Visited on 05/16/2023) (cit. on p. 25).
- [135] Shifeng Zhang et al. *FaceBoxes: A CPU Real-time Face Detector with High Accuracy*. Comment: Accepted by IJCB 2017; Added references; Released codes. Dec. 2018. arXiv: 1708.05234 [cs]. (Visited on 04/14/2023) (cit. on p. 90).
- [136] Zhou Zhang et al. “A Virtual Laboratory System with Biometric Authentication and Remote Proctoring Based on Facial Recognition”. In: *Computers in Education Journal* 7 (Dec. 2016), pp. 74–84 (cit. on pp. 33, 34).
- [137] Zhou Zhang et al. “A Virtual Proctor with Biometric Authentication for Facilitating Distance Education”. In: *Lecture Notes in Networks and Systems*. Jan. 2018, pp. 110–124. ISBN: 978-3-319-64351-9. DOI: 10.1007/978-3-319-64352-6_11 (cit. on p. 34).
- [138] He Zhao et al. “RDCFFace: Radial Distortion Correction for Face Recognition”. In: *2020 IEEE/CVF Conference on Computer Vision and Pattern Recognition (CVPR)*. Seattle, WA, USA: IEEE, June 2020, pp. 7718–7727. ISBN: 978-1-72817-168-5. DOI: 10.1109/CVPR42600.2020.00774. (Visited on 02/28/2023) (cit. on pp. 16, 91).
- [139] Jian Zhao, Shuicheng Yan, and Jiashi Feng. “Towards Age-Invariant Face Recognition”. In: *IEEE Transactions on Pattern Analysis and Machine Intelligence* 44.1 (Jan. 2022), pp. 474–487. ISSN: 1939-3539. DOI: 10.1109/TPAMI.2020.3011426 (cit. on pp. 20, 98).
- [140] Tianyue Zheng and Weihong Deng. “Cross-Pose LFW: A Database for Studying Cross-Pose Face Recognition in Unconstrained Environments”. In: () (cit. on pp. 20, 96, 98).

- [141] Tianyue Zheng, Weihong Deng, and Jiani Hu. *Cross-Age LFW: A Database for Studying Cross-Age Face Recognition in Unconstrained Environments*. Comment: 10 pages, 9 figures. Aug. 2017. arXiv: 1708.08197 [cs]. (Visited on 05/03/2023) (cit. on pp. 20, 96, 98).
- [142] Xinqi Zhu and Michael Bain. *B-CNN: Branch Convolutional Neural Network for Hierarchical Classification*. Comment: 9 pages, 8 figures. Oct. 2017. DOI: 10.48550/arXiv.1709.09890. arXiv: 1709.09890 [cs]. (Visited on 02/13/2023) (cit. on p. 7).
- [143] Zheng Zhu et al. “WebFace260M: A Benchmark Unveiling the Power of Million-Scale Deep Face Recognition”. In: *2021 IEEE/CVF Conference on Computer Vision and Pattern Recognition (CVPR)*. Datasets. Nashville, TN, USA: IEEE, June 2021, pp. 10487–10497. ISBN: 978-1-66544-509-2. DOI: 10.1109/CVPR46437.2021.01035. (Visited on 02/28/2023) (cit. on pp. 19, 94).
- [144] Fuzhen Zhuang et al. *A Comprehensive Survey on Transfer Learning*. Comment: 31 pages, 7 figures. June 2020. arXiv: 1911.02685 [cs, stat]. (Visited on 05/01/2023) (cit. on p. 12).

Appendix

Face Detection Classes

→ **Multi-stage** methods [25] include all the coarse-to-fine facial detectors that work in similar manner to the following two phases. First, bounding box proposals are generated by sliding a window through the input. Then, over one or several subsequent stages, false positives are rejected and the approved bounding boxes are refined. To complement, one widely applied object detection protocol that inspired face detection methods and perfectly describes the steps mentioned above is Faster R-CNN [86]. However, these methods can be slower and have a more complex way of training [123].

→ **Single-stage** approaches [25] are the ones that perform classification and bounding box regression without the necessity of a proposal stage, producing highly dense face locations and scales. This structure takes inspiration, once again, from general object detectors, for example, the Single Shot MultiBox detector, commonly referred to as SSD [65]. Finally, the methods included in this class are more efficient, but can incur in compromised accuracy, when compared to multi-stage.

→ **Anchor-based** techniques [67, 25, 131] detect faces by predefining anchors with different settings (scales, strides, number, etc.) on the feature maps, then performing classification and bounding box regression on them until an acceptable output is found. As proven by Liu and Tang *et al.* [67], the choice of anchors highly influences the results of prediction. Hence, it is necessary to fine-tune them on a situation-by-situation basis, otherwise, there is a limitation in generalization. Furthermore, higher densities of anchors directly generate an increase in computational overhead.

→ **Anchor-free** procedures, obviously, do not need predefined anchors in order to find faces. Alternatively, these methods address the face detection by using different techniques. For example, DenseBox [43] which attempts to predict faces by processing each pixel as a bounding box, or CenterFace [123] that treats face detection as a key-point estimation problem by predicting the center of the face and bounding boxes. Even so, relating to the accuracy of anchor-free approaches, there's still room for improvement for false positives and stability in the training stage [26].

→ **Multi-task learning** are all the methodologies that conjointly performs other tasks, namely facial landmark¹ localization, during face classification and bounding box regression [26]. CenterFace [123] is one example, and so it is the widely implemented MTCNN [133], which correlated bounding boxes and face landmarks. RetinaFace [25] is another state-of-the-art approach, it mutually detects faces, respective landmarks and performs dense 3D face regression.

→ **CPU real-time** methods, as the name suggests, include the detectors that can run on a single CPU core, in real-time, for VGA-resolution input images. A face detector can achieve great results in terms of accuracy, but for real world applications, its use can be too computational heavy, therefore, can't be deployed in real time (specially in devices that do not have a GPU) [26]. MTCNN [133], Faceboxes [135], CenterFace [123] or RetinaFace [25] are examples of this category.

→ **Problem-oriented** is a category that includes the detectors that are projected to resolve a wide range of specific problems, for example, faces that are tiny, partially occluded, blurred or scale-invariant face detection [26]. PyramidBox [103] is an example that solves the partial occluded and blurry faces, and HR [41] tackles the tiny faces challenge.

¹ A facial landmark is a key-point in a face that contributes with important geometric information, namely the eyes, nose, mouth, etc. [31]

Face Alignment Classes

→ **Landmark-based alignment** is a category of methods that exploits the facial landmarks with the aim of, through spatial transformations, calibrating the face to an established layout [26]. This can be accomplished through: coordinate regression, heatmap regression or 3D Model Fitting. **Coordinate regression-based** methodologies [31, 64, 133] consider the landmark localization as a numerical objective, i.e. a regression, thus an image is fed to a DCNN and it will output a vector of landmark coordinates. **Heatmap Regression** [24, 121, 16] is different from coordinate regression because, although it is a numerical objective task, the output is not a coordinate vector, but a map of likelihood of landmarks' locations. Finally, **3D Model Fitting** [9, 15, 122] is the category that integrates methods that consider the relation between 2D facial landmarks and the 3D shape of a generic face. The particularity of them is the reconstruction of the 3D face from a 2D face image that is then projected over a plane in order to obtain the landmarks.

→ **Landmark-free alignment**, on the other hand, integrates the approaches that do not rely on landmarks as a reference to align the face, in contrast, these type of methods incorporate the alignment into a DCNN that gives, as a result, an aligned face [26]. An example of an end-to-end method that does not depend on facial landmarks is RDCFace [138], and it rectifies distortions, applies alignment transformations and executes face representation. Hayat et al. [36] proposes a method that deals with extreme head poses. The process to register faces in an image with high pose variance can be quite challenging and often demands complex pre-processing, namely landmark localization, therefore, to address that, a DCNN is employed that does not rely on landmark localization and concomitantly register and represent faces.

Training Data

→ **CASIA-WebFace** [126], composed of 494,414 face images and 10,575 identities, was proposed as a novel dataset to overcome the problem of data dependence in face recognition and improve comparability across different methods.

→ **VGGFace** [81] was published alongside a homonymous face recognition method and, once again, with the objective of combating the lack of available large scale public datasets. It contains 2,6 million images and 2,622 different identities and a curated version, where incorrect image labels were hand-removed by humans, has 800,000 images for the same amount of identities.

→ **MS-Celeb-1M**'s [35] first intention was to provide a novel benchmark to identify celebrities that solves name ambiguities by linking a face with an entity key in a knowledge base. Second, it aimed at solving the gap in available large-scale datasets by providing a training set with, approximately, 10 million images and 100 thousand identities. Unfortunately, it is a dataset known for the presence of noisy labels.

→ **MegaFace** [77] introduced a benchmark for million-scale face recognition and provided a public large-scale training dataset that integrated 4,753,320 faces over 672,057 identities. The main difference compared to the previously mentioned datasets is that MegaFace does not use celebrities as subjects, in contrast it leverages the photographs released by Flickr under the Creative Commons license.

→ **VGGFace2** [13] is another large-scale dataset, and its main goals are: 1) covering numerous identities, 2) reduce labeling noise through automatic and manual filtering and, finally, 3) represent more realistic unconstrained scenarios due to a novel dataset generation pipeline that gathers images with a broad range of poses, age, illumination and ethnicity. All in all, this resulted in a dataset comprised of 3,31 million faces of 9131 subjects.

→ **UMDFaces-Videos** [7] is a video-based dataset composed of 22,075 videos of 3,107 subjects with 3,735,476 human annotated frames with great variation in image quality, pose, expressions and lightning. It was proposed during a study how the performance of a face verification models is impacted by the effects of: 1) the type of media used for training (only videos or still images vs a mixture of both), 2) the width and depth of a dataset, 3) the label's noise and 4) the alignment of the faces.

→ **Celeb-500k** [12] is another large-scale proposed with two issues in mind: the disparity in the scale of public datasets when compared with private ones, and determining the impact in performance from intra- and inter-class variations. That being so, Celeb-500k, consisting of 50 million images from 500 thousand persons, and Celeb-500k-2R, a cleaned version of the previous, comprised of 25 million aligned faces of 245 thousand identities, are released.

→ **IMDb-Face** [109] proposes a new dataset with based on a manually cleaned revision of MS-Celeb-1M and MegaFace. The growing demand for large-scale datasets introduced a new variable to take into consideration: the time available to annotate the data. Datasets that are well-annotated and have an enormous amount of data are notably expensive and time-consuming to develop. Therefore, automatic measures to clean the data were used, so it is expected for a certain degree of noise to be introduced in a dataset. After selecting a subset from both the originals datasets, 2 million images were manually cleaned and resulted in 1,7 million images of 59 thousand celebrities.

→ **MS1MV2** [23] is another well know dataset. It was proposed in the ArcFace face recognition method's revision paper and consists of a semi-automatic refinement of the previously mentioned MS-Celeb-1M, resulting in 5,8 million images of 85 thousand identities.

→ **RMFRD** [116] is presented in the context of the need of using a mask, mandated by the COVID-19 pandemic, and that greatly reduces the effectiveness of conventional face recognition methods. Therefore, there was a need to improve their performance and for that a dataset that provides masked faces is needed. RMFRD pioneered this need by publishing a dataset consisting of 5 thousand masked and 90 thousand unmasked faces from 525 celebrities.

→ **Glint360K** [4] is a training set presented in the Partial FC method paper. It was generated by merging and cleaning the aforementioned Celeb-500K and MS1MV2 datasets, which resulted in 17 million images of 360 thousand individuals.

→ **WebFace260M** [143] takes a giant leap in closing the gap between public available datasets and private ones. Partnered with a time-constrained face recognition protocol, the original paper presented an enormous 260 million faces and 4 million identities noisy dataset, an automatically cleaned, high quality training set with 42 million faces over 2 million identities (WebFace42M), and a smaller scale training dataset derived from the WebFace42M that has 10% of its data (WebFace4M).

→ **DigiFace-1M** [6] is a novel approach that revolutionizes the way of training face recognition models. It is a fully synthetic dataset that proposes mitigating three very relevant problems present in the majority of the conventional datasets: 1) ethical issues, 2) label noise and 3) data bias. The dataset is divided in two parts: part one contains 720 thousand images from 10 thousand identities and part two has 500 thousand images with 100 thousand identities, for a total of 1,22 million images and 110 thousand unique identities.

Test Data

→ **LFW** [42] is the most well-known face verification dataset. It was first released in 2007 as a way of evaluating the performance of face recognition methods, in a

verification or pair matching manner, under unconstrained scenarios. LFW divides the dataset in 2 views. View 1 is designed for development, and in the training set contains 1100 pairs of mismatched images and 1100 pairs of matched ones, while the test set has 500 pairs of matched and 500 pairs of unmatched faces. View 2 is intended for performance reporting and splits the data over 10 separate sets, to facilitate 10-fold cross validation, where each one has 300 positive pairs (same identity) and 300 negative pairs (different person), resulting in 6000 pairs. Overall, the dataset has 13,233 face images and 5749 identities (only 1680 persons have two or more images).

→ **YTF** [120] is a video-based benchmark that leverages the greater amount of information provided by a video in comparison to still images. By collecting videos from *Youtube* there isn't an opportunity to control the conditions, hence the footage will support a wider range of characteristic's variation, namely lighting conditions, difficult poses, motion blur, compression artifacts, etc. This resulted in 3425 videos from 1595 identities and a benchmark protocol inspired in the LFW. To evaluate performance, a pair-matching test is designed. From the database, 5000 video pairs are collected, where half are matches and the other half are not, to be divided to allow 10-fold cross validation.

→ **IJB-A** [53] aims at straying further from the saturation in recognition benchmarks by proposing more challenging benchmarks (specifically by including wider geographic distribution and full pose variation) for both verification and identification. It consists of a mix of 5712 images and 2085 videos from 500 individuals, with manual bounding boxes, facial landmarks and, most importantly, labels. IJB-A supports two protocols: search (face identification) and compare (face verification). For both the protocols, the specifications are the same, i.e., ten random training and testing splits are generated using all 500 identities then used to perform sample bootstrapping (instead of cross validation) in order to enhance the number of testing subjects. For each split, 333 subjects are randomly distributed

in the training set and the remainder 167 are placed in the testing set.

→ **CFP** [93] studies the effect of extreme pose variations, such as a profile view of a face, in face verification. During collection gender and profession balance, as well as racial diversity, were considered. A number of frontal and profile view images was also set as 10 and 4, respectively. Therefore, after cleaning the initial data, it resulted in 7000 images from 500 subjects. The experimental protocol divided the 500 identities over 10 splits (facilitating 10-fold cross validation) and randomly generated 7 matched pairs and 7 unmatched pairs per identity, resulting in a total of 7000 pairs of faces.

→ **CPLFW** [140] is another dataset that tackles the overly optimistic accuracy saturation in classic benchmarks, such as the previously mentioned LFW. To this end, evaluating performance for cross-pose faces of LFW subjects is the matter of study. It contains the same number of 13,233 images of 5749 identities like LFW and the benchmark protocol performance is the LFW *View 2* with some differences: 1) negative pairs are from people of the same race and gender, 2) class imbalance and limited positive pair's diversity is resolved by assuring that each identity has at least 2 images.

→ **CALFW** [141] has the same principles as CPLFW but applied to the age of the subjects (including the negative pairs selection and the class imbalance problem).

→ **AgeDB30** [76], similarly to CALFW, is a dataset that considers the subject's age. It distances itself from other databases by solving the noisy labelling, induced by automatic or semi-automatic methods, by doing so manually. Age-DB has 16,488 images and 568 subjects used in 4 evaluation protocols, similar to LFW's *View 2*, where the main difference between them is the age difference between pairs (5, 10, 20 and 30 years).

→ **IJB-B** [118] builds upon IJB-A and proposes solving flaws that were verified

in the previous dataset. First, the improved IJB-B dataset is larger, consisting of 21,798 images and 7,011 videos from 1,845 subjects, with a more uniform racial distribution. Second, the protocols are upgraded due to a greater number of possible comparisons between images and possible identities.

→ **TinyFace** [18] was presented to fill in the gap of low-resolution face recognition benchmarks with genuine images and not downsampled ones. It is designed for face identification, and is composed of 15,975 labelled images and 153,428 distractors, totalling 169,403 low resolution images, from 5,139 identities. The evaluation protocol is similar to the one used by MegaFace: 1) half of the identities are randomly sampled by the probe set and the other half by the gallery set, and 2) the distractor images are added to the gallery incorporating further complexity to the identification process.

→ **IJB-C** [70] adds 1661 new identities to IJB-B and new end-to-end protocols (to evaluate face detection, identification, verification, clustering) in order to better mimic real-world unconstrained recognition. They have increased diversity, both in geographic location and profession, and occlusion scenarios. IJB-C has 31,334 images and 11,779 videos from 3531 subjects.

→ **IJB-S** [48] is a manually annotated benchmark constructed by collecting images and surveillance videos that presents a challenging face recognition problem. It is a dataset with several challenging variations, namely, full pose, resolution, presence of motion blur and visual artifacts. The aforesaid are tested during 6 different face detection and identification protocols. IJB-S consists of 350 surveillance videos, 202 enrollment videos and 5656 images.

→ **RFW** [114] is a proposed benchmark dataset to evaluate the racial bias of face verification solutions. It is divided in 4 subsets regarding the race of the subjects, where each contains, approximately, 10 thousand images and 3 thousand identities,

totaling 40,607 images from 11,429 subjects. The evaluation protocol is the same as the LFW one, but the negative pairs were mined to be difficult and avoid easily saturated performance.

→ **QMUL-SurvFace** [19] is a dataset introduced as a benchmark in the *Surveillance Face recognition Challenge* for face recognition in a surveillance context, and it contains both face verification and identification protocols. By data-mining 17 public person re-identification datasets, it achieves 463,507 facial images of 15,573 identities collected in uncooperative surveillance scenarios. Consequently, it presents a high variance in resolution, motion blur, pose, occlusion, illumination and background clutter.

→ **MDMFR** [107] is brought about in light of the COVID-19 impact, where wearing a mask became mandatory and rendered unusable the traditional face recognition methods. Therefore, in conjunction with DeepMaskNet, MDMFR was released. It is a large-scale benchmark dataset designed to evaluate the performance of both masked face recognition and masked face detection algorithms. The recognition protocol contains 2896 images from 226 identities, intended to benchmark masked face recognition models.

→ **XQLFW** [54] revisits the LFW and modifies it to better evaluate cross-resolution face recognition problems. The evaluation protocol, number of images and identities remains the same (13,233 and 5749, respectively), but the negative pairs are sampled in the same manner as CPLFW [140] and CALFW [141].

→ **CAFR** [139] was introduced in 2022, in the revised paper of the AIM (Age-Invariant Model) as a large-scale benchmark dataset to advance the development of face recognition models invariant to age. It consists of 1,446,500 images from 25,000 subjects and spans a range of ages from 1 to 99 years old. The evaluation protocol divides the data in 10 splits of 2500 pair-wise disjoint subjects, where each

one has associated to it 5 matched pairs and 5 unmatched, resulting in a total of 25,000 pairs per split.

→ **FaVCI2D** [82] is face verification benchmark dataset that proposes to address three relevant flaws : 1) the pairs selected are not challenging enough, 2) the demographics of other datasets are not representative enough of the real world diversity and 3) legal and ethical questions concerning the data used. It is composed of 64,879 images and 52,411 unique identities, where 12,468 are used to create genuine matched identity pairs with balanced gender and geographic distribution.

ROC Curves

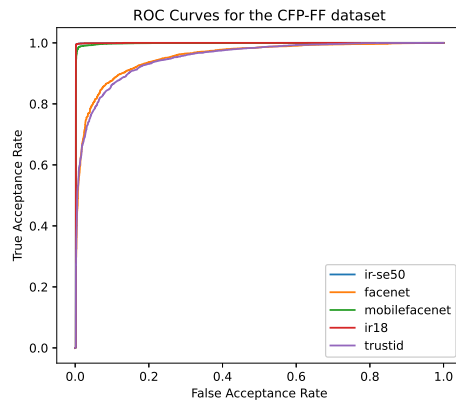


Figure 31: ROC Curves for the CFP-FF benchmark from the Frontal group.

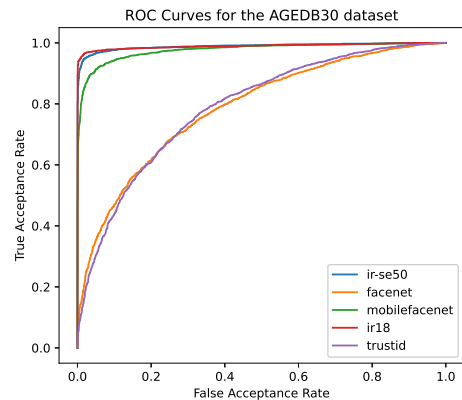


Figure 32: ROC Curves for the AgeDB30 benchmark from the Age group.

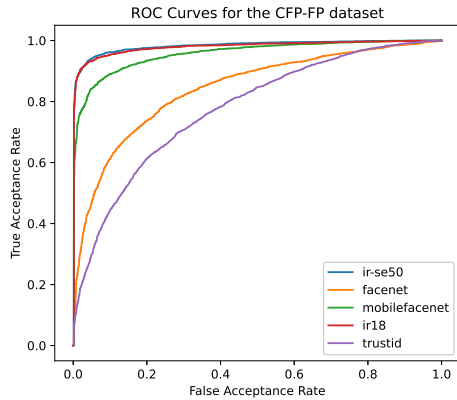


Figure 33: ROC Curves for the CFP-FP benchmark from the Pose group.

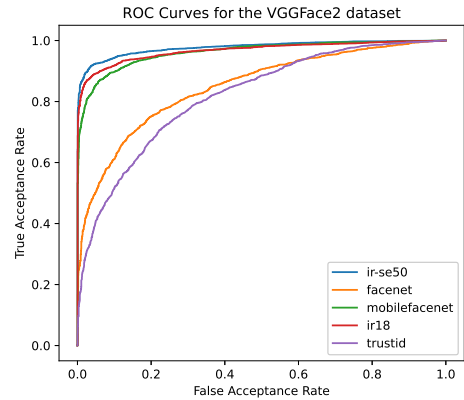


Figure 34: ROC Curves for the VGGFace2 benchmark from the Hard group.

DET Curves

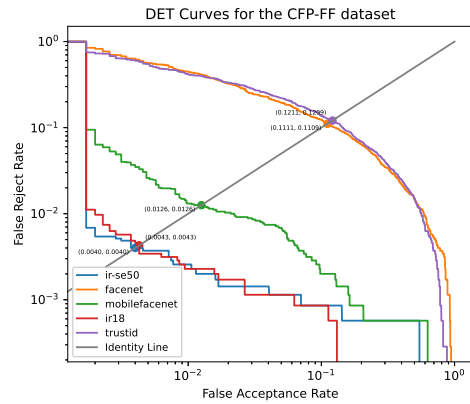


Figure 35: DET Curves for the CFP-FF benchmark from the Frontal group.

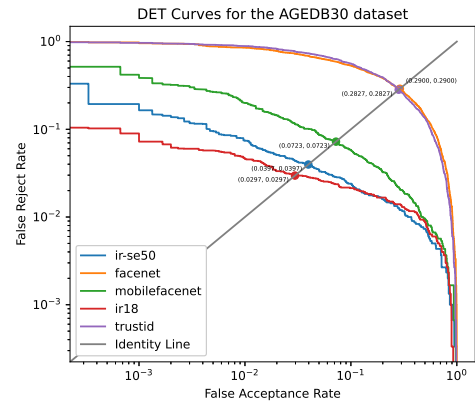


Figure 36: DET Curves for the AgeDB30 benchmark from the Age group.

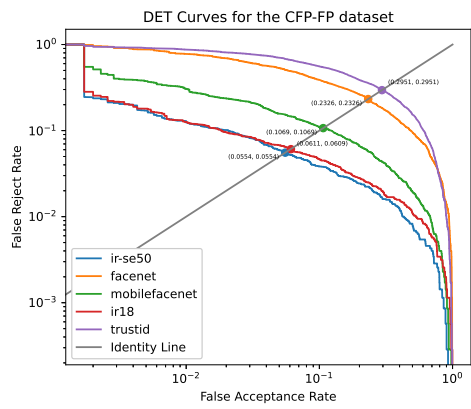


Figure 37: DET Curves for the CFP-FP benchmark from the Pose group.

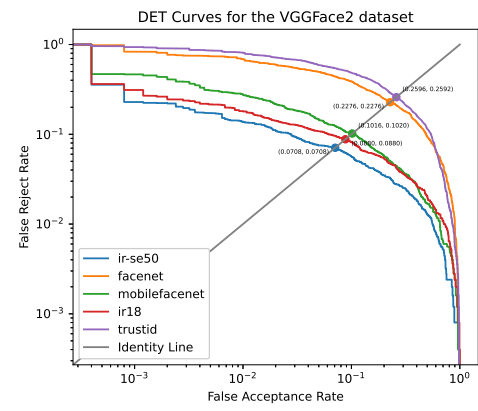


Figure 38: DET Curves for the VGGFace2 benchmark from the Hard group.